DNA-based Proximity Assays for Biomarker Detection Using Fluorescence and Electrochemistry with Improved Performance through Probe Flexibility

by

Amanda Siyanka Nellimale Kurian

A dissertation submitted to the Graduate Faculty of
Auburn University
in partial fulfillment of the
requirements for the Degree of
Doctor of Philosophy in Chemistry

Auburn, Alabama
May 6, 2023

Keywords:
Thermofluorimetric analysis, Proximity effect, Flexible probes, Electrochemistry, Analytical chemistry

Approved by

Christopher J. Easley, Chair, C. Harry Knowles Professor, Dept. of Chemistry & Biochemistry
Steven Mansoorabadi, J. Milton Harris Associate Professor, Dept. of Chemistry & Biochemistry
Wei Zhan, Professor, Dept. of Chemistry & Biochemistry
Adriana Avila-Flores, Assistant Professor, Dept. of Biological Sciences

Abstract

Detection of biomarkers is important in understanding the mechanisms underlying a disease and developing therapeutics for treatment and cure. Although there are several sensitive and specific analytical techniques revolving around complex instrumentation and labor-intensive workflows for biomolecular detection, there is a demand to develop more simpler and sensitive techniques which are easy to use, even with less technical skill and knowledge. In this dissertation, we present our contributions towards developing simpler assays for biomarker sensing leveraging DNA-based proximity assays. A key contribution of this work is the demonstration that increased probe flexibility can result in better assay performance in several platforms. In chapter 1 of this dissertation, we discuss the basic principles of using DNA strands for biomolecule analysis, where focus is directed towards fluorescence and electrochemical detection platforms.

In chapter 2 we present our attempts at developing a proximity-based assay for protein sensing using a green fluorescent protein (GFP) mimicking RNA aptamer, broccoli. The broccoli aptamer was split into two strands and fused to target sensing units, where spontaneous binding to protein of interest was expected to fuse the split RNA and form the fluorophore binding pocket. The change in fluorescence was monitored through thermofluorimetric analysis (TFA).

In chapter 3, we introduce new applications of TFA, where (1) we leveraged this technique to develop a DNA-based proximity assay for antibody detection. We also demonstrate the importance of conformational flexibility of DNA probes for enhanced assay performance. To promote hybridization of short DNA strands, ssDNA segments of the designed system were substituted with polyethylene glycol (PEG) linkers, which led to improved assay performance. This simple, mix-and-read assay was shown to function in 90 % human plasma. (2) We used this

improved system to study the valency effects of antibody oligonucleotide (AbO) conjugates using TFA, where we were able to clearly distinguish monovalent and multivalent AbOs.

Chapter 4 presents an electrochemical detection platform for antibody sensing. We adopted the flexible PEG-linker based system in chapter 3 above and combined it with the previously developed electrochemical proximity assay (ECPA) to achieve improved limits of detection compared to the developed TFA-based assay. We have demonstrated that careful positioning of PEG linkers in the signaling DNA strands improved antibody-dependent signal increase by 4-fold compared to the system without PEG modifications. Furthermore, the developed antibody sensor promoted tethered diffusion of two methylene blue molecules upon antibody addition, which also contributed to improved signal and detection limit. The assay was functional in 90 % human serum, in the presence of increased ionic strength, which aided in counteracting electric double layer effects and improved shielding effect of the DNA backbone, leading to efficient hybridization.

In chapter 5, we introduce our efforts in adopting electrochemical sensors developed for 2D gold-on-glass planar electrodes to gold microelectrodes. In this work we mainly focus on optimizing experimental design and conditions to achieve improved electrochemical sensing of biomolecules leveraging the DNA nanostructure introduced by our group.

Chapter 6 provides concluding remarks of the work detailed in this dissertation, including future improvements for projects mentioned.

Acknowledgments

I have been greatly privileged and fortunate to pursue my post graduate (Doctoral) studies in bioanalytical chemistry at the Department of Chemistry and Biochemistry, Auburn University. The peaceful and friendly atmosphere prevailing at Auburn had comfortably and immensely helped me in acquiring far and wide knowledge in the field particular. I sincerely hope that the knowledge acquired throughout my career at Auburn will be useful to many people, particularly to those who pursue further studies in similar fields.

I am sincerely grateful to my mentor, Prof. Chris Easley, for the immense support and guidance given throughout my doctoral career, and for having confidence in me. Through your mentorship I have been able to view science and research from a different dimension. Thanks to Prof. Wei Zhan, Dr. Steven Mansoorabadi, and Dr. Adriana Avila Flores for taking the time from your busy schedules to serve as my committee members. Special thanks to Dr. Pengnyu Chen for being the university reader for this dissertation.

Kudos to all members of the Easley lab who helped throughout my time at Auburn. My gratitude to the past members, Dr. Joonyul Kim, Dr. Juan Hu, Dr. Subramaniam Somasundaram, Dr. Kat Ford, Dr. Mark Holtan, Dr. Niamat Khuda, and Dr. Nan Shi. Thank you for the time taken to teach and help me understand the research in the Easley lab, and for the advice on how to navigate life as a grad student. Your experiences and words of wisdom have been of immense support. I am very grateful to my current lab mates. Thank you Asanka, Monir, Mohib, Yvette, Andresa, Joanne, and Mainul for making my time in the lab throughout these years cheerful and enjoyable and being part of my new found family. I appreciate the continuous support that you all give me to carry out my work successfully. Special thanks to Andresa and Patrick for helping me out with research related to fluorescence assay development. Having worked on fluorescent

bioassays for almost three and a half years, I transferred to working on the lab's electrochemical projects towards the latter part of my doctoral career. Thank you, Asanka and Mainul, for helping me smoothly transition into the electrochemistry arm of the lab.

As a South Asian student transitioning thousands of miles away from home I was skeptical about how long it would take me to adopt to the American culture. However, thanks to my dearest friends, Dr. Jessica Krewall, Josh Krewall (and Scout), and Mrs. Ellie O'Steen, it was not arduous. I am very grateful for the support that you all gave me since day one of arriving to USA. Auburn University had a very small Sri Lankan community upon my arrival. However, I have been fortunate enough to have several Sri Lankan friends. Asanka, Ganga, baby Maya, Dr. Isanka Jayawardane, Shanike Navaratne, and Dr. Radini Dissanayake are a few to name, who have been part of my family away from home. Thank you so much for being there to support me. The impromptu day outs, movie nights, potlucks, and trips with you all have indeed been a cure to a stressed-out soul.

My PhD journey would not have been possible without my parents. Thank you so much mama (Zareena Marjan) and dada (Henry Kurian) for being my pillars of support throughout these years. Even being miles apart, the daily conversations with the two of you have helped me keep my head high. Whenever I was feeling low, you both have been able to pull me back on track. A mere thank you is not adequate to express the continuous support that you give.

Table of Contents

List of Tables

List of Figures

Chapter 1

Introduction

1.1 The importance of biomarker detection

The study of biomolecules supports the understanding of complex metabolic processes in the body, disease recognition/ treatment, drug discovery and aids in environmental and food analysis[1]. The detection of biomarkers covers a plethora of targets ranging from ions such as sodium, potassium, and calcium to large molecules or particles such as proteins and viruses/ bacteria [2]. The Kelley group classified clinically important target analytes into three catergories namely, small molecule analytes (eg. metabolites, amino acids, neurotransmitters, and vitamins), protein analytes (eg. cardiac, hepatic, tumor, inflammatory, and other protein markers), and nucleic acid analytes (eg. bacterial, viral nucleic acids and miRNA)[2]. Crucial biomarkers are sometimes present in extremely low (pico to femto molar) concentrations. Thus, there is a need for highly sensitive and specific detection platforms [3, 4]. Biomolecules such as proteins have been identified and sometimes quantified through mass spectrometric (MS) techniques. In a nutshell, MS-based protein quantification involves trypsin digestion of proteins to their respective peptides, which are then ionized. The resulting intensities of mass to charge ratio (m/z) of the peptide fragmentation patterns are then compared with existing protein/ peptide sequence databases for target protein identification [5, 6]. Despite the sensitivity of MS-based techniques, due to the requirement of large and expensive instrumentation, difficulty in absolute quantitation, technical skill and longer analysis times, more simpler techniques have been explored[7, 8]. As such, immunoassays have been

a method of choice over several decades, ever since the development of radio-immunoassays, and have proved to be highly sensitive [7].

1.2 Sandwich immunoassays

1.2.1 Enzyme linked immunosorbent assay (ELISA)

With the advent of radio-immunoassays in the 1960s, sandwich assays have been widely used even to date for specific and sensitive biomarker detection. Although radio-immunoassays exhibited better detection limits, the use of radio isotopes as detection labels threatened a bioassay in terms of handling and workflow [7 9]. As a solution, ELISA was introduced in the 1970s, which uses chromogenic labels, rather than radio isotopes, where a change in colour was observed in the presence of specific target analyte [9].More modern forms of ELISA utilizes fluorogenic, luminescencent (electro or chemical) dyes and DNA-based techniques such as PCR which have aided not only in improving the sensitivity of the technique, but also the ability of multiplexing[9]. Since then, for almost three decades, ELISA has been the gold standard for most biomarker detection, and has been used to detect targets ranging from proteins, hormones, antigens and antibodies [9, 10].

Figure 1.1 depicts a simple illustration of sandwich ELISA. A typical heterogenous sandwich ELISA contains three basic components- two antibodies, specific to the target analyte, an enzyme, and its substrate which serves as the detection label. Here, a microwell plate is first coated with an antibody (primary or capture antibody), which has high binding specificity towards the target analyte (antigen). Due to high target specificity, when the sample is introduced, only the analyte is bound in most cases. Any other nonspecific components are removed by a washing step. Next, a secondary or detection antibody generally carrying a horseradish peroxidase (HRP)

enzyme molecule is added. This also exhibits high binding specificity towards the analyte. This is followed by another washing step to remove any unbound secondary antibody. Next, the substrate TMB (3, 3', 5, 5'-tetramethylbenzidine) is added, where necessary time is given for the reaction to happen, followed by quenching of the reaction, and measuring signal intensity. This allows us to determine the concentration of the specific target. [9-11].

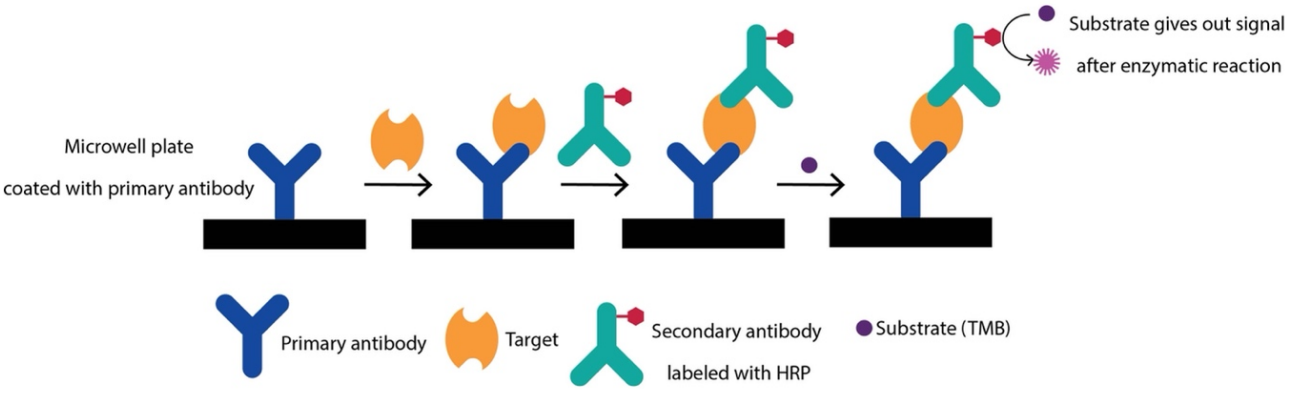

Figure 1.1 An illustration of sandwich ELISA. First a microwell plate is coated with capture antibody, followed by the addition of target. After a washing step, the detection antibody is added which binds to another antibody nonoverlapping epitope of the target. Finally, substrate is added which gives a signal readout.

Sandwich ELISA is more suitable for targets which have two independent binding epitopes. Therefore, the use of two antibodies for detection increases the specificity and sensitivity of the assay. This can also be used to detect samples with ease in complex samples matrices such as blood. Furthermore, different methods of detection can be used with the same primary/ capture antibody [10 12].

However, although this method has its advantages, it also owns certain drawbacks. Due to the use of two antibodies, the system can be used only for targets with two nonoverlapping epitopes. Also, there is a need to optimize and select the best pair of capture and detection antibodies, to get the best specificity and sensitivity. As the method uses a microwell plate (costly),

multiplexing and detecting more than one target is limited. Furthermore, each well requires a considerable volume of sample (~10 μL at least), which is detrimental for precious samples with limited volume. Also, the process requires longer times (~5-8 hrs.), skilled labor to reduce errors, and several washing steps to reduce cross reactivity.

1.2.2 Digital ELISA

Although ELISA is successful in detecting as low as pico-molar (pM) range, some biomolecules such as early-stage cancer markers, neurological disease markers, and infection markers can be found in body fluids at even lower concentrations. Thus, there is a requirement for even more sensitive detection methods [13].Walt and coworkers introduced a digital form of ELISA known as single molecule arrays (SiMoA). Here, magnetic beads carrying the captured target are restricted in ~50 fL microwells. These wells are designed in a way such that they can carry only a single fluorogenically labeled bead [13]. **Figure 1.2** depicts the general principle for SiMoA. As seen in **Figure 1.2D**, the bright areas represent wells where signal is generated by a single enzyme. Although most of the wells will have a bead, only a very few of those beads will have enzymes with catalytic activity. This is indicative of a single protein molecule bound to the capture antibody in the well [13].

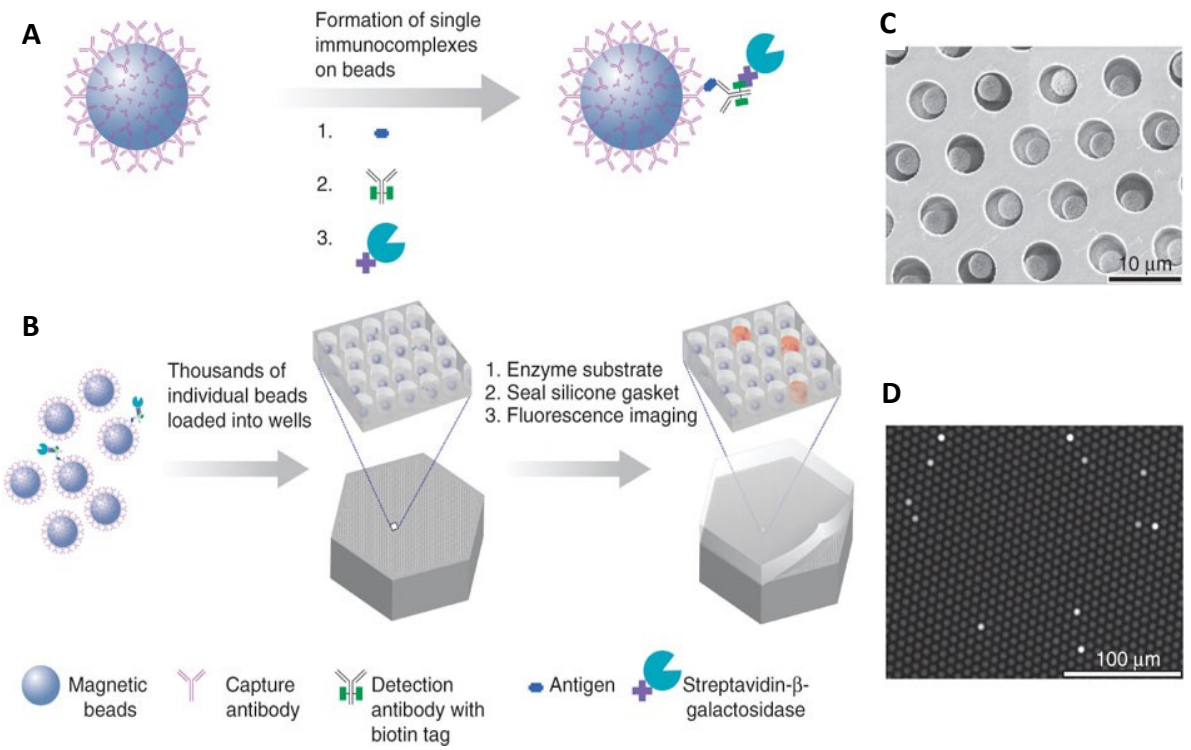

Figure 1.2 General principle of SiMoA. **A)** Antibody immobilized beads first capture the analyte, similar to conventional ELISA. **(B)** Beads are loaded to a microwell of fL volume, followed by addition of fluorogenic and enzyme substrates. **(C)** Image of beads captured in microwell. **(D)** Fluorescence of microwell plate is measured. *Reprinted with permission from reference 13. Copyright 2010, Springer Nature.*

The protein concentration is determined by counting the number of wells having a bead with a fluorescent signal and correlated with the total number of wells carrying beads. At extremely low concentrations of protein, the ratio of beads with an enzyme generating fluorescence signal to the total number of beads is less than 1:1, which results in beads with proteins to follow a Poisson distribution. Thus, at ultra-low protein concentrations, a single bead would have either a protein molecule or none. SiMoA follows a digital approach of determining concentration as opposed to an analog format, due to distinguishing a well with an enzymatic bead generating fluorescence as an 'on' well and a well without an enzyme as 'off' [13]. Therefore, this method is also known as

Digital ELISA. In this work, the authors detected 0.4 fM of prostrate-specific antigen (PSA) in the serum of patients. The better sensitivity of this approach over conventional ELISA is attributed to two factors, (A) higher sensitivity of SiMoA to labeled enzyme and (B) digital detection facilitates the low background signals [13]. Quanterix Cooperation LLC, MA now sells a complete digital analyser for SiMoA which is capable of measuring target molecules in plasma, cerebrospinal fluid, uring and cell lysates,[14]. Although high throughput, multiplexing can be achieved with a broad dynamic range and with less technical know-how, the requirement of a costly dedicated instrument, hinders its adaptability as an instrument for resource limited and point-of-care (POC) or point-of-need (PON) settings.

1.2.3 AlphaLISA

Due to multiple washing steps and narrow dynamic range of sandwich ELISA, it has been challenging to expand it to a high throughput automated assay. Thus, evolved from same principle of sandwich immunoassay and luminescent oxygen channeling immunoassay (LOCI), AlphaLISA was introduced [15-17]. This is a much simpler mix-and-read technique. The general assay principle is illustrated in **Figure 1.3**. The assay involves two types of beads, a **donor bead** that is coated with antibodies (attached through streptavidin-biotin conjugation) specific to the target and an **acceptor bead** carrying a second antibody specific to the target. The target is captured by the donor bead, which then binds to the acceptor bead. Next, the donor bead, which is a photosensitizer, is irradiated by a laser at 680 nm, produces singlet oxygen molecules ($^1O_2$) resulting in a series of reactions to generate chemiluminescence at 615 nm at the acceptor bead [15, 17]. As this follows a simple homogenous mix-and-read assay format, the handling times of the assay and complexity compared to conventional sandwich ELISA is reduced (~2-3 h). The assay

also can use as low as 1 μL of sample volume, which helps save the number of samples whose initial stock volumes are low, allows room for more automated and miniaturizable detection of targets with high sensitivity. Also, due to the amplification by bulk $^1O_2$ and background signal drop due to luminescence, AlphaLISA is highly sensitive compared to ELISA. AlphaLISA has been able to achieve limits of detection in pM ranges [15-18].

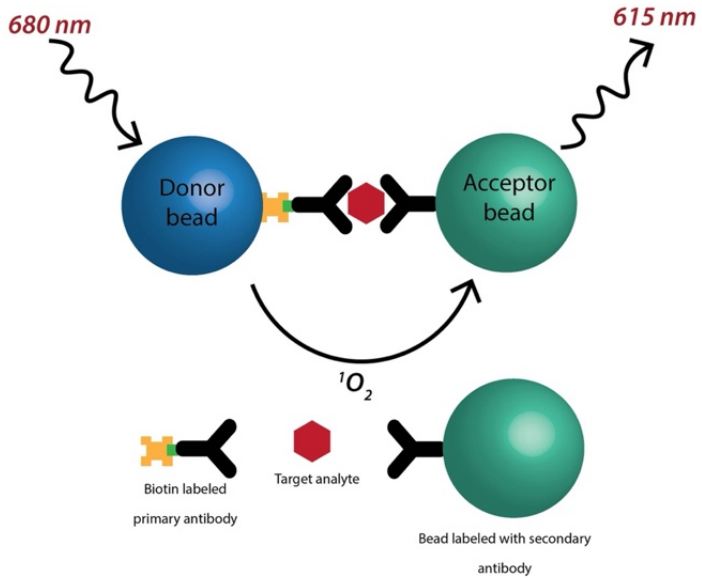

Figure 1.3 Principle of AlphaLISA. Donor bead is immobilized with capture antibody. When the analyte is added, it binds to the capture antibody, followed by binding to the secondary antibody at close proximity. The secondary antibody is immobilized to an acceptor bead. Irradiation of donor bead produces singlet O radicals, to generate chemiluminescence at the acceptor bead. The generated signal is proportional to the analyte.

Although AlphaLISA is a simple, wash-free and sensitive method, it still has the drawback of requiring a specialized instrument, which carries a specific excitation and emission wavelength filter. This feature is limited in most fluorescent devices and hampers its general usage in simple laboratories and resource limited settings.

1.3 DNA based assays

As mentioned previously, although ELISA and its more modern counterparts have achieved fM to pM limits of detection, their drawbacks have created a demand for simpler analytical techniques which are cost effective, homogenous, single-step (mix-and-read), fast and requiring less technical skill, without compromising the sensitivity and specificity [1, 2, 19, 20]. As a step towards achieving this goal, researchers are taking advantage of the changes a biomolecule undergoes in response to variations in temperature, pH, salt concentration and target [21-23]. Biosensors developed based on these natural phenomena can be easily coupled to fluorescence, electrochemical and colorimetric detection platforms to quantitatively determine biomarkers in a single-step, wash-free and limited reagent process [2, 22, 24, 25]. Taking this into account, in this dissertation, we focus on the use of oligonucleotides for biomolecule sensing.

DNA strands undergo spontaneous assembly, due to Watson and Crick base paring rules. This feature of DNA strands has made it a promising building block for biosensor development. DNA-based biosensors include DNA scaffolds, DNA walkers, proximity-based DNA sensors and DNA switches. [24, 26-32].

1.3.1 DNA-based assays: leveraging cooperative sensing for analyte detection

As mentioned above, the Watson and Crick base pairing allows the DNA strands to undergo spontaneous hybridization, due to strong binding affinities between nucleobases [33]. In an assay using cooperative sensing, this nature of spontaneous hybridization is intentionally minimized, and an analyte dependent DNA hybridization is leveraged for biomarker detection. The DNA hybridization event can be studied through fluorescence, electrochemical, and colorimetric techniques, which are then correlated to the amount of target analyte [4, 20, 24, 25, 34].

Another approach of adapting cooperative sensing is splitting a probe of interest, to destabilize it and drive its reassembly through target protein binding. This induced thermodynamic stability can be converted to a measurable signal to quantify the target protein.[24, 35, 36]Therefore, assays based on the premise of cooperative sensing hold promise for developing techniques and biosensors that are cost effective, simple (mix-and-read), sensitive, specific, and rapid. Furthermore, they could be adopted to either homogenous or surface-based assays. [20, 37-39]

The principle of analyte sensing through the proximity effect involves target induced hybridization of two short DNA strands, generally referred to as signaling oligonucleotides, of ≤ 10 base pairs (bp). These signaling oligo strands are usually tagged with signaling molecules such as fluorophore-quencher pairs or electroactive molecules such as methylene blue [4, 24]. In a solution, these signaling oligos are usually present in low concentrations (nM-pM range), which minimizes their efficient hybridization in free solution [4, 21, 24, 40, 41]. However, if these short DNA strands are bound to target recognition units (antibodies, aptamers, antibody fragments, peptide and PNAs), they can anneal to form a more thermodynamically stable duplex [4, 24]. The recognition units can bind to two nonoverlapping epitopes of a protein or two paratopes of a target antibody with high affinity. As a result, the short complementary DNA strands that were far from each other, are now brought to close proximity and are restricted within a smaller volume. This target induced entropic stabilization drives the hybridization of the shorter DNA strands, due to the increase in localized concentration from nM to μM range [4]. This formed proximity-based structure is more analogous to a simple DNA stem-loop system. Typically, the hybridization of two complementary shorter DNA strands will follow a spontaneous, intermolecular hybridization and has a lower stability at room temperature, especially if their concentrations are low in free solution.

However, if these two strands are connected through a single stranded DNA linker (ssDNA) to form a continuous DNA strand, the two shorter strands will follow intramolecular hybridization due to the formed stem-loop structure. The melting point (T_m) of this stem-loop structure is higher than that of the DNA strands that undergo intermolecular hybridization [4]. The formed proximity complex is analogous to the DNA stem-loop structure [4, 24]. **Figure 1.4** illustrates the basic principle of proximity effect.

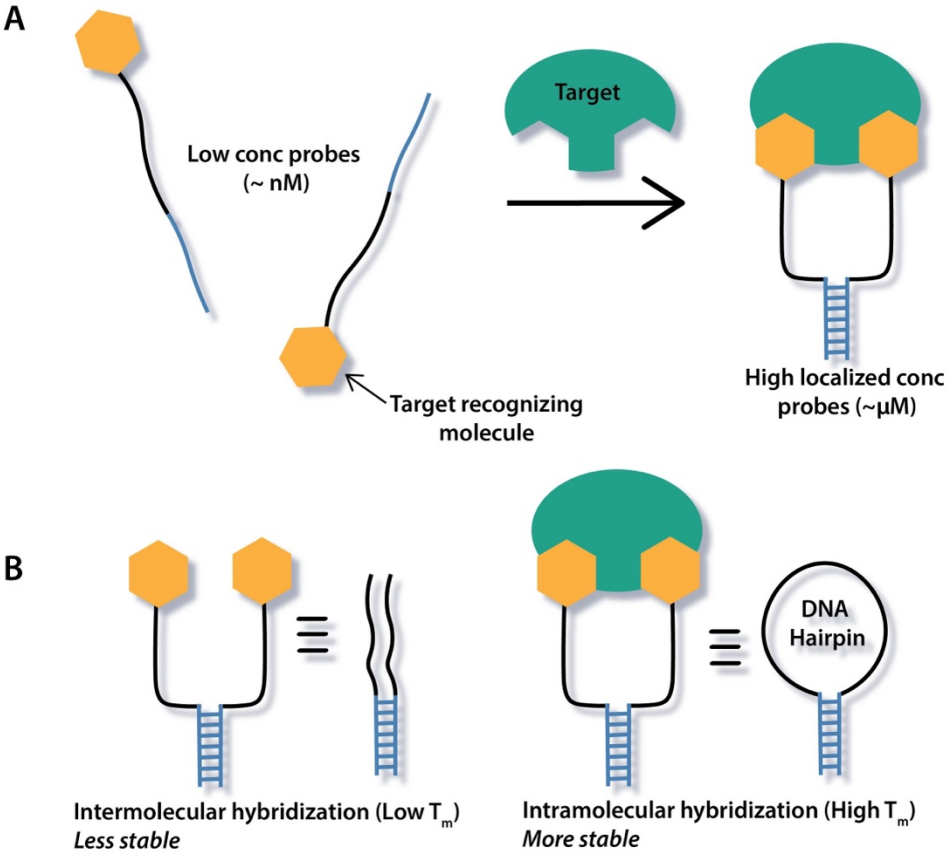

Figure 1.4 Principle of proximity effect Principle of proximity effect. **(A)** Short DNA strands tagged to analyte recognition units are in ultra-low concentrations. Addition of analyte, confines DNA strands to a smaller volume, increasing their local concentrations, which drives hybridization. **(B)** Left- target unbound system follows intermolecular hybridization and is less stable. Right- Target-bound system is similar to a stable hairpin loop and follows intramolecular hybridization

Figure 1.5 below illustrates a FRET (Förster resonance energy transfer) assay, based on thermofluorimetric analysis (TFA) for analyte sensing using antibody tagged oligonucleotides (AbOs) as signaling probes. The signaling probes carry two FRET pairs. Initially, there are free AbOs (or probes) in solution. In the presence of target, the signaling complex is formed, where a measurable FRET signal is given (**Figure 1.5** top, right). The bottom figure represents a typical derivative curve obtained by thermally scanning the melting transition of proximity complexes (i.e. following the DNA denaturation in terms of change in FRET signals, with respect to increasing temperature). As mentioned previously, the analyte-bound proximity complex gives a more thermodynamically stable complex, which is represented by the higher melting temperature (**signal peak, blue curve**). A detailed description regarding the technique of TFA and its applications will follow in **chapter 2**. Since concentration of probes in free solution initially are slightly in excess compared to what is required by the analyte, there will be a certain number of unbound probes in solution, which will not result in a measurable signal [24].Although, ideally we expect to see no measurable signal from free probes, there is still room for analyte independent, intermolecular hybridization, leading to a measurable signal (**Figure 1.5** top- center and bottom- grey curve). Therefore, when designing an isothermal assay based on proximity effect, it is critical to design necessary probe DNA in a way such that the background does not interfere with signal complex. It is important that one designs such an isothermal assay where the background is unstable enough, whilst keeping the signal within a measurable limit. For this purpose we can leverage TFA, since this provides a good understanding regarding the stability of signal and background, and select the best temperature for an isothermal assay where the background is considerably unstable, but signal is still in a measurable range. As shown in **Figure 1.5** (bottom), two curves corresponding to the background (grey) and signal (blue) are illustrated. This clearly

depicts the decrease in background peak in the presence of analyte, corresponding to its entropic stability, which gives us an idea regarding the best conditions for selecting a temperature for an isothermal assay, with minimal background interference [24].

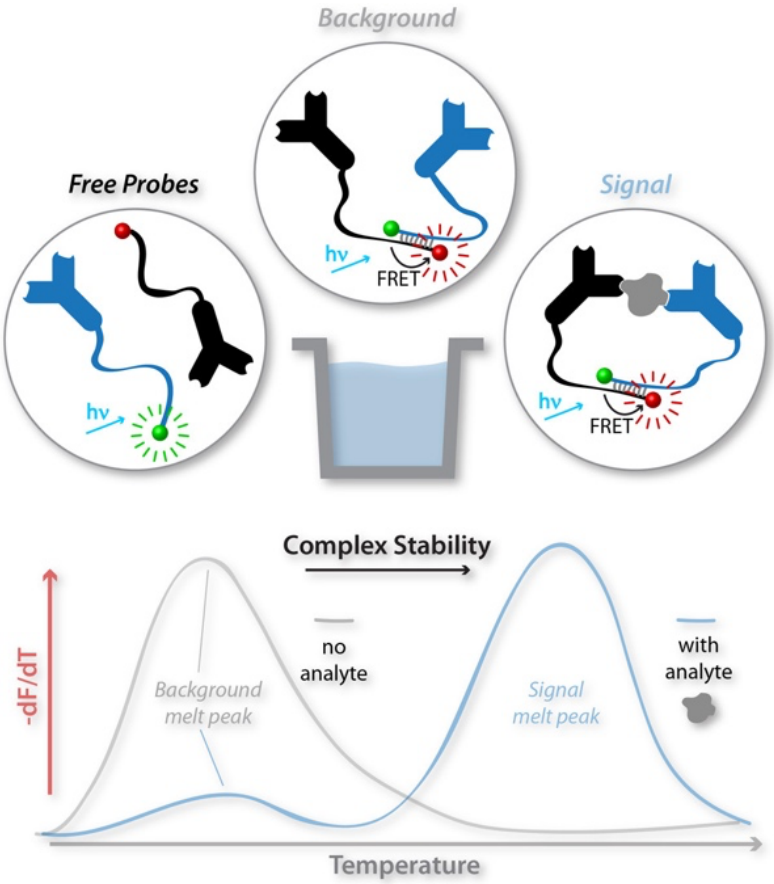

Figure 1.5 An Illustration of proximity effect, using thermofluorimetric analysis (TFA). At beginning of an assay, free probes are abundant. Upon addition of analyte, signaling DNA strands hybridize to give a measurable FRET signal. The signal complex is entropically stable and has a higher ,melting temperature, which is represented as a shift in the melt curve (bottom, blue curve). A certain number of background complexes are also formed, which are independent of analyte binding. This forms a less stable complex, which is represented by a lower melting point (bottom, grey curve). *Reprinted with permission from reference 24. Copyright 2021, American Chemical Society*.

1.3.2 Examples of assays developed based on proximity effect

In this section, we will discuss assays that were developed based on proximity effect. More recent developments on proximity based assays are highlighted in a recent review by our group [24].

1.3.2.1 Proximity ligation assay (PLA)

This assay was first introduced by the Landegren group for target protein sensing. The method combines the proximity effect with PCR amplification for quantification [37, 42, 43]. Herein, target recognizing units are first allowed to bind with the target protein, bringing probe DNA to close proximity. The 5' and 3' ends of the two DNA strands then undergo hybridization with a shorter connector strand, which aids in joining the two ends of the strands by enzymatic ligation (T4 DNA ligase) (**Figure 1.6**). Protein quantification is then achieved through PCR amplification. The probe DNA carries a primer region, which is short (20-22 nt) and will initiate fluorimetric amplification in the presence of polymerase enzyme. The DNA probes which are not bound to protein molecules will not be amplified [42, 43].

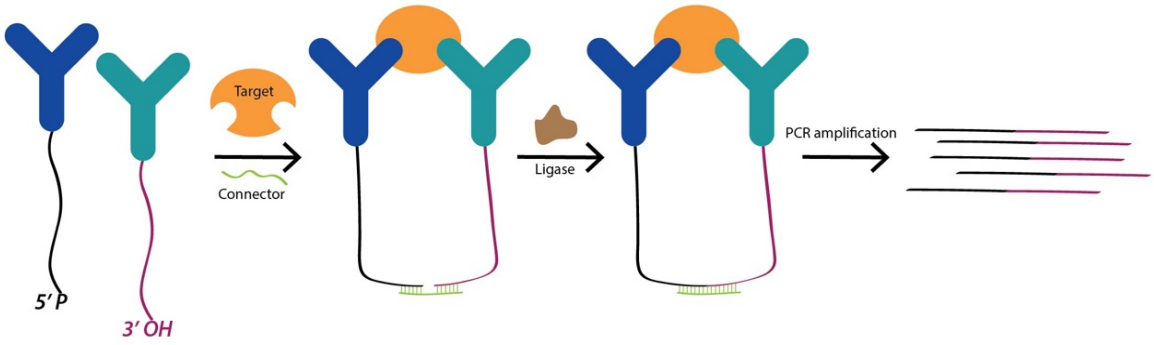

Figure 1.6 An illustration of PLA. Connector strand hybridizes to the 5' and 3' end each, when the tagged DNA strands are brought to close proximity in the presence of analyte. T4 DNA ligase seals the nick between the 5'-phosphate and 3'-OH, by forming the phosphodiester bond. The formed continuous DNA strand carries a primer sequence recognized by polymerase enzyme. Fluorescence signals generated by PCR amplification will be proportional to the amount of analyte in solution.

In their earliest work, the Landegren group demonstrated this method by detecting platelet derived growth factor, B-chain (PDGF-BB) with its corresponding aptamers. Zeptomole amounts of PDGF-BB were detected as a result of leveraging signal amplification techniques [42]. To guarantee efficient ligation, a large excess of symmetrical connector compared to the proximity probes were used. The results of this assay were comparable to that of sandwich ELISA, where PDGF-BB in human plasma was 0.2 nM based on PLA and 0.13 nM based on ELISA. Due the assay being homogenous, it did not require any washing steps, which minimized the complexity of workflow. Furthermore, this assay did not require the immobilization of recognition probes to a surface and multiplexing was easily adaptable [43]. However, the presence of ligation and amplification inhibitors in homogenous solution-based PLA was detrimental for achieving better limits of detection (LOD). In this case, a solid-phase sandwich assay version of PLA was adapted to enhance its LOD. Solid-phase immobilization did not only purify the samples reducing cross reactivity, but also pre-concentrated it [42, 43]. With the same PDGF-BB aptamer pairs the authors have been able to achieve even lower LODs compared to the homogenous PLA [42, 43].

Although aptamer pairs provided good sensitivity and specificity in protein target detction, there are only a limited number of aptamer pairs available which could be used as proximity probes. However, with the evolutions in ELISA, there are many antibodies, both mono and polyclonal that are available and are able to bind specifically to two nonoverlapping epitopes of a target protein. Therefore, in a later work, the Landegren group extended PLA to detect cytokines using antibody oligonucleotides as probes. Due to the high specificity of the antibodies, they were able to achieve better assay sensitivity, where target detection even in 1 μL samples were achieved [44]. Another advantage of this is that it requires < 1000x of antibody, compared to conventional ELISA, with less optimization steps. This aids in minimizing assay cost. Furthermore, solution-

based, homogenous PLA using antibodies offer a platform for multiplexing, provided that the targets have necessary pairs of antibodies, with limited cross reactivity [43, 44].

1.3.2.2 The proximity extension assay (PEA)

Although PLA was shown to be sensitive, its performance in human plasma was hampered due to ligase inhibition in plasma. As an alternative to PLA, the Fredriksson group introduced the proximity extension assay (PEA) [45, 46]. Herein, the authors used DNA polymerase enzyme for strand extension, followed by PCR amplification for protein quantification [46, 47]. PEA follows three basic steps (**Figure 1.7**). (a) the target protein is incubated with two AbOs, where one of the probe DNA carries a 3' linked double strand DNA (dsDNA), with a short overhang of 9 nt at the 5' end. The other probe DNA, which is 5' linked has a 9 nt complementary to that of the overhang. Protein binding brings the two DNA strands to close proximity, where the overhang hybridizes with the 5'linked probe DNA. (b) T4 DNA polymerase was added, which extended the hybridized overhang to form a full length DNA strand. (c) this DNA served as a full-length amplicon which was quantified by qPCR. The qPCR signal correlated to the target protein concentration [45, 46].

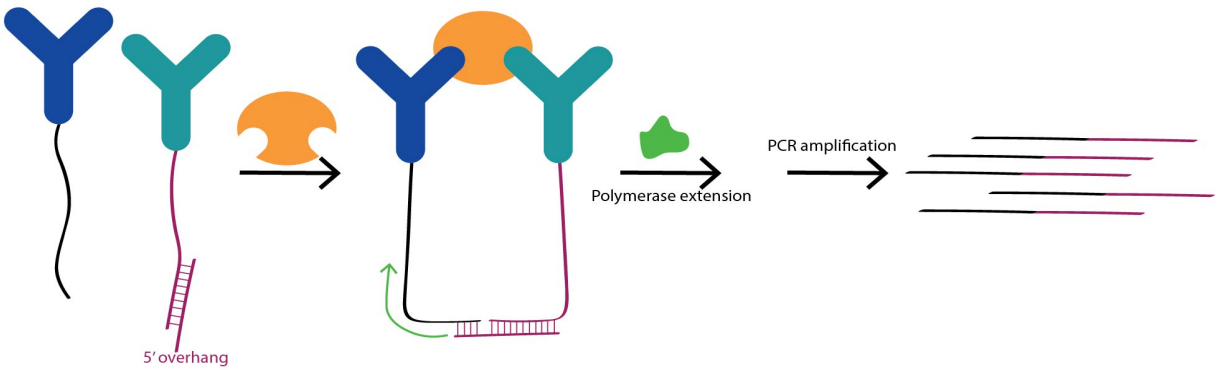

Figure 1.7 Illustration of PEA. Two DNA strands are tagged with antibodies, where one strand already carries a shorter DNA strand with a 5' overhang hybridized. Analyte addition brings the two DNA strands closer, where the 5'overhang hybridizes to part of the other DNA. Strand extension by polymerase, followed by PCR amplification helps quantify the protein.

The authors demonstrated that it was important for the polymerase enzyme to possess 3'→5' exonuclease activity, which contributed to low background and improved assay sensitivity. This was due to the fact that, exonuclease activity was able to digest any free non-adjacent ends of DNA, which will prevent them from forming any extension products through arbitrary proximity events [46]. Glial cell line derived neurotrophic factor (GDNF) and human IL-8 were spiked and detected in human plasma, where a LOD of 0.1 pM was detected for both targets [46]. To further improve the assay performance in terms of sensitivity, specificity and multiplexing the Fredriksson group included two other steps. After the polymerase extension of proximity probes, the formed PCR templates were pre-amplified by universal primers, followed by uracil glycosylase digestion to remove all the unbound primers from DNA templates. Finally, using microfluidic qPCR the existing DNA sequences were detected using specific primers. Herein, 92 well known cancer protein markers were quantified at the same time. It was observed previously that due to the requirement of proximity effect to form an amplifiable DNA template for qPCR, cross reactivity of antibody pairs used was minimal in PEA, aiding in improving its capability of adapting it for

multiple target detection [47]. Therefore, PEA bears the advantages of being rapid, simple workflow, capability of using low binding affinity target recognition units, requirement of low sample volume and capability of multiplexing [45-47].

1.3.2.3 The pincer assay

Although PLA and PEA have demonstrated to be sensitive and specific, whilst having a more simplified workflow compared to ELISA, the use enzymes and the need of a precise thermal cycling program makes it still quite cumbersome. Taking advantage of FRET, the Heyduk group introduced an even more simplified enzyme free assay known as molecular pincers [34, 40, 41, 48]. **Figure 1.8** shows an illustration of the basic principle. Herein, signaling DNA probes carry FRET pairs and include either antibodies or aptamers as analyte binders. When these bind to the target protein, the shorter signaling strands are brought to close proximity, undergoing target-induced hybridization. This results in a measurable FRET signal. The target bound complex will show a higher FRET signal compared to the background complex [34, 40, 41, 48]. Cardiac troponin I was detected as low as 40 pM using its respective antibody pairs, while insulin was detected at 100 pM using anti insulin antibodies. The assay was able to detect targets within 15-20 mins [34, 48]. To improve assay performance in complex biological fluids, the authors demonstrated the use of lanthanide chelates, instead of FRET pairs. Due to the long emission life times of lanthanide chelates any interference of autofluorescence caused by plasma will be eliminated, which enhanced the signal to background ratios. The authors were able to observe an ~2 fold improvement in assay sensitivity [34]. This method was later adopted to a surface-based assay allowing capability of multiplexing [40, 49].

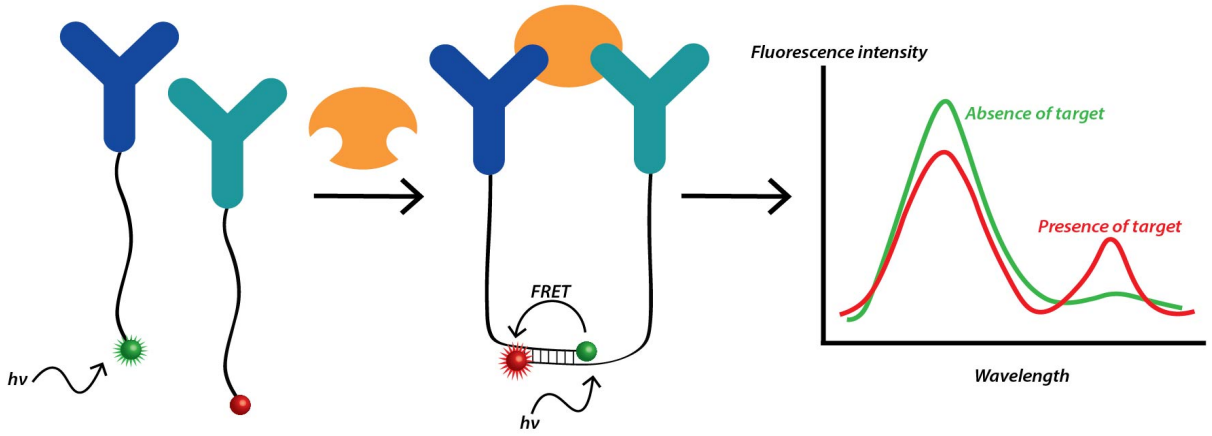

Figure 1.8 Illustration of pincer assay. Each antibody is tagged with a fluorophore. Target addition brings the two DNA strands closer to each other. Hybridization of short DNA strands then brings the FRET pairs close to each other, where the resulting change in fluorescence of the acceptor fluorophore. Change in fluorescence signal is proportional to the target concentration

1.3.2.4 The electrochemical proximity assay (ECPA)

Our lab introduced the ECPA, where proximity effect was coupled with electrochemical detection for protein quantification. **Figure 1.9** illustrates the basic principle. Herein, target binding results in assembling a 5-part circular complex which brings an electroactive redox molecule, methylene blue (MB) closer to a gold electrode surface for electron transfer [20, 25]. Each antibody-oligonucleotide conjugate is hybridized through 20 base pairs to a thiol- DNA and a MB-DNA separately. MB-DNA approaches closer to thiol-DNA, as a result of target addition, leading to the hybridization of complementary DNA strands (complementary region on MB- and thiol-DNA are shorter sequences). This brings MB closer to the gold surface, where electron transfer occurs. The generated peak current is proportional to target protein concentration.

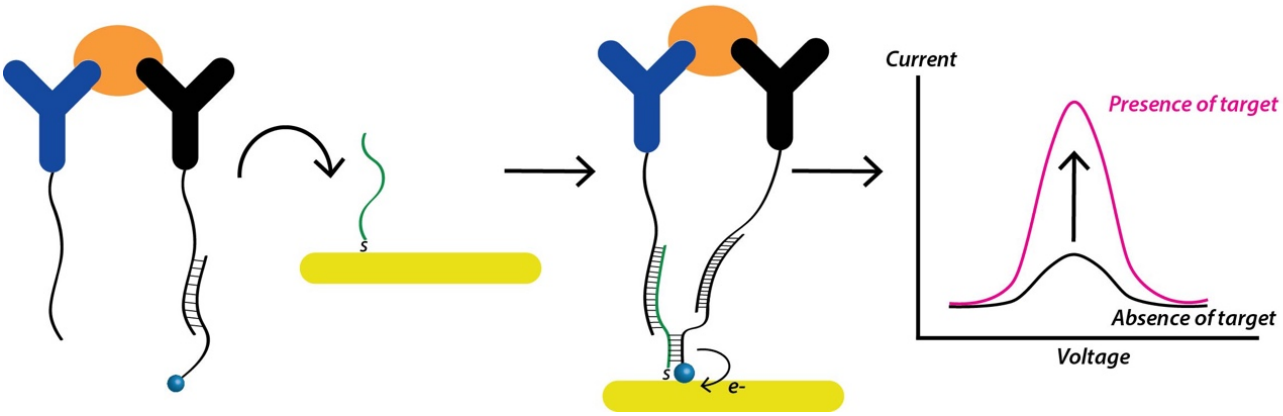

Figure 1.9 Sensing principle of ECPA. Binding of target with antibodies brings the MB-DNA closer to the electrode surface. MB-DNA hybridizes to the thiol-DNA through a short DNA strand, leading to electron transfer between the MB tag and electrode surface. Generated current is proportional to the target signal.

Leveraging ECPA, insulin and thrombin were detected in fM-pM ranges using antibody and aptamer pairs respectively as analyte binding probes. [20, 25] Since the developed ECPA was of single use, as an improvement to this first-generation sensor, a reusable ECPA was introduced for real-time protein quantification. Herein, a selected number of deoxythymidines (dTs) were substituted by deoxyuridines (dU), which allowed enzymatic cleavage of dU by uracil excision mix [25]. Following water and buffer washes after enzymatic addition removed the target bound complex, resulting in a cleaner gold electrode which now carried only the thiol-DNA on the surface. This fresh electrode was ready for a new round of sample detection. Both insulin and thrombin-based sensors demonstrated a reusability of ~19 times [25].

Later, the Ju group introduced ratiometric ECPA, REPA (**Figure 1.10**). Here, antibody 1 (Ab1) is tagged to DNA-1 with a distal MB, which is hybridized to thiol DNA carrying a ferrocene molecule (Fc) at its distal end (capture probe). Addition of target protein and the other recognition unit (Ab2-DNA-2 or detection probe) brings the DNA-1 and DNA-2 to close proximity allowing hybridization, releasing the Ab1-DNA from the capture probe, which forms a hairpin-loop

structure, bringing the Fc closer to the gold electrode surface. As a result, the Fc undergoes electron transfer, acting as "signal on" and concurrently as the MB is pushed away from the gold surface, it acts as "signal off". Due to the increase and decrease in electrochemical signals of Fc and MB respectively upon target addition, this method is considered as a ratiometric sensor. The authors demonstrated that prostrate specific antigen (PSA), a cancer marker can be detected withing 40 mins in a single step, with a LOD in pM range [50].

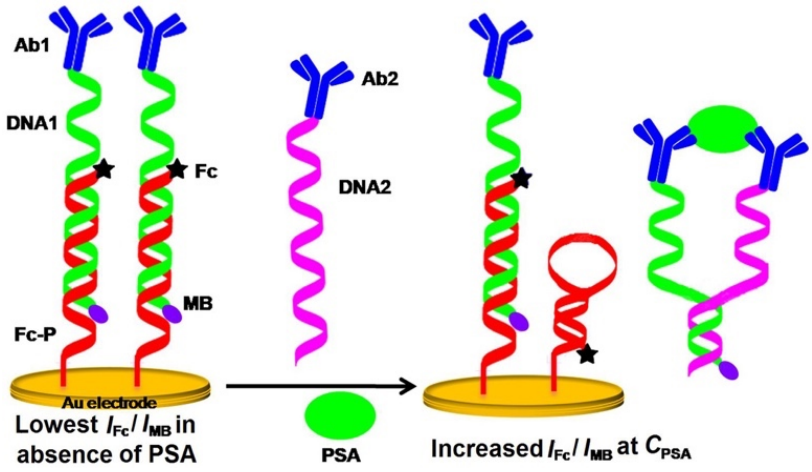

Figure 1.10 Sensing principle of REPA. DNA-1 is tagged to Ab1 and MB at its distal and proximal ends. Additionally, DNA-1 is hybridized to a thiol-DNA, which is attached to a gold surface at its proximal end and a ferrocene molecule at the distal end. Addition of DNA-2 and PSA displaces DNA-1, due proximity effect. This leads to signal reduction of MB and signal enhancement of ferrocene, making it a ratiometric sensor. *Reprinted with permission from reference 50. Copyright 2014, Springer Nature.*

In a more recent work, Alessandro Porchetta and coworkers attributed the proximity effect as "effective molarity" [24, 51]. As shown in **Figure 1.11A,** initially the capture and output DNA strands have low binding affinity towards each other but is eventually enhanced when the antibody (Ab) mimicking DNA strand (target) is added. The addition of target strand brings the capture and output strands to closer to each other, driving their hybridization due to enhanced effective

concentration. This shifts the binding curve towards a lower concentration. This system was fine tuned to accommodate antibody sensing, where the Ab-mimicking strand was replaced by small molecules recognizing paratopes of an antibody of interest (**Figure 1.11B**) [24, 51]. Sensor functionality was demonstrated by detecting both IgG and IgE antibodies, where 4 different targets were quantified in both buffer and bodily fluids [24, 51].

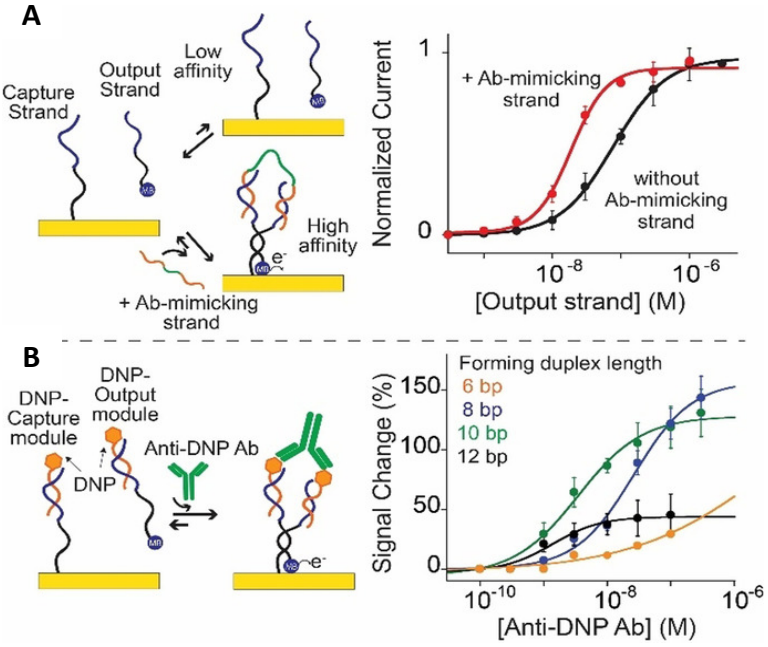

Figure 1.11 Antibody sensing through effective molarity. **(A)** When antibody-mimicking strand is added, the output strand is brought closer to the capture strand, resulting in an increase in effective molarity. The hybridization of two strands enhances MB current and shifts the binding curve towards lower concentrations (right). **(B)** System is modified to detect antibodies, where capture and output strands are now hybridized to antibody recognition units. *Reprinted with permission from reference 51. Copyright 2020, John Wiley and Sons.*

1.3.2.5 Photoelectrochemical proximity assay (PECPA)

Another approach based on ECPA was introduced by the Ju group in 2016, leveraging photoelectric effect. Herein, an Indium tin oxide (ITO) electrode was first layered with TiO_2 quantum dots (QDs), followed by a layer of Cadmium based Ab1-DNA QDs. Following the

addition of detection of Ab (Ab2-DNA), target protein and detector QD forms a proximity complex (**Figure 1.12**) [24, 38], which brings detector QD closer to the ITO surface. This resulted in a sensitized photocurrent which was proportional to the concentration of target protein. Insulin was detected at a LOD of 3.0 fM, with a dynamic range spanning from 10 fM to 10 nM [38]. They demonstrated sensor functionality in complex sample matrices with high selectivity and sensitivity. PECPA benefits from the use of nominal optical components, simple and low-cost electrochemical readout methods making it ideal for adapting the method for POC and PON, and minimal resource settings [24, 38].

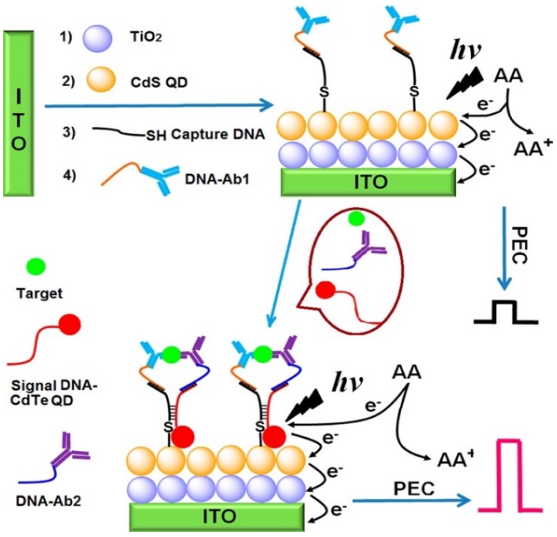

Figure 1.12 An illustration of PECPA. The ITO surface is functionalized with quantum dots(QDs), carrying target recognition units. A second DNA strand having another target recognition unit and QD (as signal transducer) is added. Target-induced hybridization brings signaling QD closer to the surface where a photoelectric current is generated, proportional to the target protein. *Reprinted with permission from reference 38. Copyright 2016, American Chemical Society.*

1.3.3 Drawbacks of assays based on proximity effect

The few examples discussed above demonstrates successful applications of proximity-based sensors as attempts of replacing the gold standard protein sensing technique, ELISA, and its modern, improved counterparts. Although this technique has the advantage of being comparatively rapid, simple mix-and-measure it bears certain disadvantages [24]

(a) Requirement of having two binding sites- The need of two nonoverlapping binding sites on target is a clear limitation to the size of biomarkers that can be detected leveraging this technique. Therefore, although larger protein molecules, viruses and cells will carry more than one binding site for recognition units, proximity effect cannot easily be used to detect smaller biomarkers such as steroids, ions etc.

(b) Limitations in adapting as competitive assays- A key feature of the recognition units used for proximity assays is its strong affinity towards the target molecule. Although lower binding affinity moieties can be used whilst coupled to purification and pre-concentrated steps with the proximity assay, it is cumbersome to displace the bound target molecule, and allow free target to compete with proximity effect. However, optical methods such as fluorescence and photo crosslinking have been used to circumvent this issue [24, 46, 52, 53].

(c) Reduction in signal at high target concentration- An important factor to consider is the ratio of signaling probes to the target detected. As illustrated in **Figure 1.13A**, initially the number of probes compared to analyte is higher, which allows accurate detection of target (region 1). However, as the amount of target increases, probe binding sites will saturate, resulting in a drop signal (region 2). As shown in **Figure 1.13A**, although assay response, "y" is the same, measured concentrations c_1 and c_2 are completely different, which leads to

a doubt regarding the amount of target quantified. However, keeping this in mind, the analyte can be diluted accordingly such that it can be quantified within region 1 [24].

(d) The degree of conjugation (DoC)- Since antibodies are widely available with the improvements to ELISA over time, antibody oligonucleotide conjugates (AbOs) have been the choice over aptamer pairs in proximity assays [34, 45]. Although it is assumed that one antibody is conjugated to a single oligonucleotide, in reality, AbO conjugates carry more than 1 DNA bound, per antibody (DoC=1). The Heyduk group demonstrated that for the commercialized pincer assay kits, best assay performance was obtained for AbO conjugates having 2-4 DNAs, per Ab [34]. Therefore, this oversimplification of AbOs can impede assay performance in terms of sensitivity [24, 34, 45, 54]. **Figure 1.13B** represents the probable configurations of AbOs, which illustrates that, as the DoC per Ab increases, the functional abundance of Ab decreases. In terms of a proximity assay, this can lead to multiple, target independent hybridizations, increasing background complexes, which will in turn converge with the signaling complex, making the assay useless [24, 45]. In a preceding chapter of this dissertation, we have attempted the comparison of multivalent AbOs (DoC>1) and custom synthesized monovalent AbOs (DoC=1), which gives us a glimpse of how assay performance can be improved if AbOs with DoC=1 is used.

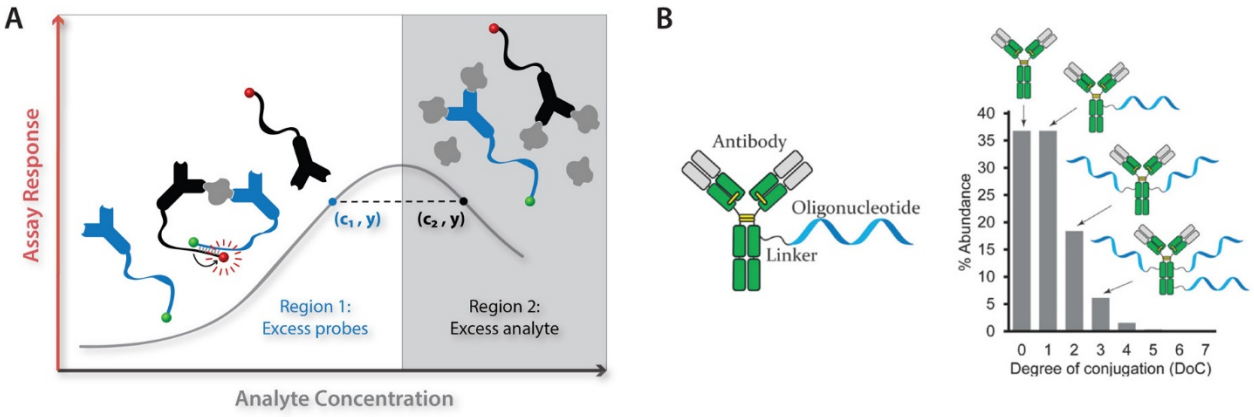

Figure 1.13 Limitations of proximity assay. **(A)** At the beginning, there is higher number of free probes in solution, compared to what is required by the analyte. This allows accurate quantification of analyte. However, as the analyte concentration increases, probe sites will be saturated, leading to a decreased signal output. **(B)** Increasing number of DNA conjugated per antibody leads to decreased abundance (functionality) of AbOs. In an assay developed using such constructs will result in higher background, leading to reduced assay sensitivity. *Reprinted with permission from 24. Copyright 2021, American Chemical Society.*

1.3.4 DNA based assays: DNA scaffolds

DNA based sensors have been developed based on their ability to change conformation or structure in response to a stimuli. Double stranded DNA scaffolds carrying target recognition units respond to external stimuli, which have been leveraged to design sensors. In this section, DNA scaffold-based sensors will be briefly discussed.

There are instances where macromolecules respond to applied electrical charge, if the macromolecule itself carries a charge [55]. Therefore, tethering such macromolecules to surfaces and manipulating their dynamics in the presence of an electrical charge and/or target molecule binding can be leveraged to develop sensors [55-60]. Ulrich Rant and coworkers demonstrated that movement of thiol-modified DNA strands attached to a gold surface can be manipulated by electrical charge and used to develop sensors that are able to detect both DNA and protein targets [55, 59, 61]. To

demonstrate the feasibility of this method, Rant and coworkers used dsDNA and ssDNA strands, of length 24-48 nucleotides (labelled with a fluorophore at distal end) tethered to a gold surface and studied changes in fluorescence in the presence of both a positive and negative applied potential. DNA are negatively charged, hence, application of a positive potential bias to the surface will attract the DNA strands, leading to quenching in fluorescence (**Figure 1.14A**). Application of a negative bias will repel the DNA from the surface which will restore the fluorescence [55]. In their earlier work they showed the importance of fine tuning the system in terms of surface density of immobilized thiols, selected potentials, salt concentrations and frequencies for manipulating dynamics of DNA movement and intrinsic differences of using ds and ssDNA strands to obtain an operatable sensor. It was noted that if a higher packing density of thiol-DNA was present, the steric hindrance and tight/ close orientation of the DNA strands will hamper the motion of DNA strands upon application of respective potentials (**Figure 1.14B**). Tightly packed surfaces will essentially keep the DNA strands upright even at positive applied potentials. When surface coverage was decreased, there was more space for DNA movement with respect to applied potentials [55]. Compared to a dsDNA, a ssDNA of similar length can is considered to be perfectly flexible. Therefore, even in the presence of an applied negative potential, the ssDNA will still remain closer to the gold surface, as opposed to a dsDNA [55, 59, 62]. Based on these criteria, the Rant group use these scaffolds to detect both DNA and protein targets [59, 61]. Leveraging the difference in flexibility of ssDNA and dsDNA, target DNA strands were detected (**Figure 1.14C**). In the absence of target DNA, no significant change in fluorescence was observed, although alternating potentials (negative and positive) were applied. However, addition of target DNA, followed by its hybridization resulted in a more rigid dsDNA which moved predictably in the presence of applied alternating potentials. Also, this system was used to detect mismatches in the target DNA strands,

by analyzing the melting transitions, whilst switching the potential [59]. In a later work the group leveraged this technique for real-time protein detection. A dsDNA tagged with a protein recognition element and a fluorophore at the distal end was used [61]. Protein target attachment slows the movement of shorter dsDNA in presence of alternating potentials, changing the rate of fluorescence modulation. This was leveraged to study the size of proteins (to Angström accuracy), post-translational protein modifications, changes in protein conformation and modifications in protein folding [61].

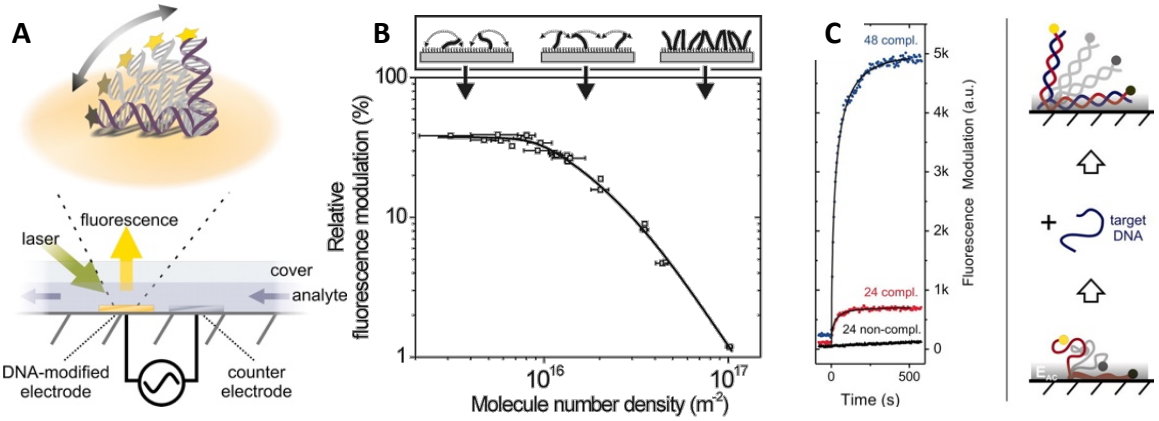

Figure 1.14 Changes in DNA orientation with respect to applied potential, work by Rant and coworkers. **(A)** Application of a potential changes the movement of DNA strand. a positive potential attracts the strand towards the surface and a negative potential pushes it away from the surface. *Reprinted with permission from reference 59. Copyright 2007, National Academy of Sciences, U. S. A.***(B)** Importance of tuning packing density of immobilized DNA on an electrode surface. A high surface density prevents DNA movement. Sufficiently low density promotes DNA movement. *Reprinted with permission from refernce 55. Copyright 2004, American Chemical Society.* **(C)** Left- Addition of target DNA changes fluorescence. Enhanced signal observed for longer complementary sequence. Right- ssDNA is more flexible, hence, their response to potential doesn't change the movement of DNA. dsDNA is more rigid and thus sensitive to changes in alternating potential. *Reprinted with permission from reference 59. Copyright 2007, National Academy of Sciences, U. S. A.*

Based on the work by the Rant group, electrochemical scaffold sensors were developed [56-58, 60, 63-66]. The Plaxco group developed several electrochemical (EC) sensors for protein detection which functioned well even in undiluted blood serum whilst being reagentless, reusable, wash-free and adaptable to microfluidic and multiplexing, demonstrating promise for POC testing [56, 57, 63, 65]. In their earlier work employing EC based DNA (E-DNA) scaffolds, low nM concentrations of anti-digoxigenin antibody and streptavidin were detected. In this sensor, a partially dsDNA was attached to a gold electrode surface through a thiol bond on the proximal end of one of DNA strands of the duplex. The distal ends of both strands of the duplex carried a target recognition unit and a redox tag (methylene blue, MB) (**Figure 1.15A**). In the absence of target, the DNA scaffold approaches the electrode with ease, allowing MB to transfer electrons efficiently, producing a larger Faradaic current. However, target binding reduces the Faradaic current due to lack of electron transfer efficiency owing to the bulk of target suppressing DNA scaffold movement (**Figure 1.15B**). It was also shown that for optimal functioning of the sensor, it is important to tune the length of the DNA strand used for the scaffold, where in this case was 19-nt. This sensor demonstrated functionality in complex matrices such as 50% blood serum [63]. Due to the weight of antibodies (~150 kDa), the decrease in electron transfer of E-DNA scaffold sensors is significant at 50 %.

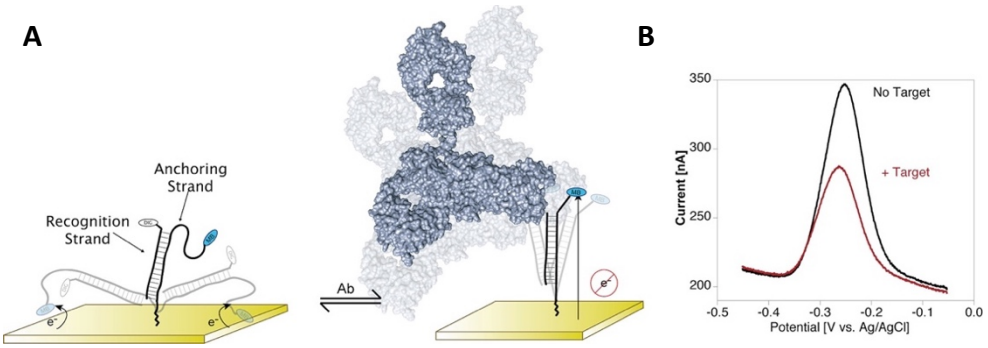

Figure 1.15 E-DNA scaffold sensors by the Plaxco group. **(A)** A dsDNA is attached to the gold surface which carries a MB-tag (anchoring strand) and target recognition unit (recognition strand). In the absence of target antibody, the dsDNA moves faster, allowing efficient electron transfer between the electrode surface and MB. Addition of antibody increases molecular weight of the system, slowing down electron transfer. **(B)** In the absence of antibody, a higher current is generated, whereas in the presence of antibody, generated current is low. *Reprinted with permission from reference 63. Copyright 2009, American Chemical Society.*

In a later work the Plaxco group adapted these sensors to detect a non-antibody, low molecular weight target chemokine IP-10 (~10kDa). Herein, a 21-reisdue polypeptide receptor of the target was used as the recognition element, which was attached to peptide nucleic acid (PNA), hybridized to a MB-DNA (**Figure 1.16**). The sensor functioned as expected giving results in low nM range. Although the limits of detection are above the clinical range (which was attributed to the lower binding affinity of the receptor to target), they were able to demonstrate good selectivity and sensitivity. However, it was successfully shown that E-DNA scaffolds can be used for detecting not only larger targets such as antibodies, but also smaller targets [56].

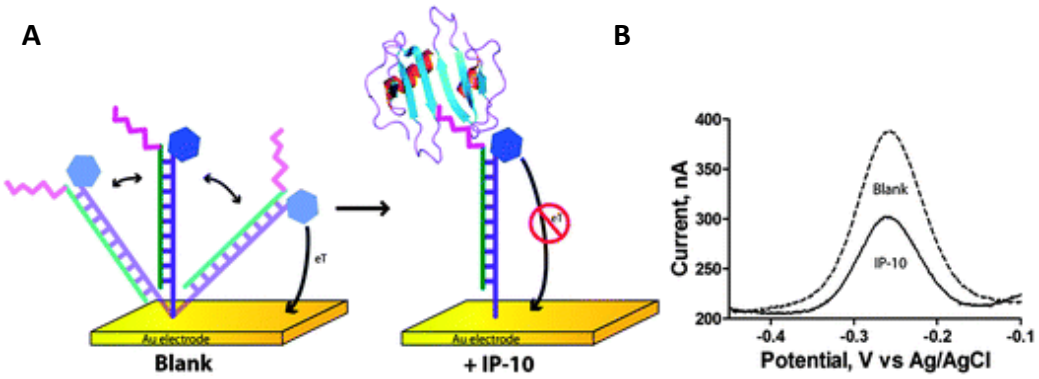

Figure 1.16 An E-DNA scaffold for protein sensing. **(A)** The recognition unit was a PNA molecule. Upon protein addition, DNA scaffold movement was slowed down. **(B)** In the absence of target protein, the higher currents observed, similar to the antibody sensor, whereas in the presence of protein, peak currents were observed to be low. *Reprinted with permission from reference 56. Copyright 2013, Royal Society of Chemistry.*

With the goal of expanding the type of protein targets that can be detected with these sensors, Plaxco and coworkers explored sensor functionality by using target recognition units of various sizes. This gives the opportunity of expanding recognition elements attached to the DNA scaffolds up to full length protein antigens [57, 65]. As size of the recognition unit increases, the change in signal of the DNA scaffold due to target binding will decrease and eventually drop to zero. **Figure 1.17** shows the change in current of a fabricated sensor before attaching the recognition element, after attaching recognition unit and after target binding. This clearly represents that recognition element hinders electron transfer compared to the unmodified sensor [65]. Several target recognition units ranging from 7 to 150 kDa were used and it was found that signal suppression begins to plateau at ~35% (with respect to unmodified sensor), when the weight reaches ~70 kDa. Based on these observations, sensors were developed by tagging full length protein antigens, including conformational epitopes for target sensing [65].

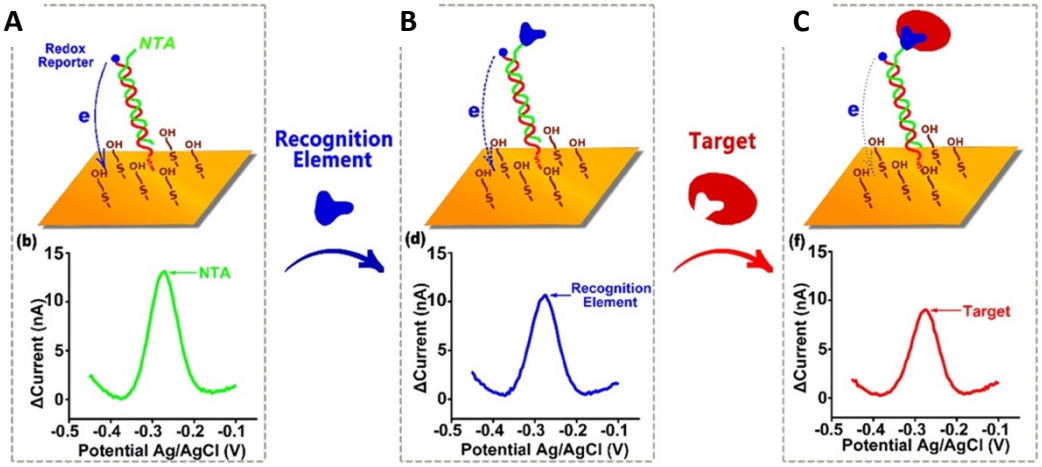

Figure 1.17 Modification of E-DNA scaffold sensors to accommodate target recognition units of different sizes. **(A)** Scaffold in the absence of recognition units has higher currents. **(B)** Addition of target recognition unit slows the electron transfer to an extent, due to the change in weight of scaffold. This gives a lower current compared to (A). **(C)** Addition of target leads to even slower electron transfer, reducing the generated current further. *Reprinted with permission from reference 65. Copyright 2018, American Chemical Society*.

In a more recent work, an antibody responsible for syphilis was detected using an almost full-length antigen as the recognition unit within 10 mins. The groundwork results of this study showed that this E-DNA based sensor was able to differentiate syphilis positive human serum from healthy human serum samples and the sensitivity of the sensor was comparable to the commercially available ELISA used for syphilis detection. The benefit of using an antigen having the folded epitopes in such E-DNA sensors is that, since all patients will not produce antibodies for one specific epitope, antibodies produced by persons for the other epitopes also can be recognized and hence helps in rapid diagnosis of the disease [57].

Inspired by the work on E-DNA scaffold sensors, our group introduced a more generalizable and novel EC sensor known as the **nucleic acid nanostructure,** to quantify of

various classes of targets, using different types of target recognition units for rapid and reagentless drop-and-read sensing [27, 30, 67]. Herein, a single DNA structure carrying a target recognition unit and redox reporter (MB) was enzymatically constructed on the surface of a gold electrode. Upon target binding, a shift in the tethered diffusion of MB results a change in electrochemical signal which can be correlated to the target concentration [27, 30, 67]. **Figure 1.18** below shows the basic principle for protein and small molecule quantification using the nanostructure. With respect to protein quantification, the assembled DNA nanostructure carries a protein recognition unit and MB tag placed close to each other and at fixed distance away from the surface. In the absence of target, the nanostructure has faster tethered diffusion, which then slows down upon target binding due to an increase in total structure mass (**Figure 1.18A**). This drops the MB signal. With respect to small molecule detection, the anchor recognition unit has a pre-bound anchor molecule which slows down the initial tethered diffusion showing decreased current. In the presence of analyte, tethered diffusion is faster since the analyte is now bound to the anchor molecule (**Figure 1.18B**). Sensor functionality was initially demonstrated by detecting streptavidin and anti-digoxigenin (larger proteins) and biotin and digoxigenin (small molecules) [30].

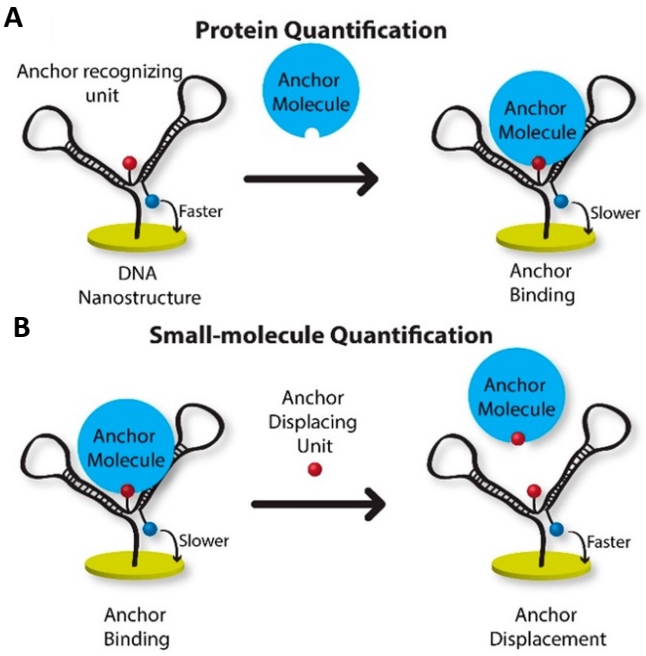

Figure 1.18 Sensing principle of DNA nanostructure. **(A)** Protein quantification using the sensor. Pre-target addition, tethered diffusion of MB is faster, generating higher currents. Post-target addition, a change in molecular weight slows down tethered diffusion leading to lower currents. **(B)** Small-molecule quantification. Protein is already attached to the nanostructure, which shows lower current. Addition of target displaces the bound protein from the nanostructure, generating higher current, due to fast tethered diffusion. Small molecules are quantified indirectly. *Reprinted with permission from reference 30. Copyright 2019, American Chemical Society.*

The DNA nanostructure included three DNA strands- a thiol-DNA binding to gold, a target recognition unit tagged DNA, and redox reporter tagged DNA. Commercial synthesis of a structure carrying three recognition units can be costly and result in a very poor yield. Alternatively, a clever method was used for assembling the DNA nanostructure, where three pieces of DNA strands were ligated enzymatically using T4-DNA ligase (**Figure 1.19**) [27, 30, 67]. The ligase-mediated construction of this structure has two key benefits, (a) low cost and (b) only the target recognition unit (red strand, **Figure 1.19**) has to be changed as a modification for various target detection [27,

[30, 67]. To validate the sensor performance further, an immunosuppressant drug, tacrolimus was detected. The circulation of tacrolimus in blood is usually detected through LC-MS/MS and this sensor was the first EC approach introduced by our group. The sensor performed successfully in both buffer and minimally diluted serum successfully [30]. Recently, the nanostructure was used for peptide quantification, leveraging the indirect method which further extended the applications of developed nanostrcuture. The peptide drug exendin-4 was electrochemically detected at a LOD of 6 nM (**Figure 1.21**) [27]. Furthermore, recently, the sensor platform was used to quantify creatine kinase (CK) and anti-CK antibody with LODs of 14 nM and 5 nM respectively, using a DNA nanostructure that was constructed using the minimized binding epitope of creatine kinase [67].

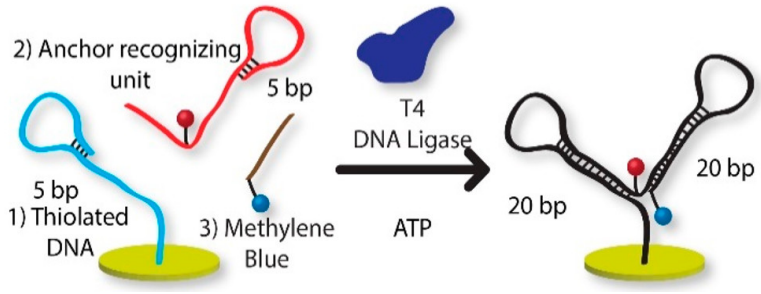

Figure 1.19 Construction of DNA nanostructure. The anchor recognition unit (red strand) and MB-DNA (brown strand) are added on to the electrode immobilized with thiol-DNA (blue strand), followed by ligase addition with cofactor, ATP. The three strands are then fused together, to form a single DNA strand which is 40 bp in length. *Reprinted with permission from reference 30. Copyright 2019, American Chemical Society.*

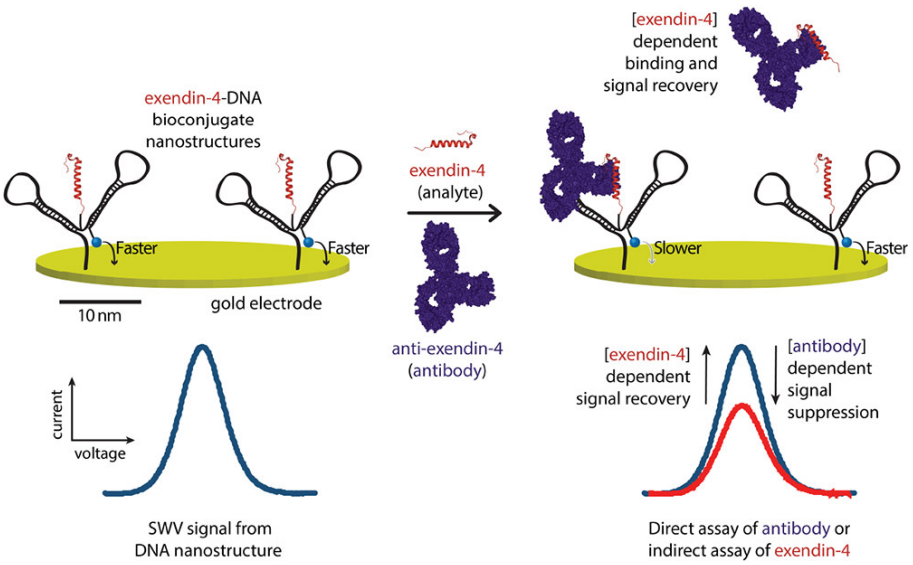

Figure 1.20 Indirect quantification of peptide, Exendin-4 using DNA-nanostructure. A nanostructure was constructed using the peptide as the recognition unit. Addition of antibody, slows down electron transfer, giving lower current. When exendin-4 was added (analyte), the antibody was displaced, which led to increased current. The change in current was proportional to the amount of analyte added. *Reprinted with permission from reference 27. Copyright 2022, American Chemical Society.*

1.4 Summary

As discussed in the preceding sections, it is important to devise methods for simpler and cost-effective assay platforms, avoiding bulkier equipment or complex methods. The work in this dissertation is focused on further improving and extending applicability of DNA-based sensors for more facile detection of target proteins/ analytes using fluorescence and electrochemical readout. **Chapter 2** introduces our attempts of using split aptamers for protein quantification, using fluorescence, more specifically TFA as an assay technique. Herein, more details on the technique of TFA, the advantages and drawbacks of aptamers in target sensing will be discussed, including experimental results. In **chapter 3**, we demonstrate the use of TFA for antibody detection,

leveraging proximity effect. In this chapter, we also point out the importance of probe flexibility and multivalency for multi-DNA-based assays. **Chapter 4** focuses on an electrochemical proximity assay, developed based on our previously introduced ECPA and TFA assay (chapter 3) for antibody detection, where we have again emphasized on probe flexibility for improved assay performance. Common electrochemical techniques used, and the process of electrode fabrication are outlined in this section. In **chapter 5,** we discuss our attempts of developing a gold microelectrode-based sensor for small molecule sensing, leveraging the prior mentioned DNA nanostructure and attempts to integrate it with 3D printed microfluidic devices.

1.5 Reference

(1) Rossetti, M.; Ippodrino, R.; Marini, B.; Palleschi, G.; Porchetta, A. Antibody-Mediated Small Molecule Detection Using Programmable DNA-Switches. *Anal Chem* **2018**, *90* (13), 8196-8201. DOI: 10.1021/acs.analchem.8b01584.
(2) Labib, M.; Sargent, E. H.; Kelley, S. O. Electrochemical methods for the analysis of clinically relevant biomolecules. *Chemical reviews* **2016**, *116* (16), 9001-9090.
(3) Yang, X.; Tang, Y.; Alt, R. R.; Xie, X.; Li, F. Emerging techniques for ultrasensitive protein analysis. *Analyst* **2016**, *141* (12), 3473-3481. DOI: 10.1039/c6an00059b.
(4) Zhang, H.; Li, F.; Dever, B.; Wang, C.; Li, X. F.; Le, X. C. Assembling DNA through affinity binding to achieve ultrasensitive protein detection. *Angew Chem Int Ed Engl* **2013**, *52* (41), 10698-10705. DOI: 10.1002/anie.201210022.
(5) Gstaiger, M.; Aebersold, R. Applying mass spectrometry-based proteomics to genetics, genomics and network biology. *Nature Reviews Genetics* **2009**, *10* (9), 617-627.
(6) Yates, J. R.; Ruse, C. I.; Nakorchevsky, A. Proteomics by mass spectrometry: approaches, advances, and applications. *Annual review of biomedical engineering* **2009**, *11* (1), 49-79.
(7) Janssen, K. P.; Knez, K.; Spasic, D.; Lammertyn, J. Nucleic acids for ultra-sensitive protein detection. *Sensors (Basel)* **2013**, *13* (1), 1353-1384. DOI: 10.3390/s130101353.
(8) Porchetta, A.; Ippodrino, R.; Marini, B.; Caruso, A.; Caccuri, F.; Ricci, F. Programmable Nucleic Acid Nanoswitches for the Rapid, Single-Step Detection of Antibodies in Bodily Fluids. *J Am Chem Soc* **2018**, *140* (3), 947-953. DOI: 10.1021/jacs.7b09347.
(9) MyBiosource. *Who invented ELISA?* MyBiosource.com, https://www.mybiosource.com/learn/ELISA (accessed 26th january 2023).
(10) Zhang, S.; Garcia-D'Angeli, A.; Brennan, J. P.; Huo, Q. Predicting detection limits of enzyme-linked immunosorbent assay (ELISA) and bioanalytical techniques in general. *Analyst* **2014**, *139* (2), 439-445.
(11) Van Weemen, B.; Schuurs, A. Immunoassay using antigen—enzyme conjugates. *FEBS letters* **1971**, *15* (3), 232-236.

(12) ThermoFisher Scientific. *Overview of ELISA*. ThermoFisher Scientific, https://www.thermofisher.com/us/en/home/life-science/protein-biology/protein-biology-learning-center/protein-biology-resource-library/pierce-protein-methods/overview-elisa.html (accessed 26 January 2023).
(13) Rissin, D. M.; Kan, C. W.; Campbell, T. G.; Howes, S. C.; Fournier, D. R.; Song, L.; Piech, T.; Patel, P. P.; Chang, L.; Rivnak, A. J. Single-molecule enzyme-linked immunosorbent assay detects serum proteins at subfemtomolar concentrations. *Nature biotechnology* **2010**, *28* (6), 595-599.
(14) Quanterix. *Simoa Technology*. https://www.quanterix.com/simoa-technology/ (accessed 26 January 2023).
(15) Beaudet, L.; Rodriguez-Suarez, R.; Venne, M.-H.; Caron, M.; Bédard, J.; Brechler, V.; Parent, S.; Bielefeld-Sévigny, M. AlphaLISA immunoassays: the no-wash alternative to ELISAs for research and drug discovery. *Nature Methods* **2008**, *5* (12), an8-an9.
(16) Ullman, E. F.; Kirakossian, H.; Switchenko, A.; Ishkanian, J.; Ericson, M.; Wartchow, C.; Pirio, M.; Pease, J.; Irvin, B.; Singh, S. Luminescent oxygen channeling assay (LOCI): sensitive, broadly applicable homogeneous immunoassay method. *Clinical chemistry* **1996**, *42* (9), 1518-1526.
(17) Zhao, H.; Lin, G.; Liu, T.; Liang, J.; Ren, Z.; Liang, R.; Chen, B.; Huang, W.; Wu, Y. Rapid quantitation of human epididymis protein 4 in human serum by amplified luminescent proximity homogeneous immunoassay (AlphaLISA). *Journal of Immunological Methods* **2016**, *437*, 64-69.
(18) Ullman, E. F.; Kirakossian, H.; Singh, S.; Wu, Z. P.; Irvin, B. R.; Pease, J. S.; Switchenko, A. C.; Irvine, J. D.; Dafforn, A.; Skold, C. N. Luminescent oxygen channeling immunoassay: measurement of particle binding kinetics by chemiluminescence. *Proceedings of the National Academy of Sciences* **1994**, *91* (12), 5426-5430.
(19) Hu, J.; Easley, C. J. Homogeneous Assays of Second Messenger Signaling and Hormone Secretion Using Thermofluorimetric Methods That Minimize Calibration Burden. *Anal Chem* **2017**, *89* (16), 8517-8523. DOI: 10.1021/acs.analchem.7b02229.
(20) Hu, J.; Wang, T.; Kim, J.; Shannon, C.; Easley, C. J. Quantitation of femtomolar protein levels via direct readout with the electrochemical proximity assay. *J Am Chem Soc* **2012**, *134* (16), 7066-7072. DOI: 10.1021/ja3000485 From NLM Medline.
(21) Harroun, S. G.; Prévost-Tremblay, C.; Lauzon, D.; Desrosiers, A.; Wang, X.; Pedro, L.; Vallée-Bélisle, A. Programmable DNA switches and their applications. *Nanoscale* **2018**, *10* (10), 4607-4641.
(22) Ranallo, S.; Rossetti, M.; Plaxco, K. W.; Vallee-Belisle, A.; Ricci, F. A Modular, DNA-Based Beacon for Single-Step Fluorescence Detection of Antibodies and Other Proteins. *Angew Chem Int Ed Engl* **2015**, *54* (45), 13214-13218. DOI: 10.1002/anie.201505179.
(23) Ranallo, S.; Sorrentino, D.; Ricci, F. Orthogonal regulation of DNA nanostructure self-assembly and disassembly using antibodies. *Nat Commun* **2019**, *10* (1), 5509. DOI: 10.1038/s41467-019-13104-6.
(24) Bezerra, A. B.; Kurian, A. S. N.; Easley, C. J. Nucleic-Acid Driven Cooperative Bioassays Using Probe Proximity or Split-Probe Techniques. *Anal Chem* **2021**, *93* (1), 198-214. DOI: 10.1021/acs.analchem.0c04364 From NLM Medline.
(25) Hu, J.; Yu, Y.; Brooks, J. C.; Godwin, L. A.; Somasundaram, S.; Torabinejad, F.; Kim, J.; Shannon, C.; Easley, C. J. A reusable electrochemical proximity assay for highly selective, real-time protein quantitation in biological matrices. *J Am Chem Soc* **2014**, *136* (23), 8467-8474. DOI: 10.1021/ja503679q From NLM Medline.

(26) Hu, J.; Kim, J.; Easley, C. J. Quantifying Aptamer-Protein Binding via Thermofluorimetric Analysis. *Anal Methods* **2015**, *7* (17), 7358-7362. DOI: 10.1039/c5ay00837a.
(27) Khuda, N.; Somasundaram, S.; Easley, C. J. Electrochemical Sensing of the Peptide Drug Exendin-4 Using a Versatile Nucleic Acid Nanostructure. *ACS Sensors* **2022**, *7* (3), 784-789. DOI: 10.1021/acssensors.1c02336.
(28) Li, F.; Lin, Y.; Lau, A.; Tang, Y.; Chen, J.; Le, X. C. Binding-Induced Molecular Amplifier as a Universal Detection Platform for Biomolecules and Biomolecular Interaction. *Anal Chem* **2018**, *90* (14), 8651-8657. DOI: 10.1021/acs.analchem.8b01985.
(29) Mahshid, S. S.; Camire, S.; Ricci, F.; Vallee-Belisle, A. A Highly Selective Electrochemical DNA-Based Sensor That Employs Steric Hindrance Effects to Detect Proteins Directly in Whole Blood. *J Am Chem Soc* **2015**, *137* (50), 15596-15599. DOI: 10.1021/jacs.5b04942.
(30) Somasundaram, S.; Easley, C. J. A Nucleic Acid Nanostructure Built through On-Electrode Ligation for Electrochemical Detection of a Broad Range of Analytes. *J Am Chem Soc* **2019**, *141* (29), 11721-11726. DOI: 10.1021/jacs.9b06229.
(31) Yang, X.; Tang, Y.; Mason, S. D.; Chen, J.; Li, F. Enzyme-Powered Three-Dimensional DNA Nanomachine for DNA Walking, Payload Release, and Biosensing. *ACS Nano* **2016**, *10* (2), 2324-2330. DOI: 10.1021/acsnano.5b07102.
(32) Zhang, H.; Lai, M.; Zuehlke, A.; Peng, H.; Li, X. F.; Le, X. C. Binding-Induced DNA Nanomachines Triggered by Proteins and Nucleic Acids. *Angew Chem Int Ed Engl* **2015**, *54* (48), 14326-14330. DOI: 10.1002/anie.201506312.
(33) Ranallo, S.; Prevost-Tremblay, C.; Idili, A.; Vallee-Belisle, A.; Ricci, F. Antibody-powered nucleic acid release using a DNA-based nanomachine. *Nat Commun* **2017**, *8*, 15150. DOI: 10.1038/ncomms15150.
(34) Heyduk, E.; Dummit, B.; Chang, Y.-H.; Heyduk, T. Molecular pincers: antibody-based homogeneous protein sensors. *Analytical chemistry* **2008**, *80* (13), 5152-5159.
(35) Morris, F. D.; Peterson, E. M.; Heemstra, J. M.; Harris, J. M. Single-molecule kinetic investigation of cocaine-dependent split-aptamer assembly. *Analytical chemistry* **2018**, *90* (21), 12964-12970.
(36) Stojanovic, M. N.; de Prada, P.; Landry, D. W. Fluorescent sensors based on aptamer self-assembly. *Journal of the American Chemical Society* **2000**, *122* (46), 11547-11548.
(37) Joonyul Kim, J. H., Rebecca S. Sollie and Christopher J. Easley. Improvement of Sensitivity and dynamic range in proximity ligation assays by assymetric connector hybridization. *ACS analytical chemistry* **2010**, *82* (16), 6976-6982.
(38) Wen, G.; Ju, H. Enhanced Photoelectrochemical Proximity Assay for Highly Selective Protein Detection in Biological Matrixes. *Anal Chem* **2016**, *88* (16), 8339-8345. DOI: 10.1021/acs.analchem.6b02740.
(39) Yang, K.; Huo, M.; Guo, Y.; Yang, Y.; Wu, J.; Ding, L.; Ju, H. Target-induced cyclic DNAzyme formation for colorimetric and chemiluminescence imaging assay of protein biomarkers. *Analyst* **2017**, *142* (19), 3740-3746. DOI: 10.1039/c7an00413c.
(40) Lass-Napiorkowska, A.; Heyduk, E.; Tian, L.; Heyduk, T. Detection methodology based on target molecule-induced sequence-specific binding to a single-stranded oligonucleotide. *Analytical chemistry* **2012**, *84* (7), 3382-3389.
(41) Tian, L.; Heyduk, T. Antigen peptide-based immunosensors for rapid detection of antibodies and antigens. *Analytical chemistry* **2009**, *81* (13), 5218-5225.

(42) Fredriksson, S.; Gullberg, M.; Jarvius, J.; Olsson, C.; Pietras, K.; Gústafsdóttir, S. M.; Östman, A.; Landegren, U. Protein detection using proximity-dependent DNA ligation assays. *Nature biotechnology* **2002**, *20* (5), 473-477.
(43) Gustafsdottir, S. M.; Schallmeiner, E.; Fredriksson, S.; Gullberg, M.; Soderberg, O.; Jarvius, M.; Jarvius, J.; Howell, M.; Landegren, U. Proximity ligation assays for sensitive and specific protein analyses. *Anal Biochem* **2005**, *345* (1), 2-9. DOI: 10.1016/j.ab.2005.01.018.
(44) Gullberg, M.; Gustafsdottir, S. M.; Schallmeiner, E.; Jarvius, J.; Bjarnegard, M.; Betsholtz, C.; Landegren, U.; Fredriksson, S. Cytokine detection by antibody-based proximity ligation. *Proc Natl Acad Sci U S A* **2004**, *101* (22), 8420-8424. DOI: 10.1073/pnas.0400552101.
(45) Dovgan, I.; Koniev, O.; Kolodych, S.; Wagner, A. Antibody–oligonucleotide conjugates as therapeutic, imaging, and detection agents. *Bioconjugate Chemistry* **2019**, *30* (10), 2483-2501.
(46) Lundberg, M.; Eriksson, A.; Tran, B.; Assarsson, E.; Fredriksson, S. Homogeneous antibody-based proximity extension assays provide sensitive and specific detection of low-abundant proteins in human blood. *Nucleic Acids Res* **2011**, *39* (15), e102. DOI: 10.1093/nar/gkr424.
(47) Assarsson, E.; Lundberg, M.; Holmquist, G.; Björkesten, J.; Bucht Thorsen, S.; Ekman, D.; Eriksson, A.; Rennel Dickens, E.; Ohlsson, S.; Edfeldt, G. Homogenous 96-plex PEA immunoassay exhibiting high sensitivity, specificity, and excellent scalability. *PloS one* **2014**, *9* (4), e95192.
(48) Heyduk, E.; Moxley, M. M.; Salvatori, A.; Corbett, J. A.; Heyduk, T. Homogeneous insulin and C-Peptide sensors for rapid assessment of insulin and C-peptide secretion by the islets. *Diabetes* **2010**, *59* (10), 2360-2365. DOI: 10.2337/db10-0088.
(49) Tian, L.; Heyduk, T. Bivalent ligands with long nanometer-scale flexible linkers. *Biochemistry* **2009**, *48* (2), 264-275.
(50) Ren, K.; Wu, J.; Yan, F.; Ju, H. Ratiometric electrochemical proximity assay for sensitive one-step protein detection. *Scientific reports* **2014**, *4* (1), 1-6.
(51) Rossetti, M.; Brannetti, S.; Mocenigo, M.; Marini, B.; Ippodrino, R.; Porchetta, A. Harnessing effective molarity to design an electrochemical dna-based platform for clinically relevant antibody detection. *Angewandte Chemie* **2020**, *132* (35), 15083-15088.
(52) Huang, Y.; Zheng, W.; Li, X. Detection of protein targets with a single binding epitope using DNA-templated photo-crosslinking and strand displacement. *Analytical biochemistry* **2018**, *545*, 84-90.
(53) Xu, L.; Zhang, H.; Yan, X.; Peng, H.; Wang, Z.; Zhang, Q.; Li, P.; Zhang, Z.; Le, X. C. Binding-induced DNA dissociation assay for small molecules: Sensing aflatoxin B1. *ACS sensors* **2018**, *3* (12), 2590-2596.
(54) Kim, J.; Hu, J.; Bezerra, A. B.; Holtan, M. D.; Brooks, J. C.; Easley, C. J. Protein quantification using controlled DNA melting transitions in bivalent probe assemblies. *Anal Chem* **2015**, *87* (19), 9576-9579. DOI: 10.1021/acs.analchem.5b03432.
(55) Rant, U.; Arinaga, K.; Fujita, S.; Yokoyama, N.; Abstreiter, G.; Tornow, M. Dynamic electrical switching of DNA layers on a metal surface. *Nano Letters* **2004**, *4* (12), 2441-2445.
(56) Bonham, A. J.; Paden, N. G.; Ricci, F.; Plaxco, K. W. Detection of IP-10 protein marker in undiluted blood serum via an electrochemical E-DNA scaffold sensor. *Analyst* **2013**, *138* (19), 5580-5583.
(57) Ogden, N. E.; Kurnik, M.; Parolo, C.; Plaxco, K. W. An electrochemical scaffold sensor for rapid syphilis diagnosis. *Analyst* **2019**, *144* (17), 5277-5283. DOI: 10.1039/c9an00455f From NLM Medline.

(58) Parolo, C.; Greenwood, A. S.; Ogden, N. E.; Kang, D.; Hawes, C.; Ortega, G.; Arroyo-Currás, N.; Plaxco, K. W. E-DNA scaffold sensors and the reagentless, single-step, measurement of HIV-diagnostic antibodies in human serum. *Microsystems & nanoengineering* **2020**, *6* (1), 1-8.
(59) Rant, U.; Arinaga, K.; Scherer, S.; Pringsheim, E.; Fujita, S.; Yokoyama, N.; Tornow, M.; Abstreiter, G. Switchable DNA interfaces for the highly sensitive detection of label-free DNA targets. *Proceedings of the National Academy of Sciences* **2007**, *104* (44), 17364-17369.
(60) White, R. J.; Plaxco, K. W. Exploiting binding-induced changes in probe flexibility for the optimization of electrochemical biosensors. *Analytical chemistry* **2010**, *82* (1), 73-76.
(61) Langer, A.; Hampel, P. A.; Kaiser, W.; Knezevic, J.; Welte, T.; Villa, V.; Maruyama, M.; Svejda, M.; Jähner, S.; Fischer, F. Protein analysis by time-resolved measurements with an electro-switchable DNA chip. *Nature Communications* **2013**, *4* (1), 1-8.
(62) Kaiser, W.; Rant, U. Conformations of end-tethered DNA molecules on gold surfaces: influences of applied electric potential, electrolyte screening, and temperature. *Journal of the American Chemical Society* **2010**, *132* (23), 7935-7945.
(63) Cash, K. J.; Ricci, F.; Plaxco, K. W. An electrochemical sensor for the detection of protein−small molecule interactions directly in serum and other complex matrices. *Journal of the American Chemical Society* **2009**, *131* (20), 6955-6957.
(64) Das, J.; Gomis, S.; Chen, J. B.; Yousefi, H.; Ahmed, S.; Mahmud, A.; Zhou, W.; Sargent, E. H.; Kelley, S. O. Reagentless biomolecular analysis using a molecular pendulum. *Nature chemistry* **2021**, *13* (5), 428-434.
(65) Kang, D.; Parolo, C.; Sun, S.; Ogden, N. E.; Dahlquist, F. W.; Plaxco, K. W. Expanding the Scope of Protein-Detecting Electrochemical DNA "Scaffold" Sensors. *ACS Sens* **2018**, *3* (7), 1271-1275. DOI: 10.1021/acssensors.8b00311.
(66) Yousefi, H.; Mahmud, A.; Chang, D.; Das, J.; Gomis, S.; Chen, J. B.; Wang, H.; Been, T.; Yip, L.; Coomes, E. Detection of SARS-CoV-2 viral particles using direct, reagent-free electrochemical sensing. *Journal of the American Chemical Society* **2021**, *143* (4), 1722-1727.
(67) Gurukandure, A.; Somasundaram, S.; Kurian, A. S.; Khuda, N.; Easley, C. J. Building a nucleic acid nanostructure with DNA-epitope conjugates for a versatile electrochemical protein detection platform. **2023**.

Chapter 2

Use of Split Broccoli Aptamer for Protein Sensing Using Thermofluorimetric Analysis (TFA)

2.1 Background

In this chapter, we use cooperative sensing towards developing an assay for protein detection through the assembly of a split green fluorescent protein (GFP) mimicking aptamer, "broccoli". We have employed thermofluorimetric analysis (TFA) as the detection method. In this section, a brief introduction of aptamers, GFP mimics, and TFA will be given.

2.1.1 Aptamers

As discussed in chapter 1, the concept of proximity effect has been explored widely in developing new means of biosensing. Several types of components are being used as target recognition units, such as antibodies, PNAs, peptides, small molecules, and aptamers in cooperative sensing. Although with the advancement in sandwich ELISA, technologies used to isolating antibodies have evolved over the decades, there is still an interest towards exploring more promising alternatives as target recognition elements having single target binding affinity [1]. Aptamers, a class of synthetic oligonucleotides (DNA and RNA) of 15-60 nt in length have gained the attention of researchers as such target recognition units, due to their unique capabilities of switching structure upon target binding and controlled synthesis [1-3]. These structures are developed by a process known as SELEX (systemic evolution of ligands by exponential enrichment), where several rounds of mutation, multiplication, selection and purification selects the best DNA/ RNA strands that bind to a particular target [2, 4, 5]. Aptamers have been developed to bind a wide range of targets from small molecules, metal ions, proteins and even cells [2, 3, 6-11]. These oligonucleotide

constructs offer several advantages over antibodies, which include flexibility in modification, long-term stability, ease of synthesis, and cost effectiveness. [2, 11-14]

The foundation of employing aptamers in assay development is its capability of undergoing a change in conformation to form a secondary or tertiary structure upon target binding [1, 2, 9, 15]. In its conformation, aptamers often carry stems and loops, which play a crucial role in forming the target binding site and stabilizing its secondary and/ or tertiary conformation [2, 14, 15]. Therefore, these conformation changes are effectively transferred into signal readouts allowing protein quantification. The most popular and preferred method of detection is fluorescence, due to the high sensitivity, specificity, ease of handling, and multiplexing capabilities. Many structure-switching aptamer-based assays are developed based on the "molecular beacon" where aptamers are labelled with FRET pairs. A change in conformation upon target binding will result in either quenching/ emitting fluorescence or increasing/ decreasing fluorescence of a dye [2, 15-18] (**Figure 2.1C**). Electrochemical approaches are also often used to quantify target analytes, which result in electrochemical aptamer-based (E-AB) sensors. Herein, the aptamer is labelled with a redox tag such as methylene blue, which upon target binding will either increase or decrease the rate of electron transfer between the redox moiety and electrode surface [19-23] (**Figure 2.1A**). Colorimetric techniques are used with standard absorbance instruments to quantify targets leveraging aptamers (**Figure 2.1B**). Although the sensitivity of colorimetric readouts are poorer than fluorescent and electrochemical techniques, these have proven to be useful in situations where point-of-care and resource poor settings are concerned, since it allows for simple handling and ability to detect color changes through the naked eye. Colorimetric detection often involves the use of nanoparticles and DNAzymes [2, 11, 24-27].

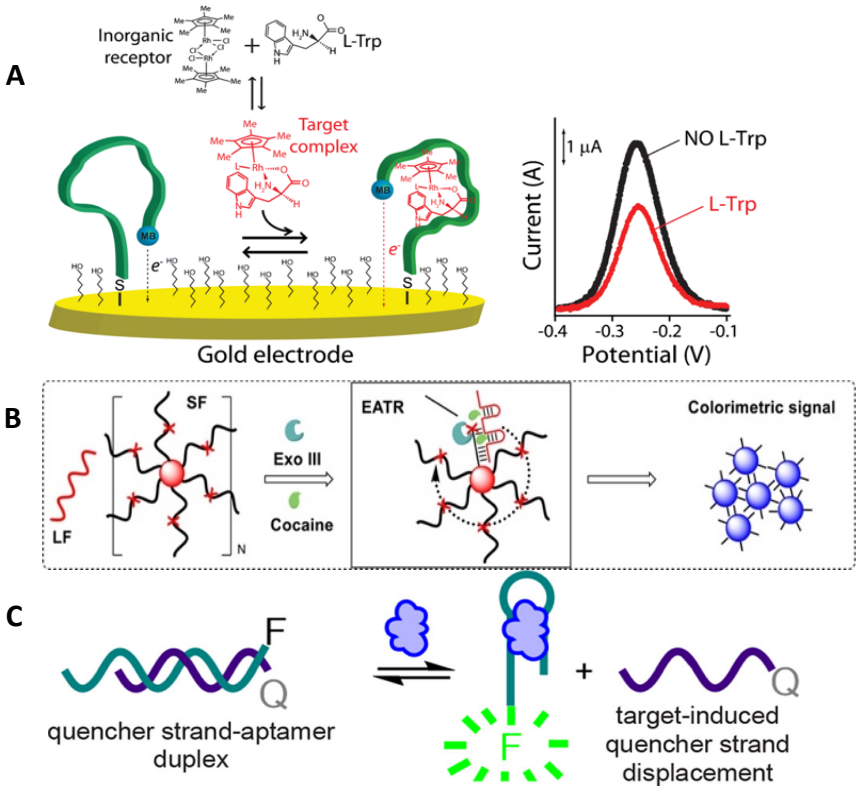

Figure 2.1 Examples of aptamer-based sensors. (A) An E-AB sensor. An aptamer modified with a thiol at the proximal end and MB at the distal end is attached to the electrode surface. In the absence of target, a higher electrochemical (EC) signal is generated. Target binding to the aptamer stabilizes the structure, generating reduced EC signal. *Reprinted with permission from reference 21. Copyright 2019, Springer Nature.* **(B)** A split aptamer sensor levering colourimetry. Aptamers are immobilized on gold nanoparticles (AuNP). In the absence of target, AuNP shows one colour, where in the presence of target, AuNP aggregates to show a different colour. *Reprinted with permission from reference 11. Copyright 2018, American Chemical Society*. **(C)** A fluorescence-based aptasensor, where initially fluorescence is quenched. Target addition changes the binding conformation of aptamer, to restore fluorescence. *Reprinted with permission from reference 1. Copyright 2018, American Chemical Society.*

2.1.2 Split Aptamers

Although structure switching aptamers have benefits, they also bear several drawbacks, impeding their extensive use in assay and biosensor development. First, many aptamers do not switch structure upon binding. They often have longer oligonucleotide strands, which leads to inefficient folding and refolding of the aptamers upon target binding and release. Likewise, it is still challenging to accurately determine the extent of folding upon target binding and also control the extent to which analyte dependent folding occurs [2, 28]. Therefore, the use of full-length aptamers in sensor development can lead to high background noise and false positives [2, 5, 28]. However, most of these drawbacks can be addressed by using split aptamer constructs.

An ingenious way of using split aptamers is to leverage the proximity effect. When an aptamer is split into sections, the cooperative binding of target can result in joining the splits, where target dependent reassembly is converted to a signal readout. Stojanovic et al. was the first to demonstrate approaches of splitting cocaine and ATP binding aptamers, showing their successful reassembly, to emit a FRET signal [2, 15]. Morris et al. demonstrated that the equilibrium upon binding of analyte results in stabilizing the aptamer and reduces its chance of dissociation [2, 5]. When the parent aptamer is split into two or more fragments, its structure is inherently destabilized. Therefore, to develop split aptamer-based assays, it is important to make sure that analyte binding pockets are not affected. In order to attain better sensitivity and specificity, parent aptamers are generally modified to have more shorter sequences, by truncating at the stems and loops which have minimal structural functionality [2, 14, 15, 29]. The splits resulting from these structures usually remain in equilibrium with the associated aptamer and target addition will form a 3-part, aptamer-target-aptamer complex [2]. Some advantages of using split aptamers in sensors include low background since assembly is highly dependent on target analyte and the incapability of forming

secondary structures in the absence of target reduces background. Also, aptamers have demonstrated a low rate of adsorption on to the surface, making it an ideal candidate for surface based assays [2, 4, 11, 30].

However, although split aptamers own certain advantages, they also possess certain disadvantages. Due to modifications and splitting a parent aptamer into fragments, its binding affinity towards a target reduces. The formed aptamer-target-aptamer sandwich complex reduces the entropy of the system, lowering the equilibrium stability. Although, this can be minimized by increasing fragment length of splits to improve stability and coupling with amplification methods for enhanced signal output, the thermal stability of longer split fragments will lead to target independent assembly of splits. This in return will increase background and reduce assay sensitivity [2, 28, 30, 31].

2.1.3 Green fluorescent protein (GFP) mimicking aptamers

Akin to the proximity effect, fluorescent proteins such as GFP, yellow Venus, mCherry and cyan can be split into two segments, and reassembled to establish fluorescence in the presence of a target. This is referred to as split protein complementation assay (PCA). PCAs have been developed for enzymes, where reassembly results in the downstream amplification of a signal of interest [2, 32-34]. Comparable to split protein assays, oligonucleotide split aptamer analogs leveraging fluorescence have been developed. Fluorescent proteins have greatly influenced the understanding of interactions, regulation and tracking of proteins within cells. Similarly, it is important to understand the function and regulation of RNAs within cells, which has been challenging to achieve [2, 35]. To improve the understanding of the role of RNA in cells, the Jaffrey group developed a series of fluorescent RNA aptamers through SELEX, which bound to the fluorophore resembled

in GFPs [2, 35-37]. The fluorophore in GFPs is 4-hydroxybenzilidene imidazolinone (HBI), which emits green fluorescence when enclosed within the protein. The group first developed the spinach aptamer (**Figure 2.2B, left**), for a modified synthetic form of HBI, 3,5-difluoro-4-hydroxybenzylidene imidazolinone (DFHBI) (**Figure 2.2A**). In absence of the aptamer, DFHBI was nonfluorescent in free solution. However, upon binding to spinach, the dye emitted fluorescence. The synthesized dye exhibited no cytotoxic effects and emitted low background fluorescence when introduced to cells. Spinach was fused to other RNAs through one of the stem-loop structures and used to successfully to image within cells [35]. Aptamers of thrombin, adenosine, SAM, guanosine, and GTP [35, 38]. **Figure 2.2C** represents the sensing principle of fusing aptamers with spinach.

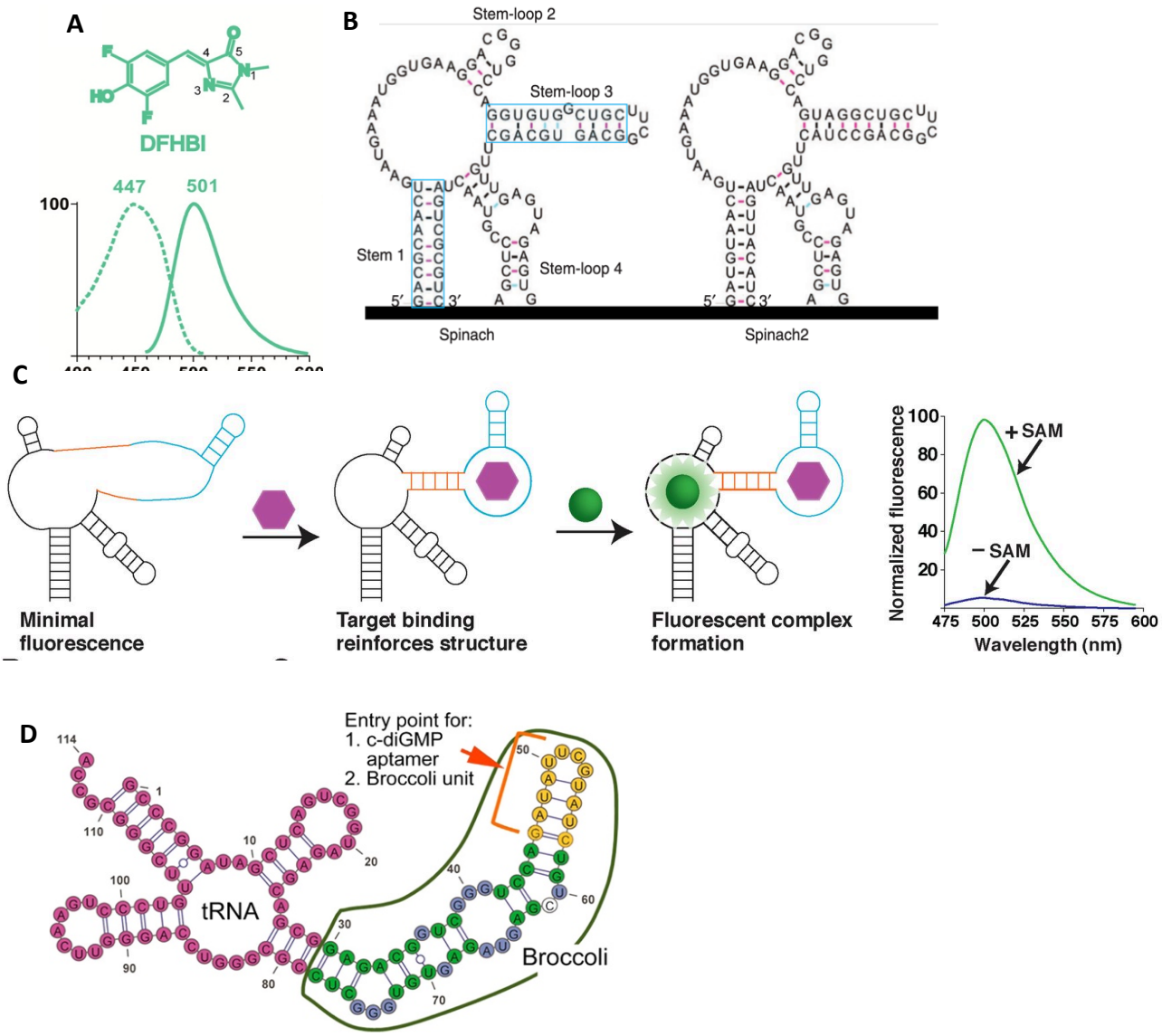

Figure 2.2 Spinach and its variants. **(A)** The synthetic fluorophore DFHBI, analogous to HBI, the fluorophore found in green fluorescent protein. *Reprinted with permission from reference 39.Copyright2014,AmericanChemicalSociety* (https://pubs.acs.org/doi/full/10.1021/ja410819x)*.**(B)** Left-Spinach aptamer. Right- Spinach2, a modified version of spinach aptamer, where the stem-loop 3 and stem 1 were modified slightly. *Reprinted with permission from reference 37. Copyright 2013, Springer Nature.* **(C)** Fusing spinach aptamer to other aptamers for analyte sensing. Left- Black represents the spinach aptamer, attached to another aptamer of interest (orange and blue). Improper folding of spinach the absence

of target. Target binding to the recognition aptamer induces proper folding of spinach, leading to fluoresce DFHBI, as the fluorophore binding pocket is formed properly. Right- Fluorescence signals of DFHBI in the presence and absence of target molecule. *Reprinted with permission from reference 122. Copyright 2012, Science*. **(D)** The broccoli aptamer. A 49-nt aptamer, which is less Mg^{2+} dependent and RNase resistant compared to the first-generation spinach aptamer. *Reprinted with permission from reference 36. Copyright 2014, American Chemical Society* (https://pubs.acs.org/doi/full/10.1021/ja508478x)*

**Any further permissions related to cited articles must be directed to ACS*

Although spinach aptamer demonstrated some success in cellular imaging, when appended to other aptamer constructs, the DFHBI-spinach complex gave low signals due to poor thermal stability and misfolding within cells. Therefore, the Jaffrey group developed a more stable and brighter spinach aptamer, spinach2 (**Figure 2.2B, right**) [37]. Due to the versatility of spinach in cellular imaging, the goal of Jaffrey group was focused on improving the brightness of these GFP-mimicking aptamers. After the development of spinach2, a much shorter version of spinach was evolved, known as broccoli. Broccoli aptamer was 49-nt in length as opposed to the much longer parent aptamer spinach (~94-nt). Compared to spinach2, broccoli exhibited improved folding, much brighter fluorescence, low magnesium ion dependance for folding and stability within cells [36]. Within cells, RNAs are suffer degradation by RNases. Therefore, spinach and its earlier variants required a tRNA scaffold to be fused so that are being targeted by the RNases and degraded [2]. However, broccoli was found to be more stable within cells, even without the need of appending additional tRNA scaffold (**Figure 2.2D).**

Owing to the success of GFP mimicking aptamers, these have also been split into fragments and used to develop assays based on proximity effect. Rogers et al. demonstrated that the full-length spinach aptamer can be split into two segments and reconstituted to turn on fluorescence of DFHBI. Herein, the splits were hybridized to a DNA blocker, which prevented the annealing of

split aptamer fragments. However, in the presence of target DNA strand, the blocker DNA was displaced via toehold mediated strand displacement allowing the split aptamer strands to recombine and fluoresce DFHBI [2, 40]. Kikuchi et al. also demonstrated proximity-based split spinach recombination by modifying each split to carry a DNA strand that recognized a particular target DNA. In the presence of target DNA, recognition DNA annealing leads to bringing the split aptamers to close proximity. In the presence of DFHBI, the fluorophore binding pocket is formed and turns on its fluorescence [2, 41, 42]. Ricci and coworkers leveraged split spinach reassembly to quantify antibodies. Herein, each split was tagged with an antibody recognizing small molecule. In the absence of target antibody, the splits would not reassemble and thus DFHBI did not fluoresce. However, in the presence of target, the recognition element binding brings the two splits closer to result in turning on the fluorescence of DFHBI [43]. Alam et.al demonstrated the first ever split broccoli reassembly *in vivo*. Here, the aptamer was split into two segments and were brought together and stabilized through a 3-way junction RNA construct. They showed that this split broccoli reassembly resulted in a digital output and was able to maintain performance, even when it was fused with other RNA constructs to result in a stand-alone AND gate construct, *in vivo* [44]. Wang et al. also demonstrated that split broccoli aptamers could be used for *in vivo* cell imaging. Here, the aptamer was split at its loop and each split was modified to carry a segment of target mRNA recognizing unit, which was then encoded within cells. In the presence of target mRNA, broccoli splits will be brought closer, turning on the fluorescence of DFHBI. This system was successfully used to monitor mRNA within cells in real time [45].

Inspired by GFP mimicking split aptamers for analyte sensing, we attempted to develop an in vitro assay for protein detection using split broccoli aptamer and leveraging thermofluorimetric

analysis (TFA) as the signal readout method which has thus far not been used in this manner. The following section describes the basic principle of TFA.

2.1.4 Thermofluorometric analysis (TFA)

A prerequisite for proximity complex bound to the target is that it should be stable enough to be measurable over the background complex. As mentioned in chapter 1, the interaction of DNA with the target results in an increase in melting temperature of the proximity complex, rendering a much higher value, compared to the target-independent DNA hybridization event. Although most proximity assays have developed to be isothermal assays, it is important that at assay temperature the background is either fully or partially destabilized, whilst the signaling complexes are clearly detectable. Though assay performance at room temperature can be fine-tuned by optimizing the concentration of signaling probes and probe to analyte ratios, temperature dependance of the system in presence and absence can also assist in evaluating optimized assay performance, as it will be an indicator of the complexes' entropic stability [2]

Native stability of a protein is altered upon ligand binding (metal ions, cofactors and inhibitors). The variations in protein stability is often studied based on their thermodynamics parameters, which are derived from thermal denaturation curves of a protein [46, 47]. These curves can provide important information regarding amino acid residues that enhance stability, parameters that contribute towards protein folding and its structure [46]. The stability of a protein depends on its **Gibbs free energy of folding** (ΔG_U) [46, 48]. When a protein which is in its native, folded form is heated, it gradually unfolds and destabilizes as ΔG_U decreases and becomes zero. An equilibrium is established between the folded and unfolded states as their concentrations become equal. The temperature at this stage is referred to as the **melting temperature** (T_m) of the protein [48]. Binding of ligands to specific sites of the protein shifts the T_m due to alterations in

stability [47, 49]. Generally, ligand binding leads to an increase in ΔG_U of the protein, leading to an increase in T_m, compared to the free protein. This signifies a stabilization in the protein structure, which is proportional to the concentration and binding affinity of ligand [47, 48]. Thermal analysis of proteins is performed using a real-time qPCR instrument. Apart from the capability of performing several tests in a single run, the instrument also offers a broad window for scanning temperature, prevents sample evaporation. This technique also requires considerably low sample volumes, while allowing to study samples of appreciably low concentrations [47, 49]. The fluorescent dyes used for thermal analysis are generally non-fluorescent in polar solvents but are highly fluorescent in non-polar environments. Thus, upon unfolding of a protein these dyes could bind to the hydrophobic sites and fluoresce [47, 48]. Pantoliano et al. successfully demonstrated the screening of approximately 100 therapeutically important drugs through thermal analysis. This work also showed that certain proteins that can bind multiple ligands simultaneously had varying melting temperatures amongst their free, single- and multi- ligand bound protein [47].

Based on the concept of thermal analysis of DNA melting, our lab has demonstrated the use of TFA to monitor changes in melting of shorter DNA strands in the presence and absence of target protein binding. Herein, essentially two systems are compared- a signal complex and background complex [6, 50, 51]. As mentioned previously, due to the stability of target binding, signal complex will melt at a higher temperature compared to the background complex, formed as a result of target- independent hybridization (**Figure 2.3A**). Analysis of the derivative melt curves (dF/dT) of the signal and background complexes clearly indicates a separation between the signal and background, which also demonstrated a concentration dependent separation (**Figure 2.3B**, top). Furthermore, subtraction of the background curve (zero-target) from rest of the derivative curves

will show a clear separation between the background (minima) and background (maxima curves) (**Figure 2.3B**, bottom) [50].

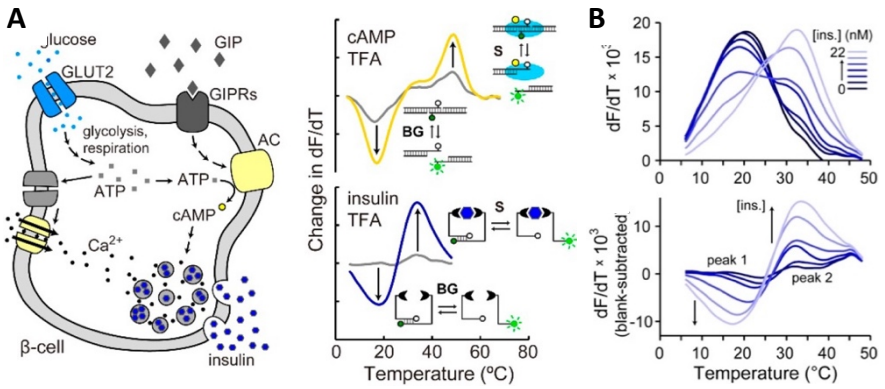

Figure 2.3 Principle of thermofluorimetric analysis (TFA). **(A)** Signaling complex is formed as a result of target binding, which is entropically stable, giving a higher melting temperature. **(B)** Top- Derivative curve (dF/dT) shows a shift in melt curve towards a higher temperature. As the concentration of target analyte increases, the melt peaks at higher temperature becomes sharper. Bottom- subtraction of background melt curve from the rest of the derivative curves analytically separates the signal from the background, where growing minima represents the background and growing maxima represents the signal. *Reprinted with permission from reference 50. Copyright 2017, American Chemical Society*

In the past, our group used this technique to successfully detect thrombin (using thrombin aptamers), insulin (using insulin-antibody oligos), and small molecule cyclic AMP (cAMP) in low concentrations [6, 50, 51]. Key advantages of TFA include- the non-physical separation of signal from background, ease of correcting for complex-matrix autofluorescence due to the interpretation of derivative curves, repurposing a simple qPCR instrument, simple-mix-and-read format compared to ELISA, use of considerably small sample volumes, and the capability of adopting to an isothermal assay as temperature could be selected to eliminate or minimize background

interference [2, 6, 50, 51]. However, along with these advantages, TFA still carries certain drawbacks: limit of detection (LOD) is not as impressive as ELISA (due to the lack of downstream amplification processes), limitations of sensitive optics in qPCR instrument, and scanning up to higher temperatures can lead to not only melt DNA, but also the analyzing protein, making it important to pay close attention to the temperature selected for thermal scanning. In the following sections we describe a TFA-based proximity assay for protein sensing using split broccoli aptamer and its fluorophore, DFHBI.

2.2 Methods and reagents

2.2.1 Reagents

Customized RNA and DNA strands were purchased from Integrated DNA Technologies (IDT) (Coralville, Iowa). All oligonucleotide sequences are given in **Table 2.1** below. Thrombin (from human plasma), HEPES (4,2-hydroxyethyl-1-piperazineethanesulfonic acid) and phenol-chloroform (5:1) were from Sigma Aldrich (St. Louis, MO). Sodium chloride, magnesium chloride hexahydrate and bovine serum albumin were purchased from OmniPur. Potassium chloride was obtained from BDH. Ammonium acetate from VWR and ethyl alcohol (absolute, anhydrous) purchased from Pharmco Aaper (NY). DFHBI and DFHBI-1T were purchased from Lucerna.Inc (Brooklyn, NY). AmpliScribe T7-flash in vitro transcription kit (Lucigen brand), 2.5 mM dNTP mix-PCR grade (Invitrogen brand) and DNase, RNase-free UltraPure distilled water (Invitrogen brand) were from ThermoFisher Scientific. Monarch PCR and DNA cleanup kit (5μg), Q5 hot start high-fidelity DNA polymerase (including 5X Q5 reaction buffer) and 5X Q5 high GC enhancer were purchased from New England BioLabs. Inc (MA). For TFA measurements, the BioRad real time qPCR instrument (CFX 96) was used. For isothermal fluorescence measurements

the Beckman Coulter fluorescence plate reader was used.

Sequence name	**Sequence (5' to 3')**
Full-length Broccoli aptamer	GAGACGGUCGGGUCCAGAUAUUCGUAUCUGUCGAGUA GAGUGUGGGCUC
Split Broccol-1	GAGACGGUCGGGUCCAGAUAUUCG
Split Broccoli-2	UAUCUGUCGAGUA GAGUGUGGGCUC
Thrombin aptamer (**ThrA**)	AGTCCGTGGTAGGGCAGGTTGGGGTGACTTTTTTTTTTTTTTTTTATATTTT TTTTTTCTCGCGGAUUUGAACCCUAACG
Thrombin aptamer (**ThrB**)	TAGGAAAAGGAGGAGGGTGGGATTGGTGTGTGTTTTTTTTTTTTTTTTTTT TTTTTTTTTTTTTTGGTTGGTGTGGTTGG
Broccoli aptamer with T7 promoter (DNA) (**T7_Broccoli**)	AGAACATAATACGACTCACTATAGCGGAGACGGTCGGGTCCAGATATTCG TATCTGTCGAGTA GAGTGTGGGCTC CGC
Reversed primer for Broccoli aptamer (**Broccoli_RevP**)	GCGGAGCCCACACTCTA
T7 Promoter for split broccoli aptamer with thrombin binding arm (Strand 1) (**T7_Mod_Split1**)	TAATACGACTCACTATAGCTCCTCCTTTTCCTAGAGACGGTCGGGTCCAGA TATTC
Reversed primer for modified split1 (**Rev_P_Split1**)	GAATATCTGGACCCGACCGTCTC
T7 Promoter for split broccoli aptamer with thrombin binding arm (Strand 2) (**T7_Mod_Split2**)	TAATACGACTCACTATA*GTATCTGTCGAGTAGAGTGTGGGCTC*CG TTAGGGTTCAAAT
Reversed primer for modified split2 **(Rev_P_Split2)**	ATTTGAACCCTAACGGAGCC
DNA Loop	TAGGAAAAGGAGGAGGGTGGCCCACTTAAACCTCAATCCACCCACTTAA ACCTCAATCCACGCGGAUUUGAACCCUAACG

Table 2.1 DNA and RNA sequences used in chapter 2.

2.2.2 TFA experiments

Stock solutions of oligonucleotides were dissolved in IDTE buffer, purchased from IDT. All working solutions were prepared in assay buffer containing 40 mM HEPES, 100 mM KCl and 1 mM $MgCl_2$. Broccoli aptamer and the split broccoli aptamers of specific concentrations were mixed with the DFHBI fluorophore (final concentration, 5 μM), to a total assay volume of 20 μL. The solutions were then placed in the RT-qPCR instrument. Solution mixture was first incubated at 37 °C for 10 min, followed by further incubating at 4°C for 10 min. A complete thermal scan was performed from 4-95 °C, with a 0.5 °C increment and 10 s equilibration time between each interval. The SYBR green channel (λ_{em}= 520 ± 10 nM and λ_{ex} = 470 ± 20 nM) was used to measure fluorescence intensity of all experiments. A solution of DFHBI (5 μM) in assay buffer was used as the blank. In instances where thrombin was quantified, the split broccoli aptamers were modified with thrombin binding arms and mixed with thrombin aptamers A and B, DFHBI (5 μM), thrombin or buffer (corresponding to 0 nM thrombin) where the same incubation steps and thermal scanning procedure was followed. The split broccoli and thrombin aptamers were either 25 or 50 nM final concentration, whereas thrombin concentrations were either 25, 50 or 100 nM. In instances where a DNA loop was used as the target, the DNA loop was mixed with the split broccoli aptamers and DFHBI at a final concentration of either 25 nM or 50 nM (for DNA loop and split broccoli aptamers). Again, the same incubation steps and thermal scanning procedure was followed.

2.2.3 Isothermal fluorescence measurements

Necessary concentrations of broccoli or split broccoli aptamer was mixed with DFHBI (5 μM) and transferred to the plate reader where, solutions were incubated for 10 min at 25 °C, followed by fluorescence measurement. Excitation and emission filters selected were 485 nm and 535 nm respectively. Assay volumes were either 40 μL or 20 μL, depending on the well plate used (96-well or 384-well plate formats respectively). Blank/ background solution consisted of DFHBI (5 μM), in assay buffer. In instances where thrombin was detected, similar concentrations (as in section 2.2.2) of thrombin aptamers and split broccoli were mixed with DFHBI and thrombin or buffer. Similar incubation step and fluorescence measurement as above was followed. When DNA loop was used as the target, similar concentrations of DNA loop and split broccoli aptamer (as mentioned in section 2.2.2) were mixed with DFHBI, followed by the same incubation procedure and fluorescence detection method.

2.2.4 DNA template preparation for *in vitro* RNA transcription

Prior to in vitro transcription, reversed PCR primers and ssDNA (containing the T7 promoter region) templates necessary for specific sequences of RNA were designed and purchased from IDT. A basic illustration of dsDNA template formation and *in vitro* transcription is given shown in **Figure 2.4** below. For dsDNA template synthesis, the procedure for **Q5 hot start high fidelity DNA polymerase** provided by NEB was followed with few modifications. The following reagents were mixed and added to a PCR tube, followed by running one PCR cycle, to form the dsDNA.

1. Template with T7 promoter (x μM) 1 μL
2. Reversed primer (x μM) 1 μL
3. 5x polymerase buffer 4 μL

4. 5x GC enhancer 4 μL
5. dNTPs (2.5 mM) 4 μL
6. Q5 polymerase 0.5 μL
7. Water 5.5 μL
8. Total volume of mixture= 20 μL

After the dsDNA synthesis was completed, it was purified using the Monarch PCR cleanup kit. The manufacturer's procedure was followed with slight modifications as needed.

1. The dsDNA was first diluted with necessary amount of binding buffer provided in the kit.
2. The diluted DNA was then transferred to the purification column and was spun down for 1 min at 15,000-16,000 rpm in the centrifuge machine.
3. Washing buffer provided in the kit was added to the column according to the given procedure and spun again for 1 min at the same speed as above. This step was repeated once more.
4. The columns were then transferred to new microcentrifuge tubes, followed by the addition of 10 μL of water.
5. The tubes were again centrifuged at the same time and speed as above.
6. Afterwards, the column was removed, whereas the synthesized and cleaned dsDNA template was collected into a new microcentrifuge tube.
7. The concentration of this solution was determined using the Nanodrop 1000, and the template was store in -20 °C until further use.

2.2.5 *In vitro* transcription

Reagents provided in the AmpliScribe T7-flash transcription kit was thawed at room temperature in the following order and was mixed. The manufacturer's protocol was followed with slight modifications.

Nuclease free water	x μL
dsDNA template	3 μL (~ 0.1 μg)
Transcription buffer	1 μL
ATP	
CTP	
GTP	
UTP	0.9 μL each
DTT (100 mM)	1 μL
RNase inhibitor	0.25 uL
T7 RNA polymerase	1 μL

This mixture was incubated at 37 °C for 4-6 hrs, followed by incubation at 65 °C for further 10-15 min, to deactivate the enzyme. Next, RNase free DNaseI was added to digest any remaining dsDNA template. Herein, 0.5 μL of DNase was added and incubated at 37 °C for 15 min, followed by enzyme deactivation at 65 °C, for 15 min. Purification of synthesized RNA was performed as follows-

1. 1 volume of 5 M ammonium acetate was added, followed by incubating on ice for 10-15 min. This commences precipitation of RNA.
2. To complete precipitation, excess ammonium acetate was removed, followed by the addition of 2 volumes of absolute ethanol. This was then kept at -20 °C for at least 20 min. **To make sure that the DNA template and remnants were removed, phenol-chloroform extraction was performed, prior to addition of absolute ethanol (phenol: chloroform, 5:1, pH 4.5- 5).*

3. The solution with the precipitated pellet was next centrifuged at top speed for ~15 min
4. The ethanol solution was removed, followed by washing the pellet with 20 µL of 70 % ethanol solution. The ethanol was drained the pellet was air dried for 15 min.
5. The formed pellet was then dissolved in necessary storage buffer and concentration of synthesized RNA was determined using the Nanodrop 1000 (Nucleic acid function, on RNA setting) and was the aliquoted and store at -20 °C until used .

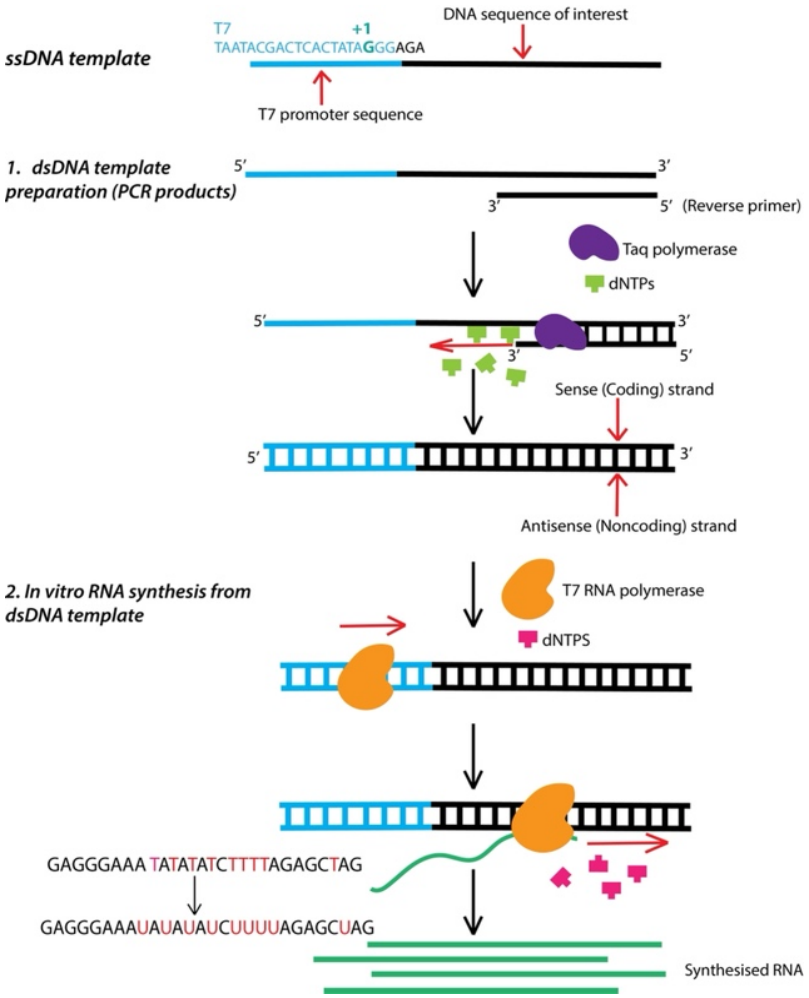

Figure 2.4 An illustration of in vitro RNA transcription. A customized ssDNA template including the DNA sequence of interest and T7 promoter region were purchased. A dsDNA template is synthesized using 1-2 cycles of PCR amplification, where the ssDNA is converted to a dsDNA. This dsDNA carries an antisense (noncoding) and sense (coding) strands, used for RNA synthesis. During in vitro RNA synthesis, the RNA polymerase recognizes the coding strand and adds dNTPs

giving several copies of the corresponding RNA strand. Finally, the RNA is purified, extracted and stored in a freezer, till used.

2.2.6 Data analysis

Data analysis was performed in Microsoft excel. A detailed representation of data analysis for TFA is shown **in chapter 3, experiments, and methods section.**

2.3 Results and discussion

Spinach and broccoli aptamers have a specific G-quadruplex binding pocket for the fluorophore, DFHBI. Upon binding, the fluorophore is stabilized, and excitation energy is released as light (fluorescence) (**Figure 2.5A**). As mentioned previously, the Ricci group demonstrated that splitting the spinach aptamer destabilizes the DFHBI binding pocket, resulting in low fluorescence. They modified the split aptamers to carry digoxigenin molecules on one end, where in the presence of anti-digoxigenin the splits were brought to close proximity. The proximity effect resulted in the reassembly of split spinach and stabilized the DFHBI molecule, turning on its fluorescence. The fluorescence intensity was proportional to the amount of anti-digoxigenin [43]. Based on this work, we hypothesized that splitting the 49-nt broccoli (a more brighter and robust variant of spinach) at its hairpin loop into two fragments of 24- and 25-nt and fusing them to recognition units can turn on fluorescence of DFHBI in the presence of a target analyte. We used TFA to assess the quantity of target, with the objective of developing a simple-mix-and read assay. As a first step we studied the capability of differentiating between the monomeric, full length broccoli aptamer and split aptamers using TFA. In the presence of full-length broccoli, DFHBI turns on its fluorescence and in the presence of splits, DFHBI fluorescence should be comparable to that of the background (only DFHBI in buffer) (**Figure 2.5B**).

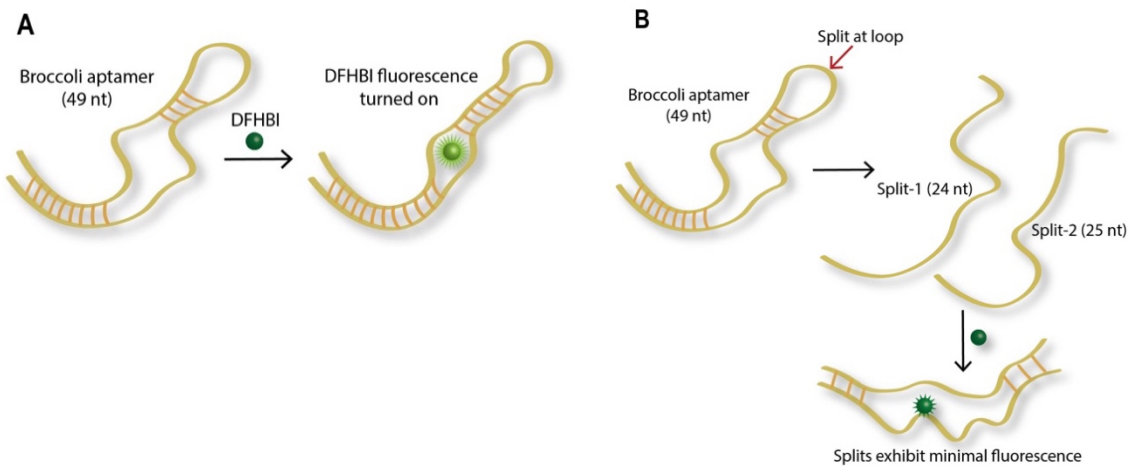

Figure 2.5 Broccoli aptamer interaction with DFHBI. **(A)** The full-length aptamer can turn of fluorescence of DFHBI in solution. **(B)** Splitting of the aptamer at the hairpin loop to two segments leads to very minimal fluorescence in solution, as the DFHBI binding pocket is destabilized.

Figure 2.6A illustrates the principle of identifying between full-length and split broccoli aptamers using TFA. When 500 nM of full-length broccoli and 500 nM split broccoli were thermally scanned, we observed that splitting at the hairpin loop led to decreased fluorescence as hypothesized. **Figure 2.6B** and **Figure 2.6C** shows the clear difference in change of DFHBI fluorescence, where a sharp drop is observed in the melting curve for the fully functional aptamer, as opposed to the split aptamers. This was clearly visible in the derivative curve, where a sharp melt peak at ~ 44 °C was observed for the full-length aptamer, whereas, at the same temperature there was no such significant observation for the splits. To further confirm that splitting broccoli led to loss/ reduced DFHBI fluorescence, we performed isothermal fluorescence measurements at 25 °C, for the same concentrations of full-length broccoli and split broccoli in the presence of DFHBI. As shown in **Figure 2.6D** the split aptamers had fluorescence nearly comparable to the blank, further supporting our hypothesis.

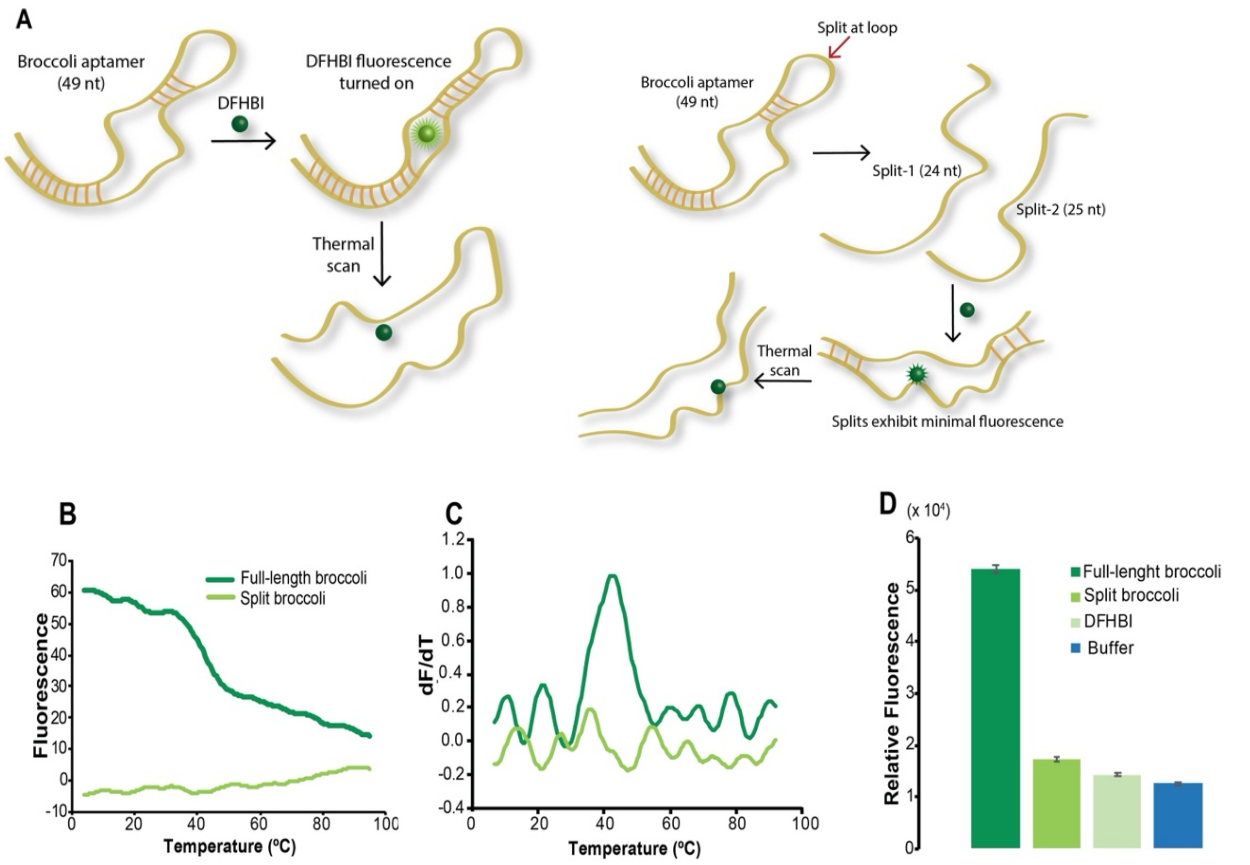

Figure 2.6 TFA for understanding full-length and split-broccoli constructs. **(A)** Left- When full-length broccoli aptamer is thermally scanned, the fluorescence gradually drops, since the aptamer thermally denatures. Right- Spit aptamers don't show significant difference in fluorescence, due to destabilized DFHBI binding pocket. **(B)** Fluorescence curves showing the clear difference between full-length and split aptamers. Sharp melting transition is observed for the full aptamer. **(C)** Derivative curve showing a sharp melting peak at ~ 44 °C for full-length aptamer, whereas no such peak was seen for the splits. **(D)** Isothermal fluorescence measurements confirming the TFA results.

Since our goal was to develop a simple, mix-and-read signal turn on assay using the split broccoli aptamers, it is important that the assay functions at low volumes as well as considerably low probe concentrations. As shown in **Figure 2.6**, for 500 nM of aptamer splits we were able to observe a loss/ decrease in fluorescence. Therefore, we visualized that, even at reduced

concentrations we should be able to observe a difference between the thermal melt curves of full-length and split broccoli aptamer. First, we performed isothermal measurements at 25 °C for full-length broccoli having concentrations of 12.5, 25 and 50 nM. As shown in **Figure 2.7A**, compared to the blank (DFHBI 5 μM) we were able to observe a linear increase in fluorescence with increasing aptamer concentration. Next, we performed thermal scans for 25 and 50 nM of full-length and split broccoli aptamers. As shown in **Figure 2.7B** and **Figure 2.7C** we were able to observe clear melting transition for full-length broccoli compared to its splits, where a melt peak was observed at ~ 40 °C for full-length aptamer. This suggested that we can use TFA to distinguish between the full-length and split aptamers, at considerably low concentrations.

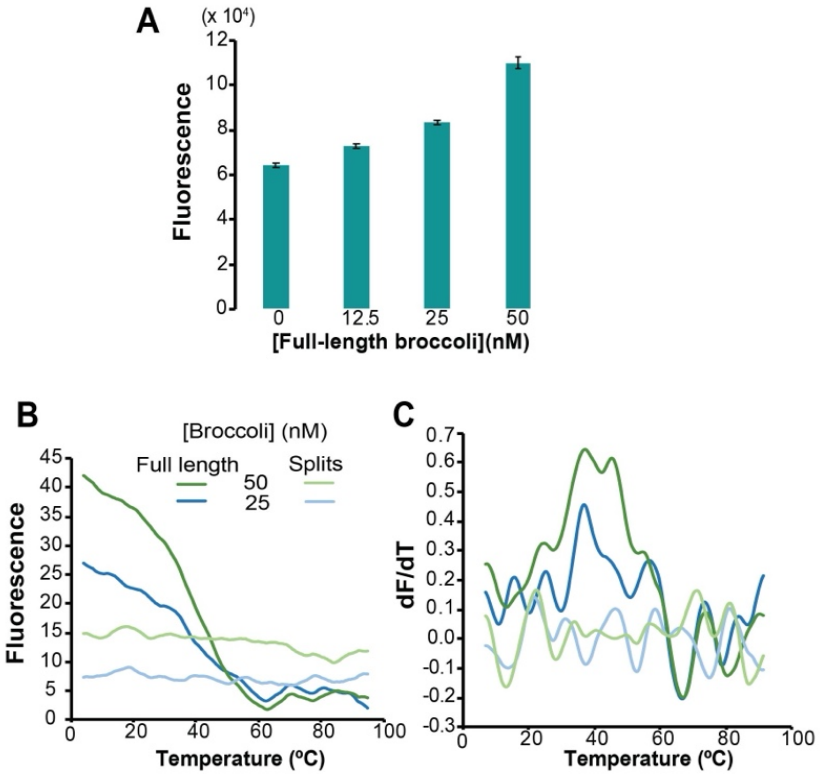

Figure 2.7 Comparison of low concentration broccoli aptamers. **(A)** Isothermal fluorescence shows that low concentration of full-length aptamers can be studied in buffer. **(B)** Thermal scan also shows that low concentrations of full-length broccoli aptamer can be distinguished from its splits. **(C)** The dF/dT curves further confirm the observations.

To utilize split broccoli aptamers in proximity-based assays, it is important that the splits are fused to target recognition elements such as small molecules, aptamers, peptides, or antibodies. With that in mind, we modified the split aptamers for thrombin detection. Thrombin aptamers A and B bind to two nonoverlapping epitopes of the thrombin molecule. Our group and others have used this system for thrombin detection leveraging proximity effect successfully, owing to the strong binding specificities of the two aptamers to thrombin [7, 17, 52]. Therefore, we sought to use thrombin to demonstrate the proof-of-concept. Specifically, we included a 15-nt RNA sequence to the 3'- and 5'- terminals of each split broccoli aptamer (split-1 and split-2 respectively) which was complementary to another 15-nt DNA sequence on thrombin aptamer A and thrombin aptamer B respectively (**Figure 2.8A**). The modifications were carefully done and analyzed on NUPACK open-source software to make sure that the 15-nt sequence would not interact with the individual aptamer sequences to form stable secondary constructs.

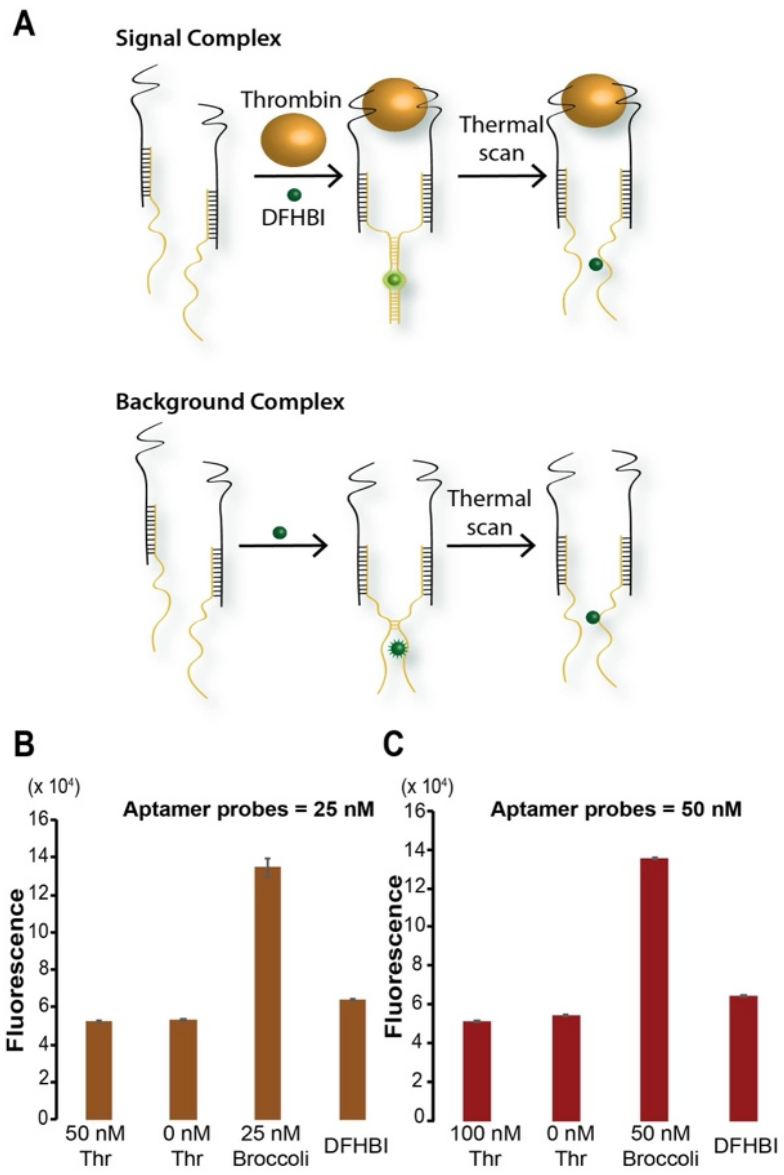

Figure 2.8 Thrombin sensing leveraging split broccoli aptamers. **(A)** Sensing principle. Thrombin aptamers (black) were hybridized to the split broccoli aptamers (beige) through 15bp. Top- incubation with thrombin, brings the split aptamers to close proximity, which will form the DFHBI binding pocket, where DFHBI will light up. Thermal scanning would result in gradual decrease in fluorescence, due to melting of split aptamers and destabilization of fluorophore binding pocket. Bottom- In the absence of thrombin, the split aptamers will not be able to hybridize and form the DFHBI binding pocket, as the aptamer strands are placed far apart from each other. **(B)** Isothermal fluorescence measurements for system depicted in (A) above. Split aptamer, hybridized to thrombin aptamers are 25 nM. The concentration of thrombin measured is 50 nM. **(C)** Isothermal

fluorescence for aptamer constructs having 50 nM concentration, with 100 nM thrombin detected. As observed, for both (B) and (C) above, fluorescence of DFHBI in the presence of thrombin is comparable to that of the blank, indicating that DFHBI binding pocket has not formed.

A substantial disadvantage of using RNA for bioassays is its instability. RNAs are usually more unstable than DNA due to it being prone to rapid degradation by RNase enzymes [2]. For our initial experiments thus far, we utilized commercially synthesized RNA strands, which were aliquoted and stored at -80 or -20 °C, till further use. However, we noticed that aliquots cannot be used over longer period as observed by the fluctuating fluorescence measurements. To confirm this, we compared an older aliquot (placed in ~2 °C – 8 °C for ~ 2 months) with a fresh aliquot stored at either -20 °C or -80 °C. Herein, isothermal fluorescence measurements were performed for two concentrations of full-length broccoli aptamer (20 and 40 nM) of a new and older aliquot. The older samples exhibited poor fluorescence compared to the newer aliquots which indicated possible RNA degradation (**Figure 2.9**). Since purchasing synthetic RNA can be costly, we opted to synthesizing the broccoli aptamers (full-length, splits and modified splits) in the lab using commercially available *in vitro* transcription kit, as described in the methods section above. The benefit of this method is that from a small amount of DNA template, few micrograms of RNA can be synthesized with considerable purity and less effort. Therefore, for all other experiments which precedes, we utilized in-lab synthesized RNA strands.

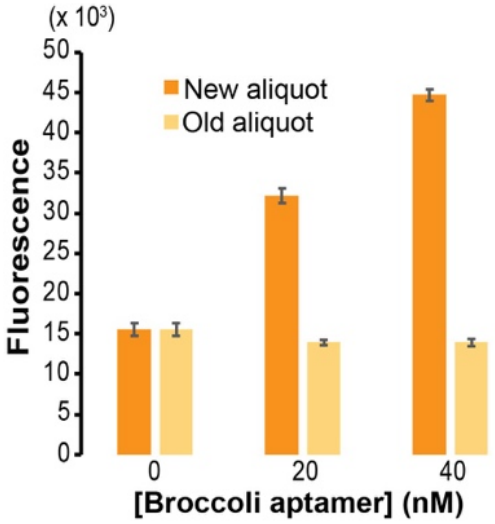

Figure 2.9 Stability comparison of RNA aliquots. Isothermal fluorescence measurements were performed for a new and older aliquot of full-length broccoli aptamer, where we observed significant drop in fluorescence signal for the older aliquot, which was indicative of RNA degradation.

Following in vitro transcription, as shown in **Figure 2.8A**, we incubated the split broccoli aptamers with the respective thrombin aptamers. We hypothesized that binding of these thrombin aptamers to thrombin would bring the two split broccoli strands to close proximity and form the DFHBI binding pocket, leading to an enhanced fluorescence which will be comparable to that of the full-length broccoli aptamer. However, the isothermal fluorescence measurements showed that irrespective of the presence or absence of target (thrombin), DFHBI fluorescence was not restored and was comparable to the intensity of free DFHBI in solution (**Figure 2.8B and Figure 2.8C**). For further confirmation, we used a DNA loop as a target (**Figure 2.10A**). As illustrated, in the presence of loop, we would expect the reassembly of split broccoli. However, similar to thrombin experiments we did not see an increased fluorescence as hypothesized, which implied that the split-broccoli aptamer wasn't reassembling the binding pocket of DFHBI. Further, we performed

thermal scans for both the thrombin and DNA loop systems. Herein, similar to the isothermal fluorescent measurements, we didn't observe clear melting, which implied the reassembly of broccoli splits did not take place (**Figure 2.10B** and **Figure 2.10C**). However, the TFA results marginally suggests that there is a possibility of the split aptamers reforming, since it can be observed that split broccoli in the presence of thrombin or DNA loop shows higher fluorescence, in comparison to the aptamers without the respective targets.

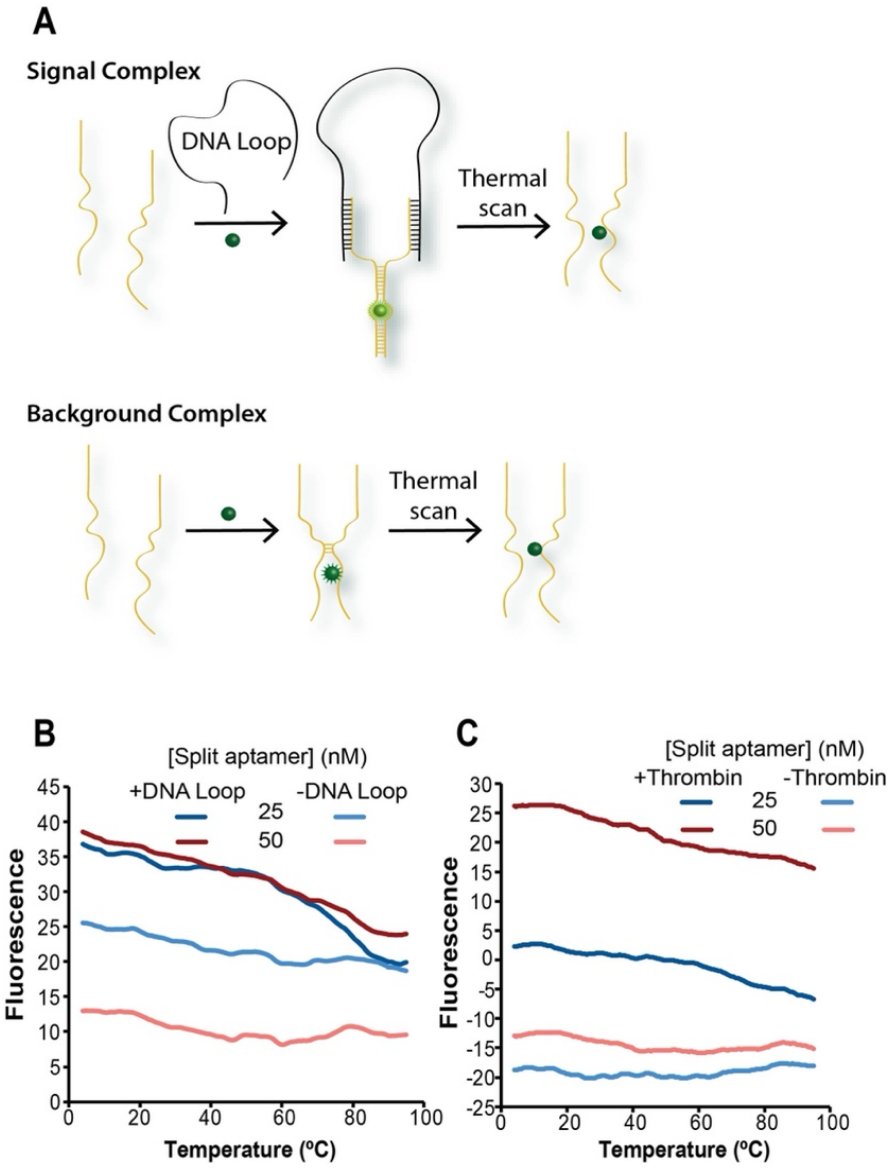

Figure 2.10 (A) Detection of a DNA loop as target leveraging designed split broccoli aptamers. Top- The DNA loop is expected to bring the splits closer and turn on DFHBI fluorescence. Bottom- In the absence of DNA loop, the DFHBI binding pocket will not be formed, as the splits cannot reassemble. **(B)** DNA melt curve for split aptamers, where DNA loop was used as the target. **(C)** DNA melt curve for the split aptamers, where thrombin was used as the target. For both (B) and (C) above, although obvious melt curves were not seen, the melting transitions of split aptamers in the presence of respective targets are slightly higher and steeper that the aptamers in the absence of target.

2.4 Conclusions

In this chapter, we have attempted the design of a proximity assay using the complementation of split broccoli aptamer in the presence of a target analyte (thrombin or DNA), using TFA. Although splitting the full-length 49-nt broccoli aptamer at functionally minimal loop into two fragments resulted in destabilizing the fluorophore (DFHBI) binding pocket, in the presence of target the splits did not seem to reassemble. Furthermore, from the TFA data it was evident that although melting transitions were clearly visible for full-length broccoli and changes in melting transitions of the full-length aptamer was discernible from the split aptamers, the fluorescence measurements (raw fluorescence) was observed at the detection limit of the BioRad qPCR instrument. Therefore, limitations in the instrument's optical system did not permit the successful identification of minute changes. However, the results marginally suggested that the split aptamers might be binding weakly to form the DFHBI binding pocket and stabilizing the DFHBI molecule weakly. Also, although the aptamer was split at a loop, it might be important to pay closer attention to its functionality and assess its contribution towards stability, although it was placed far from the presumed G-quadruplex binding pocket of DFHBI. It is possible that, splitting at that region disrupts its thermodynamic stability, hampering proper folding of the split aptamer even in the presence of target analyte.

2.5 Reference

(1) Feagin, T. A.; Maganzini, N.; Soh, H. T. Strategies for creating structure-switching aptamers. *ACS sensors* **2018**, *3* (9), 1611-1615.
(2) Bezerra, A. B.; Kurian, A. S. N.; Easley, C. J. Nucleic-Acid Driven Cooperative Bioassays Using Probe Proximity or Split-Probe Techniques. *Anal Chem* **2021**, *93* (1), 198-214. DOI: 10.1021/acs.analchem.0c04364 From NLM Medline.
(3) Hamaguchi, N.; Ellington, A.; Stanton, M. Aptamer beacons for the direct detection of proteins. *Analytical biochemistry* **2001**, *294* (2), 126-131.
(4) Liu, X.; Li, X.; Lu, Y.; Cao, J.; Li, F. A split aptamer-based imaging solution for the visualization of latent fingerprints. *Analytical Methods* **2018**, *10* (19), 2281-2286.
(5) Morris, F. D.; Peterson, E. M.; Heemstra, J. M.; Harris, J. M. Single-molecule kinetic investigation of cocaine-dependent split-aptamer assembly. *Analytical chemistry* **2018**, *90* (21), 12964-12970.
(6) Hu, J.; Kim, J.; Easley, C. J. Quantifying Aptamer-Protein Binding via Thermofluorimetric Analysis. *Anal Methods* **2015**, *7* (17), 7358-7362. DOI: 10.1039/c5ay00837a.
(7) Hu, J.; Yu, Y.; Brooks, J. C.; Godwin, L. A.; Somasundaram, S.; Torabinejad, F.; Kim, J.; Shannon, C.; Easley, C. J. A reusable electrochemical proximity assay for highly selective, real-time protein quantitation in biological matrices. *J Am Chem Soc* **2014**, *136* (23), 8467-8474. DOI: 10.1021/ja503679q From NLM Medline.
(8) Sun, Y.; Yuan, B.; Deng, M.; Wang, Q.; Huang, J.; Guo, Q.; Liu, J.; Yang, X.; Wang, K. A light-up fluorescence assay for tumor cell detection based on bifunctional split aptamers. *Analyst* **2018**, *143* (15), 3579-3585.
(9) Tang, J.; He, X.; Lei, Y.; Shi, H.; Guo, Q.; Liu, J.; He, D.; Wang, K. Temperature-responsive split aptamers coupled with polymerase chain reaction for label-free and sensitive detection of cancer cells. *Chemical Communications* **2017**, *53* (87), 11889-11892.
(10) Wei, Y.; Zhou, W.; Liu, J.; Chai, Y.; Xiang, Y.; Yuan, R. Label-free and homogeneous aptamer proximity binding assay for fluorescent detection of protein biomarkers in human serum. *Talanta* **2015**, *141*, 230-234.
(11) Yu, H.; Canoura, J.; Guntupalli, B.; Alkhamis, O.; Xiao, Y. Sensitive detection of small-molecule targets using cooperative binding split aptamers and enzyme-assisted target recycling. *Analytical chemistry* **2018**, *90* (3), 1748-1758.
(12) Chen, J.; Zhang, J.; Li, J.; Yang, H.-H.; Fu, F.; Chen, G. An ultrasensitive signal-on electrochemical aptasensor via target-induced conjunction of split aptamer fragments. *Biosensors and Bioelectronics* **2010**, *25* (5), 996-1000.
(13) Ocaña, C.; Hayat, A.; Mishra, R.; Vasilescu, A.; Del Valle, M.; Marty, J.-L. A novel electrochemical aptamer–antibody sandwich assay for lysozyme detection. *Analyst* **2015**, *140* (12), 4148-4153.
(14) Zhao, T.; Liu, R.; Ding, X.; Zhao, J.; Yu, H.; Wang, L.; Xu, Q.; Wang, X.; Lou, X.; He, M. Nanoprobe-enhanced, split aptamer-based electrochemical sandwich assay for ultrasensitive detection of small molecules. *Analytical chemistry* **2015**, *87* (15), 7712-7719.
(15) Stojanovic, M. N.; de Prada, P.; Landry, D. W. Fluorescent sensors based on aptamer self-assembly. *Journal of the American Chemical Society* **2000**, *122* (46), 11547-11548.

(16) Ebrahimi, S. B.; Samanta, D.; Cheng, H. F.; Nathan, L. I.; Mirkin, C. A. Forced intercalation (FIT)-aptamers. *Journal of the American Chemical Society* **2019**, *141* (35), 13744-13748.
(17) Heyduk, E.; Heyduk, T. Nucleic acid-based fluorescence sensors for detecting proteins. *Analytical Chemistry* **2005**, *77* (4), 1147-1156.
(18) Yuan, B.; Sun, Y.; Guo, Q.; Huang, J.; Yang, X.; Chen, Y.; Wen, X.; Meng, X.; Liu, J.; Wang, K. High signal-to-background ratio detection of cancer cells with activatable strategy based on target-induced self-assembly of split aptamers. *Analytical Chemistry* **2017**, *89* (17), 9347-9353.
(19) Arroyo-Currás, N.; Somerson, J.; Vieira, P. A.; Ploense, K. L.; Kippin, T. E.; Plaxco, K. W. Real-time measurement of small molecules directly in awake, ambulatory animals. *Proceedings of the National Academy of Sciences* **2017**, *114* (4), 645-650.
(20) Dauphin-Ducharme, P.; Yang, K.; Arroyo-Currás, N.; Ploense, K. L.; Zhang, Y.; Gerson, J.; Kurnik, M.; Kippin, T. E.; Stojanovic, M. N.; Plaxco, K. W. Electrochemical aptamer-based sensors for improved therapeutic drug monitoring and high-precision, feedback-controlled drug delivery. *ACS sensors* **2019**, *4* (10), 2832-2837.
(21) Idili, A.; Gerson, J.; Parolo, C.; Kippin, T.; Plaxco, K. W. An electrochemical aptamer-based sensor for the rapid and convenient measurement of l-tryptophan. *Analytical and bioanalytical chemistry* **2019**, *411* (19), 4629-4635.
(22) Lai, R. Y.; Plaxco, K. W.; Heeger, A. J. Aptamer-based electrochemical detection of picomolar platelet-derived growth factor directly in blood serum. *Analytical chemistry* **2007**, *79* (1), 229-233.
(23) Li, H.; Arroyo-Curras, N.; Kang, D.; Ricci, F.; Plaxco, K. W. Dual-reporter drift correction to enhance the performance of electrochemical aptamer-based sensors in whole blood. *Journal of the American Chemical Society* **2016**, *138* (49), 15809-15812.
(24) Duan, W.; Wang, X.; Wang, H.; Li, F. Fluorescent and colorimetric dual-mode aptasensor for thrombin detection based on target-induced conjunction of split aptamer fragments. *Talanta* **2018**, *180*, 76-80.
(25) Nie, J.; Deng, Y.; Deng, Q.-P.; Zhang, D.-W.; Zhou, Y.-L.; Zhang, X.-X. A self-assemble aptamer fragment/target complex based high-throughput colorimetric aptasensor using enzyme linked aptamer assay. *Talanta* **2013**, *106*, 309-314.
(26) Wang, Y.; Li, H.; Zhou, J.; Qi, Q.; Fu, L. A colorimetric and fluorescent gold nanoparticle-based dual-mode aptasensor for parvalbumin detection. *Microchemical Journal* **2020**, *159*, 105413.
(27) Xia, F.; Zuo, X.; Yang, R.; Xiao, Y.; Kang, D.; Vallée-Bélisle, A.; Gong, X.; Yuen, J. D.; Hsu, B. B.; Heeger, A. J. Colorimetric detection of DNA, small molecules, proteins, and ions using unmodified gold nanoparticles and conjugated polyelectrolytes. *Proceedings of the National Academy of Sciences* **2010**, *107* (24), 10837-10841.
(28) Jin, F.; Lian, Y.; Li, J.; Zheng, J.; Hu, Y.; Liu, J.; Huang, J.; Yang, R. Molecule-binding dependent assembly of split aptamer and γ-cyclodextrin: A sensitive excimer signaling approach for aptamer biosensors. *Analytica Chimica Acta* **2013**, *799*, 44-50.
(29) Zuo, X.; Xiao, Y.; Plaxco, K. W. High specificity, electrochemical sandwich assays based on single aptamer sequences and suitable for the direct detection of small-molecule targets in blood and other complex matrices. *Journal of the American Chemical Society* **2009**, *131* (20), 6944-6945.

(30) Zhang, H.; Liu, Y.; Zhang, K.; Ji, J.; Liu, J.; Liu, B. Single molecule fluorescent colocalization of split aptamers for ultrasensitive detection of biomolecules. *Analytical chemistry* **2018**, *90* (15), 9315-9321.
(31) Yang, J.; Dou, B.; Yuan, R.; Xiang, Y. Aptamer/protein proximity binding-triggered molecular machine for amplified electrochemical sensing of thrombin. *Analytical chemistry* **2017**, *89* (9), 5138-5143.
(32) Nagai, T.; Ibata, K.; Park, E. S.; Kubota, M.; Mikoshiba, K.; Miyawaki, A. A variant of yellow fluorescent protein with fast and efficient maturation for cell-biological applications. *Nature biotechnology* **2002**, *20* (1), 87-90.
(33) Shaner, N. C.; Campbell, R. E.; Steinbach, P. A.; Giepmans, B. N.; Palmer, A. E.; Tsien, R. Y. Improved monomeric red, orange and yellow fluorescent proteins derived from Discosoma sp. red fluorescent protein. *Nature biotechnology* **2004**, *22* (12), 1567-1572.
(34) Vidi, P.-A.; Ejendal, K. F.; Przybyla, J. A.; Watts, V. J. Fluorescent protein complementation assays: new tools to study G protein-coupled receptor oligomerization and GPCR-mediated signaling. *Molecular and cellular endocrinology* **2011**, *331* (2), 185-193.
(35) Paige, J. S.; Wu, K. Y.; Jaffrey, S. R. RNA mimics of green fluorescent protein. *Science* **2011**, *333* (6042), 642-646.
(36) Filonov, G. S.; Moon, J. D.; Svensen, N.; Jaffrey, S. R. Broccoli: rapid selection of an RNA mimic of green fluorescent protein by fluorescence-based selection and directed evolution. *Journal of the American Chemical Society* **2014**, *136* (46), 16299-16308.
(37) Strack, R. L.; Disney, M. D.; Jaffrey, S. R. A superfolding Spinach2 reveals the dynamic nature of trinucleotide repeat–containing RNA. *Nature methods* **2013**, *10* (12), 1219-1224.
(38) Paige, J. S.; Nguyen-Duc, T.; Song, W.; Jaffrey, S. R. Fluorescence imaging of cellular metabolites with RNA. *Science* **2012**, *335* (6073), 1194-1194.
(39) Song, W.; Strack, R. L.; Svensen, N.; Jaffrey, S. R. Plug-and-play fluorophores extend the spectral properties of Spinach. *Journal of the American Chemical Society* **2014**, *136* (4), 1198-1201.
(40) Rogers, T. A.; Andrews, G. E.; Jaeger, L.; Grabow, W. W. Fluorescent monitoring of RNA assembly and processing using the split-spinach aptamer. *ACS synthetic biology* **2015**, *4* (2), 162-166.
(41) Kikuchi, N.; Kolpashchikov, D. M. Split spinach aptamer for highly selective recognition of DNA and RNA at ambient temperatures. *ChemBioChem* **2016**, *17* (17), 1589-1592.
(42) Kikuchi, N.; Kolpashchikov, D. M. A universal split spinach aptamer (USSA) for nucleic acid analysis and DNA computation. *Chemical Communications* **2017**, *53* (36), 4977-4980.
(43) Bertucci, A.; Porchetta, A.; Ricci, F. Antibody-templated assembly of an RNA mimic of green fluorescent protein. *Analytical chemistry* **2018**, *90* (2), 1049-1053.
(44) Alam, K. K.; Tawiah, K. D.; Lichte, M. F.; Porciani, D.; Burke, D. H. A fluorescent split aptamer for visualizing RNA–RNA assembly in vivo. *ACS synthetic biology* **2017**, *6* (9), 1710-1721.
(45) Wang, Z.; Luo, Y.; Xie, X.; Hu, X.; Song, H.; Zhao, Y.; Shi, J.; Wang, L.; Glinsky, G.; Chen, N. In Situ Spatial Complementation of Aptamer-Mediated Recognition Enables Live-Cell Imaging of Native RNA Transcripts in Real Time. *Angewandte Chemie* **2018**, *130* (4), 984-988.
(46) Johnson, R. J.; Savas, C. J.; Kartje, Z.; Hoops, G. C. Rapid and adaptable measurement of protein thermal stability by differential scanning fluorimetry: updating a common biochemical laboratory experiment. *Journal of chemical education* **2014**, *91* (7), 1077-1080.

(47) Pantoliano, M. W.; Petrella, E. C.; Kwasnoski, J. D.; Lobanov, V. S.; Myslik, J.; Graf, E.; Carver, T.; Asel, E.; Springer, B. A.; Lane, P. High-density miniaturized thermal shift assays as a general strategy for drug discovery. *Journal of biomolecular screening* **2001**, *6* (6), 429-440.
(48) Niesen, F. H.; Berglund, H.; Vedadi, M. The use of differential scanning fluorimetry to detect ligand interactions that promote protein stability. *Nature protocols* **2007**, *2* (9), 2212-2221.
(49) Rodrigues, J. V.; Prosinecki, V.; Marrucho, I.; Rebelo, L. P. N.; Gomes, C. M. Protein stability in an ionic liquid milieu: on the use of differential scanning fluorimetry. *Physical Chemistry Chemical Physics* **2011**, *13* (30), 13614-13616.
(50) Hu, J.; Easley, C. J. Homogeneous Assays of Second Messenger Signaling and Hormone Secretion Using Thermofluorimetric Methods That Minimize Calibration Burden. *Anal Chem* **2017**, *89* (16), 8517-8523. DOI: 10.1021/acs.analchem.7b02229.
(51) Kim, J.; Hu, J.; Bezerra, A. B.; Holtan, M. D.; Brooks, J. C.; Easley, C. J. Protein quantification using controlled DNA melting transitions in bivalent probe assemblies. *Anal Chem* **2015**, *87* (19), 9576-9579. DOI: 10.1021/acs.analchem.5b03432.
(52) Hu, J.; Kim, J.; Easley, C. J. Quantifying aptamer–protein binding via thermofluorimetric analysis. *Analytical Methods* **2015**, *7* (17), 7358-7362.

Chapter 3

Thermofluorimetric Analysis (TFA) using Probes with Flexible Spacers: Application to Direct Antibody Sensing and to Antibody-Oligonucleotide (AbO) Conjugate Valency Monitoring

This chapter is adopted from the submitted publication "Thermofluorimetric analysis (TFA) using probes with flexible spacers: application to direct antibody sensing and to antibody-oligonulceotide (AbO) conjugate valency monitoring" (Kurian, A. S. N., Gurukandure, A., Dovgan I., Kolodych, S. and Easley, C. J. ChemRxiv 2023)

3.1 Background

Protein molecules serve as crucial biomarkers which aid in understanding complex metabolic processes, disease diagnosis, and drug discovery [1-4]. During onset of a disease, pathologically important proteins are produced by the body at extremely low concentrations and released to body fluids [4]. Thus, it is vital to establish highly sensitive and specific detection platforms for protein biomarker sensing [1, 2, 4-6]. Enzyme linked immunosorbent assay (ELISA) is considered as the gold standard for biomarker detection even to date, achieving picomolar (pM) detection limits with high specificity and flexibility [3, 5, 7]. With its extensive application over several decades, ELISA has been evolved further to achieve even lower detection limits in techniques such as digital ELISA (SiMOA) and Alpha-LISA [8, 9]. Despite the fM to pM range limits of detection (LOD) achieved, the methods still suffer from drawbacks such as inclusion of several time consuming and laborious washing steps, limited capability of multiplexing, requirement of

special reagents or specific equipment [6-8, 10]. These limitations have created a substantial demand to explore alternative assays that are simpler, yet sensitive and specific, with single step (mix-and-read) format and cost effectiveness [1, 5, 7, 10-12].

A step towards achieving this goal is to leverage nucleic acid hybridizations, to translate changes experienced by a biomolecule in response to binding with a specific target [13-17]. This includes DNA walkers, DNA scaffolds, DNA nanostructures, and target induced DNA hybridization [12, 18, 19]. Among the nucleic acid based sensors developed, target driven hybridization of affinity ligand tagged short DNA strands have demonstrated to be a promising technique [1, 12, 18, 20-22]. A key advantage of this technique is its simple mix-and-read format, which can be adopted to either a homogenous or surface based assay [1, 15, 20, 23-25]. This proximity dependent annealing can be converted into a signal readout by coupling to fluorescent, electrochemical, or colorimetric detection platforms [5, 13, 18, 19, 26].

For biomarker sensing in complex matrices, detrimental effects of serum autofluorescence can be rectified by employing chemiluminescence and time-resolved fluorescence, yet these techniques require special reagents and equipment [10, 26]. Our group employs thermofluorimetric analysis (TFA) [10, 14, 20, 27] to simplify workflow and instrumentation needs. We have successfully demonstrated that analysis of DNA melt curves from standard real-time quantitative polymerase chain reaction (qPCR) instrumentation can be leveraged to assess analyte quantities (insulin, thrombin, and cyclic AMP), allowing a more straightforward differentiation between signal (target dependent annealing) and background (target independent annealing) [10, 14, 20, 27]. This TFA technique repurposes commonly used qPCR instruments to generate dF/dT melting curves, allowing mix-and-read workflows, analytical (not physical) separation of complexes, and removal of autofluorescence in complex biological matrices such as plasma or serum.

Antibodies, a subclass of proteins generated by the immune system in response to foreign antigens, are important as disease-related biomarkers or therapeutic agents, especially in the field of oncology [1, 18, 28, 29]. In parallel, antibodies have found widespread use as bioanalytical probes for assays such as ELISA, SiMOA, and Alpha-LISA, and antibody-oligonucleotide conjugates (AbOs) have been employed in other enzyme-linked oligonucleotide assays (ELONA) [30] and in many proximity dependent annealing assays[5, 13, 26, 30]. To develop simpler and sensitive analytical tools for antibody detection and for AbO conjugate characterization, herein we present two novel TFA based approaches with mix-and-read workflow. First, we leverage proximity-based assembly of antigen-tagged, short DNA strands to promote quenching of fluorescence upon antibody binding. The antibody assay is functional in both buffer and human plasma samples. Interestingly, we found that DNA probe flexibility is a critical parameter in such assays. Conformational rigidity of antibody-bound probe complexes was reduced using polyethylene glycol (PEG) spacers in the DNA strands, rendering considerable flexibility to the system and giving more efficient DNA hybridization and significantly improved signal. We then adapted this improved TFA system to study AbO conjugate valency, permitting clear discrimination of monovalent from multivalent AbOs. These more flexible, mix-and-read antibody and AbO conjugate sensors based on TFA should be applicable for quantifying various other antibodies and AbOs in the future.

3.2 Materials and reagents

3.2.1 Reagents

Customized DNA strands were purchased from Integrated DNA Technologies (IDT) (Coralville, Iowa). Monovalent insulin antibody oligonucleotides were custom synthesized by Syndivia (Strasbourg, France). Multivalent insulin antibody oligonucleotides were custom synthesized by Mediomics, LLC (St. Louis, MO) using anti-insulin antibodies (clones 8E2 and 3A6) purchased from Fitzgerald Industries. Human insulin solution was purchased from Millipore Sigma. DNA strand sequences are given in Table 3.1. Sodium chloride, magnesium chloride hexahydrate, bovine serum albumin and tris (hydroxymethyl) aminomethane were purchased from OmniPur. Potassium chloride was obtained from BDH. Calcium chloride dihydrate, HEPES (4,2-hydroxyethyl-1-piperazineethanesulfonicacid), and thrombin (from human plasma) were purchased from Sigma Aldrich (St. Louis, Missouri). Anti-digoxigenin antibody (mouse monoclonal) was purchased from Roche, and human plasma was purchased from BioIVT. Buffers, anti-digoxigenin and thrombin were prepared in DNase, RNAse free UltraPure distilled water (ThermoFisher Scientific, Invitrogen brand). For thermal scans in TFA the BioRad RT-qPCR instrument (CFX 96) or ABI 7500 (ThermoFisher Scientific, Applied Biosystems brand) real time PCR machine was used.

Sequence name	Sequence (5’ to 3’)
DNA loop	TAGGAAAAGGAGGAGGGTGGCCCACTTAAACCTCAATCCACC CACTTAAACCTCAATCCACGCGGAUUUGAACCCUAACG
Split loop-1	CCCACTTAAACCTCAATCCACGCGGATTTGAACCCTAACG
Split loop-2	TAGGAAAAGGAGGAGGGTGGCCCACTTAAACCTCAATCCA
Digoxigenin tagged DNA (**Dig-DNA-1**)	/5DiGN/CCCACTTAAACCTCAATCCACGCGGAUUUGAACCCUA ACG
Digoxigenin tagged DNA (**Dig-DNA-2**)	TAGGAAAAGGAGGAGGGTGGCCCACTTAAACCTCAATCCA/3D iG_N/
Thrombin aptamer (**Thr1**)	AGTCCGTGGTAGGGCAGGTTGGGGTGACTTTTTTTTTTTTTTT TATATTTTTTTTTCTCGCGGAUUUGAACCCUAACG
Thrombin aptamer (**Thr2)**	TAGGAAAAGGAGGAGGGTGGGATTGGTGTGTGTTTTTTTTTTT TTTTTTTTTTTTTTTTTTTTTGGTTGGTGTGGTTGG
FAM-DNA	CCACCCTCCTCCTTTTCCTATCTCTCCCTCGTCACCATGC/36-FAM/
Quencher-DNA	/5IABkFQ/GCATGGTATTTTTCGTTTTTTCGTTAGGGTTCAAATC CGC
PEG modified FAM-DNA **(PEG-FAM-DNA)**	CCACCCTCCTCCTTTTCCT/iSp18/iSp18/iSp18/iSp18/ACCATGC/36 -FAM/
PEG modified quencher-DNA **(PEG-Q-DNA**)	/5IABkFQ/GCATGGT/iSp18/iSp18/iSp18/iSp18/CGTTAGGGTTCAA ATCCGC

Monovalent insulin antibody oligonucleotide (1)	/5DBCON//iSp18/CCC ACT TAA ACCTCA ATC CAC GCG GAU UUG AAC CCU AAC G
Mono:Insulin Antibody oligonucleotide (2)	TAG GAA AAG GAG GAG GGT GGC CCA CTT AAA CCT CAA TCC A/iSp18//3DBCON/
Multivalent Insulin AbO (1)	5AmMC6//iSp18/ CCC ACT TAA ACCTCA ATCCAC GCG GAU UUG AAC CCU AAC G
Multivalent Insulin AbO (2)	TAG GAA AAG GAG GAG GGT GGC CCA CTTAAA CCT CAA TCC A /iSp18//3AmMO/

Table 3.1 DNA sequences used in this study

3.2.2 TFA using DNA loop as target

Stock solutions of all DNA strands purchased from IDT were dissolved in the company's IDTE buffer (pH 7.5). All working solutions of DNA were prepared in tris assay buffer (50 mM Tris-HCl, pH 7.5, 100 mM NaCl, 1 mM $MgCl_2$ and 0.1% BSA). For experiments using DNA loop as target, the total volume of an assay tube was 20 µL. Specifically, 10 µL of DNA loop solution was mixed with 5 µL each of probe DNA (FAM and quencher tagged strands), to result in a final concentration of 40 nM loop, 60 nM FAM-DNA, and 60 nM quencher DNA. The background was prepared by mixing 5 µL of each probe DNA solution with 5 µL of each split loop. The final concentrations were 40 nM split loop (each strand), 60 nM FAM-DNA, and 60 nM quencher DNA. A control solution was prepared by diluting FAM DNA in assay buffer to a final concentration of 60 nM. This was used as the fluorescence maximum. A 20 µL solution of assay buffer was used as a blank. All tubes after mixing were incubated at room temperature for 30 min. The solutions were then placed in the RT-qPCR instrument (Bio-Rad CFX96) for thermal scanning and fluorescence readout. Here, the solutions were further incubated at 4 °C for 10 min, followed by thermal scanning from 4 °C to 70 °C, with a 0.5 °C increment and 10 s equilibration time between each

interval. The FAM channel in the instrument (λ_{em}= 522 ± 8 nM and λ_{ex} = 470 ± 20 nM) was used to measure fluorescence intensity for all experiments.

3.2.3 TFA for antibody detection

Anti-digoxigenin (anti-dig) antibody samples used in the assay were diluted using tris assay buffer. Total assay volume for anti-dig based TFA was 30 µL. Specifically, 10 µL of anti-dig solution was mixed with 5 µL of each probe DNA (FAM-DNA and quencher-DNA) and 5 µL of each digoxigenin tagged DNA (dig-DNA-1 and dig-DNA-2). The background was prepared by mixing 5 µL each of FAM-DNA, quencher-DNA, dig-DNA-1, and dig-DNA-2. Background (0 nM anti-dig) did not include anti-dig solution, but instead included 10 µL of buffer. In each case, final concentrations of all four DNA strands in assay solution was 60 nM. Final concentrations of anti-dig solutions were 30 nM or 40 nM. A maximum fluorescence control was prepared using FAM-DNA solution at 60 nM, and a 30 µL buffer solution was used as the blank. Initially, all four DNA strands were mixed and incubated at room temperature for 30 min. Anti-dig was added afterwards and incubated for 15 min at 37 °C. Following this step, samples were transferred into the RT-qPCR instrument for TFA. The samples were incubated at 4 °C for 10 min, followed by thermal scanning from 4 °C to 70 °C, with 0.5 °C increment and 10 s equilibration time between each interval. The FAM channel was selected for measuring fluorescence emission, as before.

3.2.4 Calibration curve for anti-dig detection

A series of anti-dig solutions were analyzed through TFA, using the method described above. These were prepared in assay buffer and mixed with probe DNA solutions and dig-tagged DNA solutions to result in final concentrations ranging from 0-64 nM. The final assay volume was

30 µL. Final concentrations of FAM-DNA, quencher-DNA, dig-DNA-1, and dig-DNA-2 were 64 nM. A maximum fluorescence control was prepared using FAM-DNA solution at 64 nM, and a 30 µL buffer solution was used as the blank.

3.2.5 Anti-dig detection in human plasma

TFA experiments were performed to detect antibodies in 90% human plasma. The total assay volume was 30 µL, where 27 µL of human plasma solution was mixed with a 3 µL mixture having the four DNA strands and anti-dig antibody. The final concentrations of the probe DNAs and digoxigenin tagged DNAs were 64 nM. Two concentrations of anti-dig (32 nM and 50 nM) were analyzed in plasma. The background sample was prepared by mixing the probe DNAs and digoxigenin tagged DNAs in plasma solution and did not include anti-dig. Two controls were used in this case. A fluorescence maximum was prepared by diluting the FAM-DNA strand in assay buffer, followed by plasma, to yield a final FAM-DNA concentration of 64 nM in 90% human plasma. A fluorescence minimum was prepared by mixing assay buffer and plasma only, to obtain a 90% plasma solution. In parallel to plasma experiments, the similar concentrations of anti-dig were analyzed in assay buffer. The TFA measurement procedure was performed as mentioned previously.

3.2.6 Thrombin sensing with TFA

To provide a proximity assay platform for comparison, the above methodology was also used to detect thrombin, using a labeled aptamer pair. Working solutions of thrombin, its aptamers (ThrA, ThrB), and probe DNAs were prepared in thrombin assay buffer (TAB) (50 mM tris-HCl, pH 7.5, 100 mM NaCl, 50 mM KCl, 1 mM MgCl2 and 0.1% BSA). The final assay volume was 30 µL. Two different concentrations of thrombin (10 µL) were incubated with a mixture of the two

probe DNAs and 5 μL each of the two thrombin aptamers (ThrA and ThrB). The background included all four DNA strands in TAB without thrombin protein. Final concentrations of thrombin in assay solutions were 30 nM or 40 nM, whereas the probe DNAs and thrombin aptamers were 60 nM each. The control was prepared by diluting FAM-DNA to a final concentration of 60 nM in TAB. The TFA measurement procedure was performed as mentioned previously.

3.2.7 Antibody oligonucleotide (AbO) valency comparison

Working solutions of monovalent AbOs, multivalent AbOs, DNA loop (control experiment), signaling DNA, and insulin were prepared in BMHH buffer (HEPES 10 mM; pH 7.5, 125 mM NaCl, 5.7 mM KCl, 2.5 mM $CaCl_2$, 1.2 mM $MgCl_2$, 0.1% BSA). First the two types of AbOs were incubated individually with FAM-DNA and quencher-DNA for 30 min at room temperature, followed by incubation with insulin for further 20 min at 37 °C. The final concentrations of monovalent or multivalent AbOs, FAM-DNA, and quencher-DNA were 25 nM, where insulin was 20 nM. When used, Loop-DNA was also diluted to 25 nM. The final assay volume was 20 μL. A FAM-DNA control and a buffer blank were used as described above. All these samples were transferred to the ABI real time PCR instrument (due to later malfunctions in the other instrument) for TFA. Samples were further incubated at 4 °C (10 min), followed by thermal scan from 4 to 70 °C (1% setting, 10 s equilibration), with a temperature ramp between 0.36 and 0.38 °C s^{-1}.

3.2.8 Polyacrylamide gel electrophoresis (PAGE) of AbO conjugates

Purification PAGE protocol: AbOs (0.6 - 1.3 nmol) were mixed with 4x Laemmli sample buffer and were purified with Tris-Glycine (pH 8.5) PAGE (5%) in a 1.5 mm gel using 40 µL of sample per well. Separations were run at 200 V for 40 min. The product-containing bands were cut from the gel using a scalpel and extracted by passive diffusion in phosphate-buffered saline (PBS) buffer (1x; pH 7.4) overnight. The samples were filtered through 0.22 µm filters and were concentrated using a VivaSpin column (0.5 mL; MWCO: 30 kDa) before analysis by 10% PAGE (below).

Analytical PAGE protocol: 9 µL (6 pmol) of the conjugates (0.1 g L^{-1} of protein content) were mixed with Laemmli sample buffer (3 µL, 4x, containing 10x SYBR Gold) and analyzed with Tris-Glycine (pH 8.5) PAGE (10%) using 12 µL of sample per well. Separations were run at 200 V for 40 min.

3.2.9 Data analysis

Data processing was done using Microsoft Excel. Raw fluorescence signals versus temperature, obtained from a qPCR instrument, were first background corrected using a buffer blank solution, then normalized to the high temperature data, then normalized again using signal from a free FAM-DNA solution. These data were differentiated by calculating the dF/dT, and dF/dT difference curves were also used in some analyses (**Figure 3.1**)

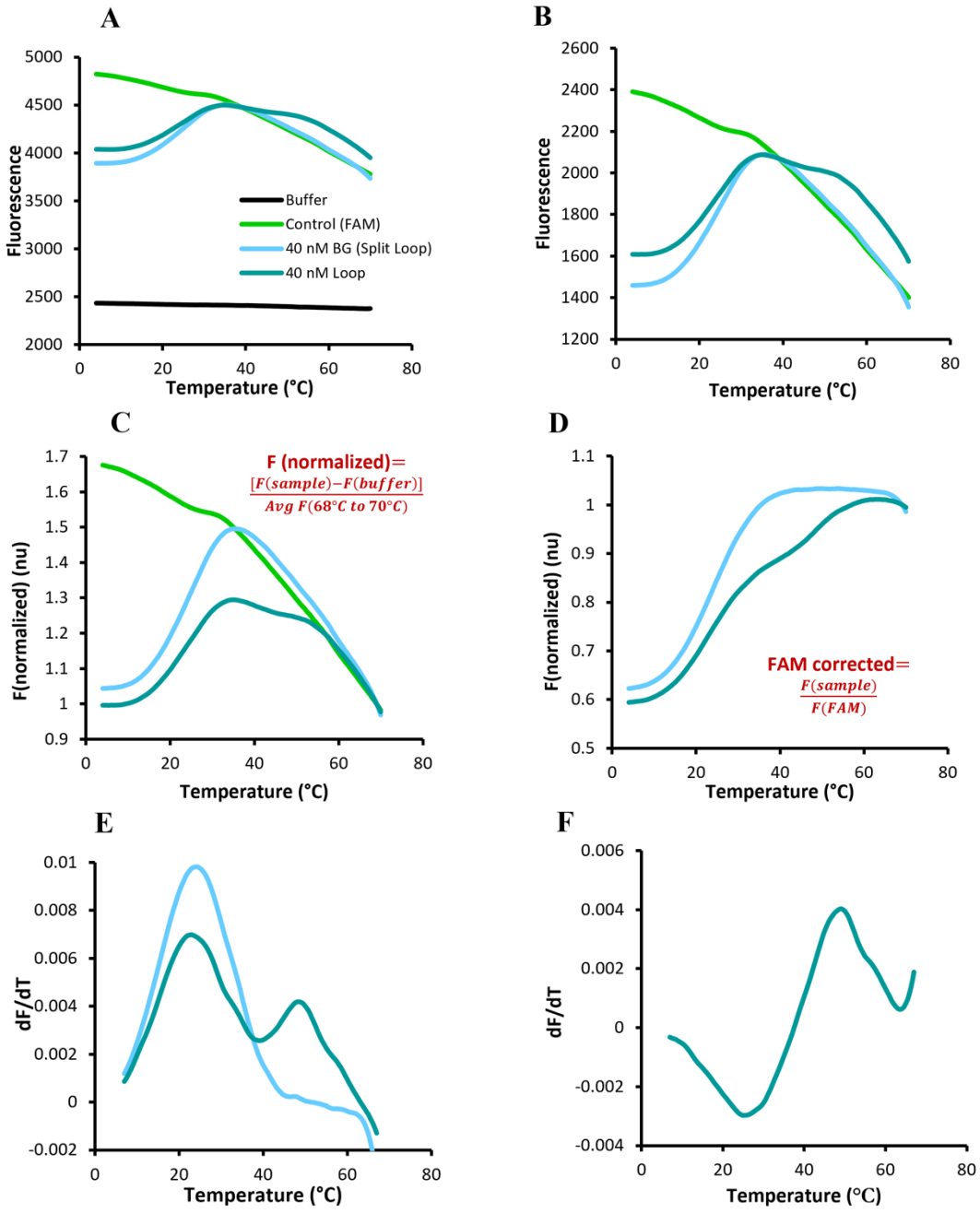

Figure 3.1 Data analysis demonstration using DNA loop samples, using Microsoft Excel **(A)** Raw fluorescence data obtained from qPCR instrument. **(B)** Subtraction of buffer fluorescence from each set of data, to correct for instrument background (black trace). **(C)** Normalized fluorescence of each set of data, to the average fluorescence values in 68 to 70 °C range. **(D)** Each set of data is corrected to the maximum fluorescence of the FAM strand (green trace). **(E)** A 13-point Savitzky-Golay filter was used to obtain the first derivative curve, dF/dT from the data set in (D) above. **(F)**

Subtraction of blank dF/dT curve (light blue trace), from derivative data obtained in **(E)** above. The appearance of two peaks in low temperature and high temperatures clearly indicates the proximity dependent changes. (Similar data analysis was performed for both anti-digoxigenin and thrombin detection).

3.3 Results and discussion

3.3.1 System designs

Inspired by our previous work on the electrochemical proximity assay (ECPA) and Heyduk's molecular pincer assay, we have developed a Förster resonance energy transfer (FRET) based assay for antibody sensing, leveraging thermal denaturation curves of DNA [5, 15, 26, 31]. Herein, the antibody sensing system carries four DNA strands, where two are labelled with small antigen molecules that bind to an antibody (**Figure 3.2A**). The remaining two strands act as signaling oligonucleotides. One end of each strand is labelled with a fluorescent molecule (FAM) or quencher molecule (BHQ), with 7 bases complementary to each other. The opposite ends of the two signaling strands are complementary to the antigen labeled strands, through 20 base pairs (bp). Addition of target antibody results in the spontaneous binding of antigens, which brings the FAM and quencher labelled strands into close proximity. Due to the drastic increase in local concentrations of the two signaling oligonucleotides, the short 7 bases undergo hybridization, leading to quenched fluorescence. This target-induced hybridization of short DNA strands results in a more entropically stable complex, which is analogous to a stem loop [22]. Thermal scanning of this system will result in denaturation of the 7 bp and eventually restore fluorescence.

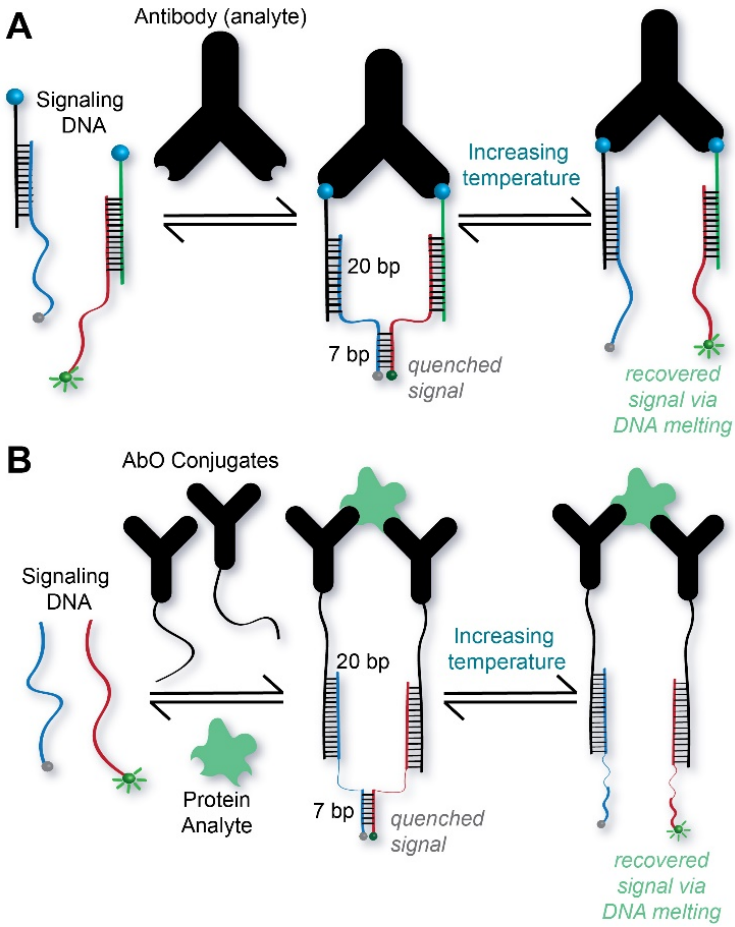

Figure 3.2 General mechanisms for proximity-based antibody or AbO conjugate sensing, leveraging TFA. **(A)** Spontaneous binding of antigens to the two paratopes of the antibody analyte promotes hybridization of signaling oligos, leading to quenched fluorescence. Without antibody, signaling oligos are most stable in the unhybridized form (leftmost). **(B)** Similar signaling probes can be used to detect protein analytes or AbO conjugates. Relative quantities of all of these complexes can be studied by thermal melting and TFA.

The second system presented in this work uses similar signaling DNA strands based on FAM-labeled DNA and a quencher-labeled DNA, yet in this case the FRET signal reports either the presence of a protein analyte or and AbO conjugate (**Figure 3.2B**). In further work discussed below, this proximity assay system is used in a unique fashion to evaluate the valency of the AbO conjugates.

3.3.2 TFA using DNA loop as target

Initially, to experimentally mimic the probe-target proximity complexes (signal) in **Figure 3.2**, we used an 80 nucleotide (80-nt) DNA loop. As given in **Figure 3.3A**, the DNA loop carried 20-nt complementary regions at both ends, designed to bind the probe (signaling) DNAs. Incubation of the DNA loop with probe DNAs led to stabilization of the 7 bp segments, akin to intramolecular hybridization. This resulted in FRET based quenching. Split loop strands (40 nt each) bound to probe DNAs, mimicking the background complex, which is formed because of intermolecular hybridization. Considering the innate stability of intramolecular over intermolecular hybridization, the signal molecule will possess a higher melting temperature (T_m) than the background [22, 27]. By analyzing the differential melt curves (dF/dT), we were able to observe a clear separation between signal and background melt peaks at ~43 °C and ~20 °C respectively (**Figure 3.3B**).

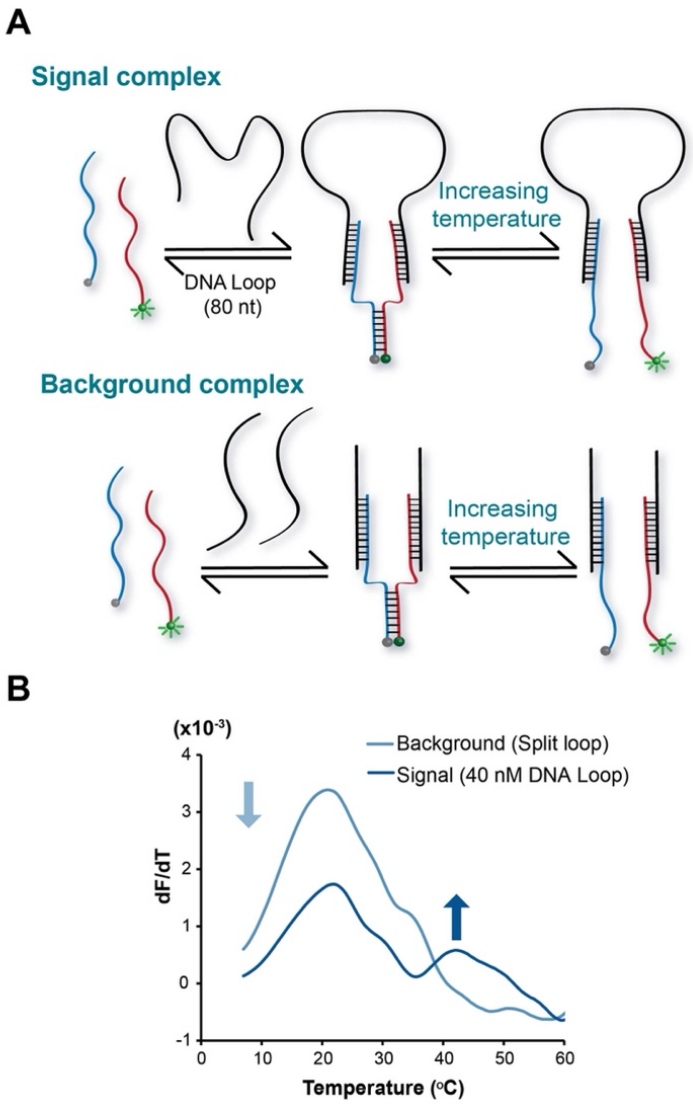

Figure 3.3 Use of a DNA loop-based experimental model to mimic probe-target interaction. **(A)** 80 nt DNA loop mimicked the signaling complex (top) and a split version of the loop, carrying two 40 nt DNA strands, mimicked the background complex (bottom). **(B)** dF/dT curves which show a clear loop-dependent signal and background peak separation at high (~43 °C) and low (~20 °C) temperatures.

3.3.3 TFA for antibody detection

Since experiments with the DNA loop model were successful, we advanced forward by modifying the system for antibody detection. To do so, we used the anti-digoxigenin antibody (anti-dig) and its antigen, digoxigenin (dig). As shown in **Figure 3.2A**, spontaneous binding of dig-labelled signaling DNA to anti-dig should lead to quenching of fluorescence. This signaling complex, like the DNA loop model, should be more stable compared to the background complex. The background complex is formed through hybridization of two dig-labelled signaling DNA only (i.e. in the absence of anti-dig) **(Figure 3.4A)**. Therefore, when analyzing dF/dT curves, similar to the loop, we should be able to observe two melt peaks: a high T_m corresponding to the signal and a low T_m corresponding to the background. However, when interpreting both fluorescence and dF/dT curves for this assay, we did not observe an obvious change in the melt transition (compared to control, FAM-DNA) or an obvious melt peak at higher temperatures (which should correspond to the "signal") (**Figure 3.4B and 3.4C**). Although there may have been a slight antibody-dependent shoulder present near the background T_m, the overall quenching efficiency of the system was observed to be only ~5% to 8%. Together, these results suggested that the assay developed for antibody detection was not functioning as hypothesized.

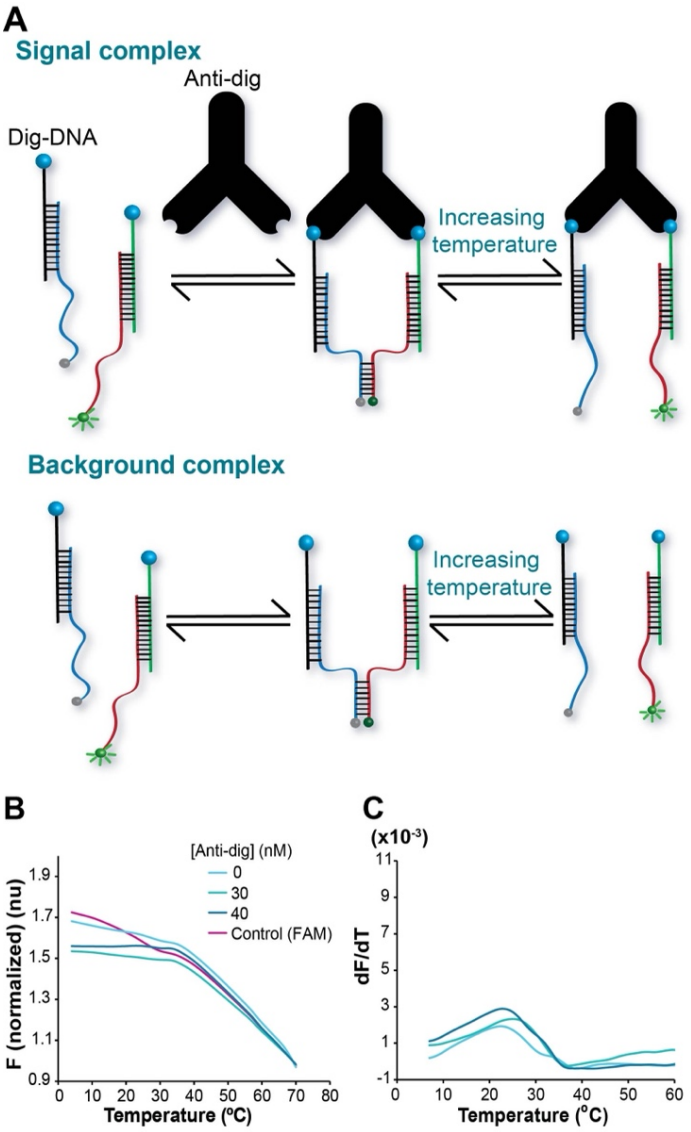

Figure 3.4 Antibody sensing with TFA without flexible linkers. **(A)** Mechanism for antibody sensing using anti-dig and digoxigenin. Signaling complex is formed as a result of antibody binding (top) and background complex is formed in the absence of target antibody (bottom). **(B)** Normalized fluorescence showed poor quenching, and **(C)** dF/dT curves did not show an obvious signal peak at high temperatures, although a background peak at ~23 °C was present.

3.3.4 Assay improvement through probe flexibility

We reasoned that poor quenching was a result of weak hybridization between the shorter 7 bp region of the signaling strands. As shown in **Figure 3.5A** (left), a 14-nt ssDNA linker separates the 20-bp complementary region (to dig-labelled DNA) from the shorter 7 bp region of the signaling DNA strand. The complete length of the DNA strands (dig-DNA hybridized to signaling DNA) is theoretically longer (~30 nm) than the maximum distance (~15 nm) separating the two paratopes and should therefore, ideally allow the 7 bp to hybridize[32]. However, we hypothesized that the conformational rigidity imposed on the system due to the use of four DNA strands may be preventing the efficient hybridization of the shorter 7 bp region. More specifically, the 14-nt ssDNA (~8.8 nm) linkers of the signaling DNA strands were perhaps too rigid to promote annealing of the 7 bp. Therefore, we assumed that if this ~8.8 nm linker was made more flexible, efficient binding could be promoted and result in increased quenching (i.e. higher FRET efficiency) of the sensor in the presence of target antibody.

Polyethylene glycol (PEG) linkers have been used in instances where protein molecules such as enzymes or antibodies are required to be attached with oligonucleotides, such that sufficient flexibility to the system is introduced. The Heyduk group used PEG linkers in their FRET-based sensors to improve assay performance, since it considerably reduced steric effects [23, 26, 31, 33, 34], and the Plaxco group also used this approach to increase current response in electrochemical antibody sensors[35]. Therefore, as a potential improvement to our system's design, we substituted the ssDNA linker (~8.8 nm) with a similar length of commercially synthesized DNA with PEG spacers (~9.6 nm) (**Figure 3.5A**, right). This modification also reduced the molecular weight of the linker by ~3.4 fold. In comparison to the original TFA based assay, a drastic increase in quenching efficiency was observed (from ~8% to ~40%) using the PEG spacers (**Figure 3.5B**).

Additionally, we began to observe two clear melt peaks in the dF/dT curves, one at ~23 °C (corresponding to the background) and another new peak at higher temperature of ~40 °C (corresponding to the signal) (**Figure 3C**). The T_m of the background peak with PEG spacers was essentially equivalent to that of the more rigid ssDNA spacers, which would be expected since background 7 bp annealing should be independent of spacer flexibility. It is noteworthy that the dF/dT peaks for background at ~23 °C were also more intense using the flexible probes (0.011 in **Figure 3.5C** versus 0.003 in **Figure 3.4C**); this represents another advantage from an assay standpoint. We have not yet performed extensive modeling of the complex formation and equilibria involved, thus the reasoning for this increase is still under investigation. The working hypothesis is that the equilibrium is shifted further toward signal complexes by using flexible linkers on the probes, thereby further stabilizing background complexes as well.

Based on previous studies of proximity assay systems[22, 27, 34] the new signal peak at ~40 °C in **Figure 3.5C** indicates that the PEG spacers introduced further entropic stabilization to the full proximity complex. For additional confirmation, this effect was validated with our previously developed assay system [27], a thrombin-sensing proximity assay using aptamer probes. As shown in **Figure 3.6** and the accompanying text, flexible PEG spacers improved the thrombin proximity assay in a similar fashion, increasing TFA peak heights and providing further distinction between signal and background peaks.

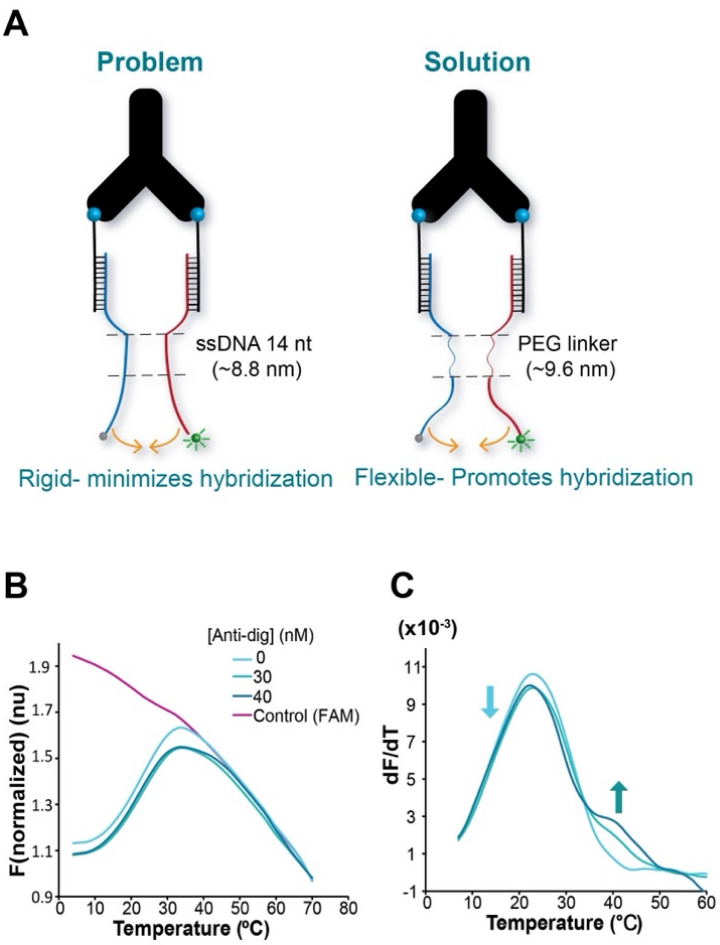

Figure 3.5 (A) The relative rigidity of the ssDNA linker likely prevents efficient hybridization of the 7 bp (left). Substitution of 14 nt ssDNA linker with PEG spacers promoted efficient hybridization (right). **(B)** PEG modification led to efficient quenching of fluorescence at lower temperatures (left), and dF/dT curves now showed two melt peaks at high and low temperatures, corresponding to signal and background respectively.

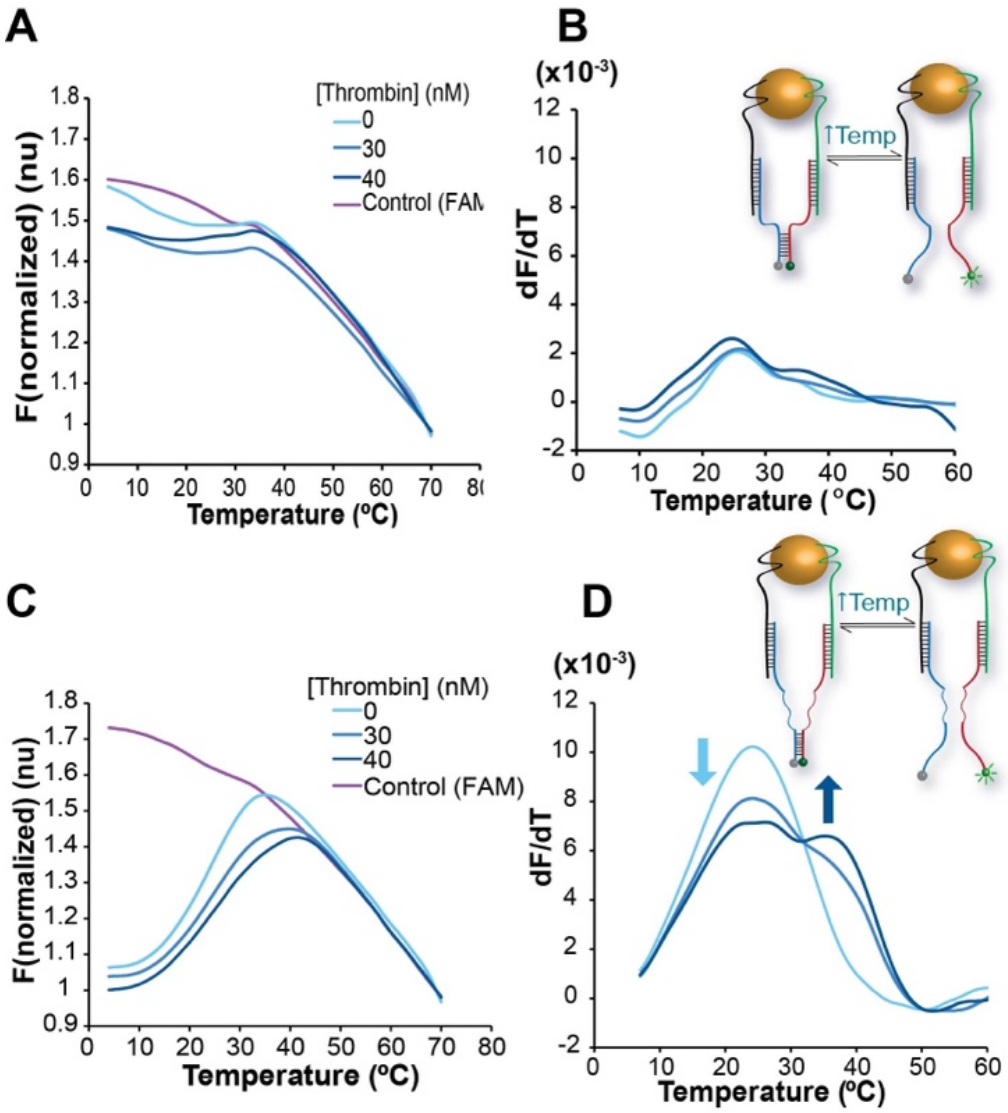

Figure 3.6 Assay response to thrombin, pre- and post-modification with PEG spacers. **(A)** Fluorescence curves showing poor quenching with ssDNA spacers. **(B)** Derivative curve does not show clear signal peaks at higher temperatures. **(C)** PEG spacers resulted in more efficient quenching post-modification, as hypothesized. **(D)** dF/dT curves with PEG spacers showed clearly defined background and signal peaks, which were concentration dependent.

The sensor with more flexible probes (**Figure 3.5A**) was then calibrated for antibody quantification. As the concentration of the anti-dig analyte was increased, not only did the peaks shift to higher temperatures, but also an increase in peak heights at ~40 °C and decrease in peak

heights at ~23 °C were observed. This indicated that the developed TFA based sensor was responding to target concentrations, as expected (**Figure 3.7A**, left). Further treatment of data, i.e. subtraction of background (0 nM anti-dig) derivative from the target derivative curves also demonstrated a clear growing minima and maxima for the background and signal curves respectively, in a concentration dependent fashion (**Figure 3.7A**, right). Followed by this, we assessed the limit of detection (LOD) of the system to be 7 nM of anti-dig, based on 3σ of the blank (**Figure 3.7B**).

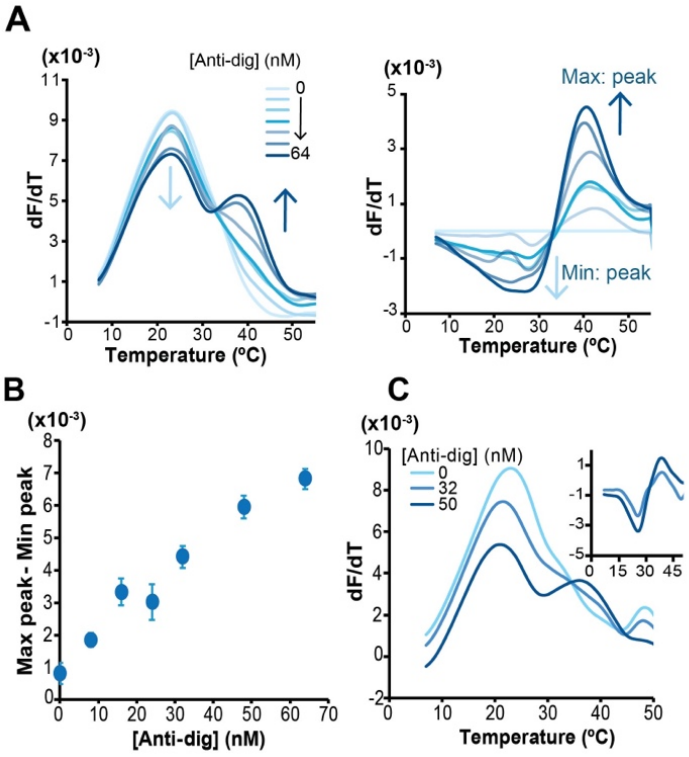

Figure 3.7 (A) dF/dT curves from anti-dig detection in buffer. Concentration dependent changes in background and signal peaks (left). Background subtracted dF/dT curves show clear differences in signal and background in response to anti-dig (right), a key feature in discriminating signal from background in complex matrices. **(B)** Calibration curve obtained by subtracting the minimum peak height (background) from corresponding maximum peak height (signal). **(C)** Detection of anti-dig in 90 % human plasma. Inset shows a clear differentiation of signal and background after background correction.

3.3.5 Antibody sensing in human plasma

Although a number of promising FRET based techniques have been developed for antibody detection, their applications are often hampered in biological fluids due to enzymatic degradation of samples and autofluorescence. While methods have been adopted to minimize enzymatic degradation, autofluorescence still makes it challenging to analyze targets in biological fluids. As mentioned earlier, a key advantage of TFA is its ability to negate effects of autofluorescence [10, 14, 27]. Here, we applied the developed assay to detect anti-dig mixed in minimally diluted, 90% human plasma. As shown in **Figure 3.7C**, we were able to observe two clear melt peaks for 32 nM and 50 nM anti-dig in 90% plasma, in a concentration dependent manner.

3.3.6 Application of TFA to the study of antibody oligonucleotide (AbO) conjugate valency

Antibodies produced by the immune system are not only relevant as analytes, but they are also used in detecting other clinically relevant biomarkers. With the development and evolution of sandwich immunoassays, antibodies have been used to detect targets such as small molecules, proteins, cells, and viruses [36]. Antibodies have also been coupled to oligonucleotides (AbOs), and these conjugates are extensively used in proximity-based analyte detection [10, 15, 31, 36-38]. Although these constructs are useful in analyte sensing, assay sensitivity can be compromised when multivalent AbOs result in increased target-independent DNA hybridization (background). The degree of degree of conjugation (DoC) defines the average number of DNA strands bound to an antibody molecule [20, 36], and AbOs with DoC > 1 are usually less desirable for assay systems than those with DoC = 1.

Typically, cumbersome gel-based separations (as in **Figure 3.10**) that require larger reagent volumes are used to study AbO valency. Here, we show that our TFA approach can be useful as an

alternative, simplified readout with minimized reagent consumption. A proximity FRET immunoassay protocol for insulin sensing was designed (**Figure 3.2B** and **Figure 3.8A**), which was similar to previous studies [10, 16, 31] except for the inclusion of the flexible linkers. Custom synthesized and purified monovalent insulin-binding AbOs (DoC = 1) were prepared, and FRET probes with flexible PEG linkers were used for TFA studies to determine signal and background levels. Both multivalent and monovalent AbOs were used for comparison (**Figure 3.8A**). TFA studies were also carried out using a DNA loop as a control system that should more closely resemble monovalent AbO probes with DoC = 1.

TFA data from thermal scans are shown in **Figure 3.8B-E**. The DNA loop (**Figure 3.8B**) behaved as expected—similar to the system in **Figure 3.3B**—where the split loop resulted in only one background peak at ~22 °C, while the complete loop gave two peaks, i.e. background (~22 °C) and signal (~50 °C) peaks. Monovalent AbOs (**Figure 3.8C**) exhibited a very similar background peak at ~24 °C. Upon addition of 20 nM insulin analyte, while there was not a clearly observed signal melting peak, the intensity around 50 °C shifted higher than the background, and the background peak at ~24 °C shifted lower. Additional dF/dT difference data is shown in **Figure 3.9**, confirming the insulin responsiveness. Multivalent AbOs (**Figure 3.8D**) were less responsive to insulin, and the background peak was much wider and appeared to contain a mixture of distinct complexes. Interestingly, it appeared that TFA peak widths (in dF/dT curves) were more useful at distinguishing monovalent from multivalent AbOs. As seen in the TFA data and highlighted further in **Figure 3.8E**, when a more homogeneous population of probes was analyzed by TFA, e.g. the DNA loop or the monovalent AbOs, the background peak widths at half height were smaller ($\Delta T \approx 15$ °C). By contrast, the heterogeneous, multivalent probes showed much wider TFA peaks ($\Delta T \approx 27$ °C).

Due to the limited availability and the difficulty in synthesizing monovalent AbOs, additional measurements were not carried out in this work. Although further optimization could feasibly be performed in future studies, these data do confirm that TFA, when using flexible PEG spacers in the DNA strands, can be a useful tool to screen for valency and purity of AbO conjugates. Along with the simple, mix-and-read workflow of TFA, the low cost of this approach is an advantage as well. TFA studies required only 0.5 pmol of AbO probes per well, while the analytical gel separation protocol (**Figure 3.10** and methods) required 6 pmol of AbO probes per well. Our TFA approach thus gave a 12-fold reduction in the required amount for analyzing this precious reagent.

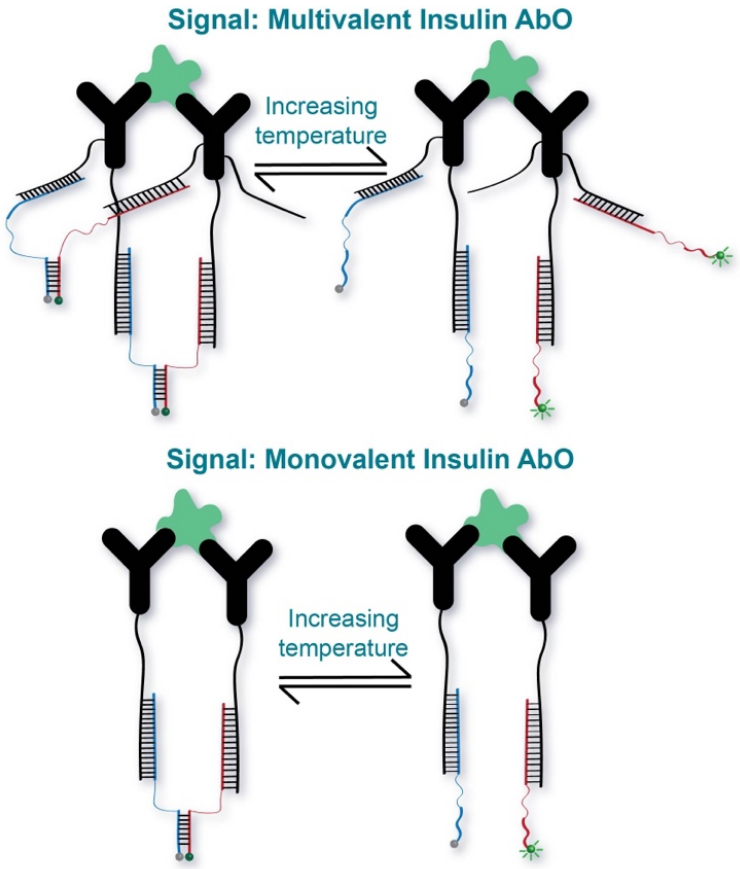
Signal: Multivalent Insulin AbO
Increasing temperature
Signal: Monovalent Insulin AbO
Increasing temperature

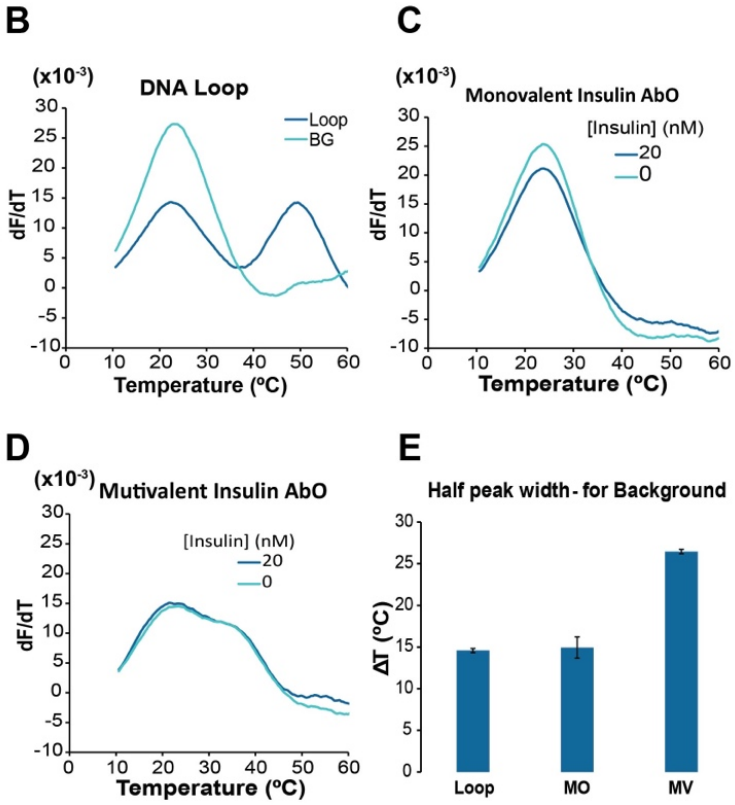
B
(x10-3)
DNA Loop
Loop
BG
dF/dT
Temperature (ºC)
C
(x10-3)
Monovalent Insulin AbO
[Insulin] (nM)
20
0
dF/dT
Temperature (ºC)
D
(x10-3)
Mutivalent Insulin AbO
[Insulin] (nM)
20
0
dF/dT
Temperature (ºC)
E
Half peak width - for Background
ΔT (ºC)
Loop
MO
MV

Figure 3.8 TFA with flexible linkers was validated for studying AbO conjugate valency. **(A)** Proximity immunoassays for insulin sensing were developed with both multivalent and monovalent AbOs containing flexible DNA linkers. Multivalent AbOs (top) can lead to more than one hybridization event per probe, while monovalent AbOs (bottom) should eliminate this possibility. **(B)** DNA loop control system, showing defined signal and background peaks. **(C)** TFA scans of monovalent AbOs were similar to the DNA loop, while **(D)** multivalent AbOs showed broad peaks and limited insulin response. **(E)** TFA peak widths at half height in dF/dT curves were useful for distinguishing the valency of AbOs.

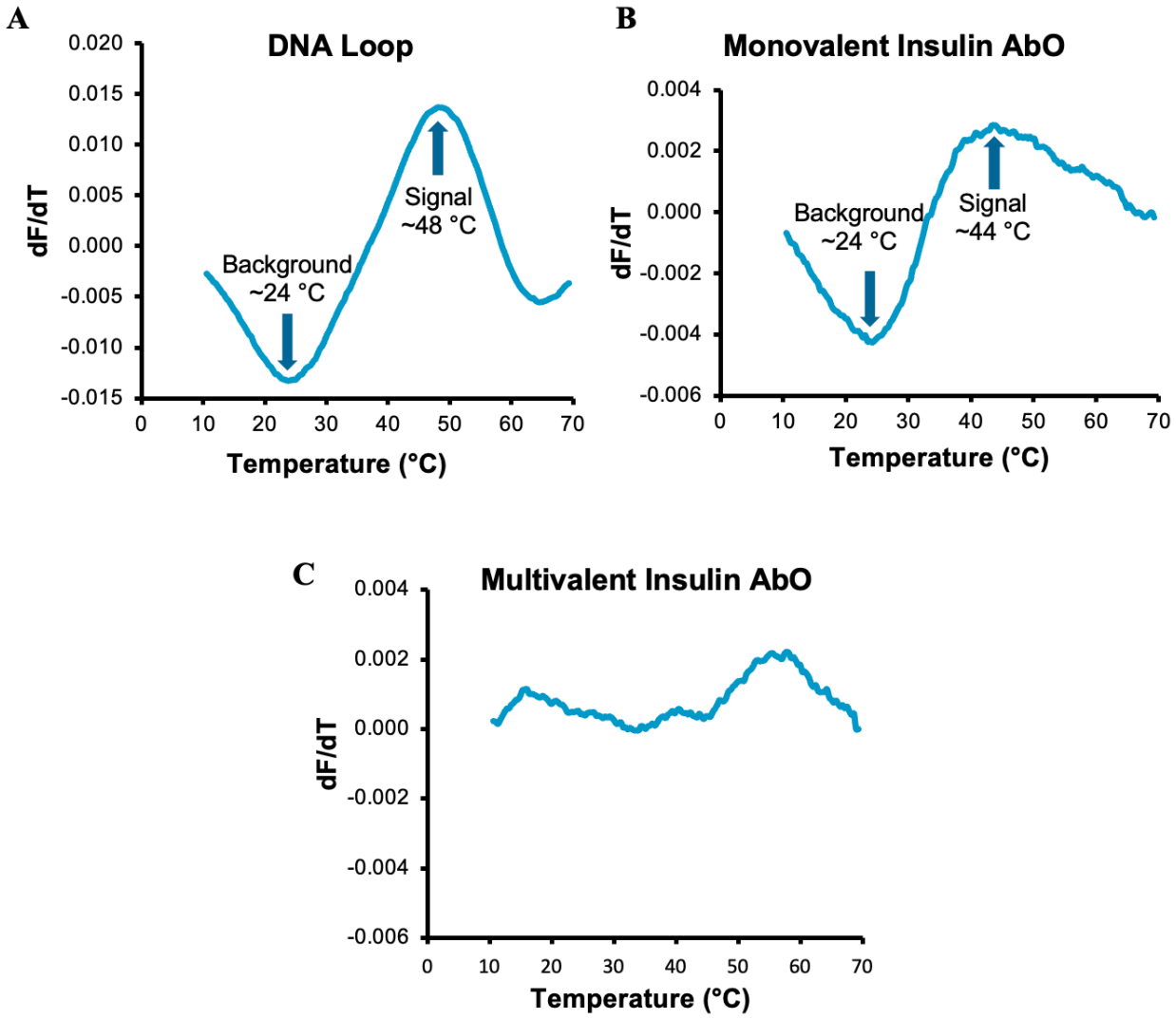

Figure 3.9 AbO valency studies with dF/dT difference curves, where the background curve has been subtracted from the signal curve. **(A)** The curve for the DNA loop demonstrates a clearly separated minima and maxima curve corresponding to the background and signal, respectively. **(B)** In response to insulin addition, monovalent AbO constructs also demonstrated a similar dF/dT difference curve structure compared to the DNA loop, with a minimum corresponding to the background and a maximum corresponding to insulin-dependent signal complex. **(C)** While the dF/dT difference curve for multivalent insulin AbOs did indicate a possible signal peak around 55 °C, the majority of the curve showed nearly a zero insulin-dependent change, and the overall structure of the curve was significantly different from the DNA loop control system.

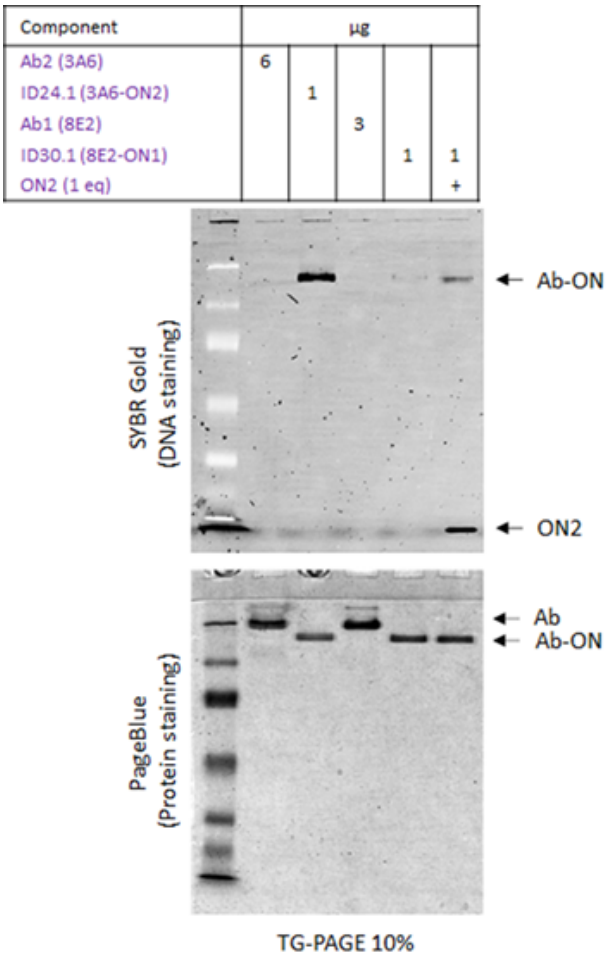

Figure 3.10 Gel images of monovalent insulin AbO. Analytical native PAGE 10% of: lane 1 - molecular ladder, lane 2 - anti-insuline Ab 3A6, lane 3 - AbO conjugate 3A6-ON2, lane 4 - anti-insuline Ab 8E2, lane 5 - AbO conjugate 8E2-ON1, lane 6 - 8E2-ON1 + 1 equiv of ON2. The table

above gel shows amount of loaded protein per well: 1 ug of Ab = 7 pmol. The complementary ON2 was added (lane 6) to visualize better the SYBR Gold staining of 8E2-ON1 by forming a dsDNA-Ab conjugate.

3.4 Conclusions

This work reports several unique applications of thermofluorimetric analysis (TFA), which can be achieved with a fast, mix-and-read workflow using standard qPCR instrumentation. First, a new antibody sensing TFA assay was developed. During the assay development, it was discovered that flexible spacers (PEG) within the signaling DNA strands gave drastic improvements in the assay performance, an effect that we expect to be generalizable based on its similar performance in aptamer based assay (see supporting material). This TFA sensor should provide a fast, easily accessible technique for users to quantify antibody amounts. Secondly, a related TFA method was developed to evaluate antibody-oligonucleotide (AbO) conjugate valency, where clear discrimination of monovalent AbOs from multivalent AbOs was demonstrated using TFA peak widths, even with a 12-fold reduction in AbO amounts analyzed. To our knowledge, this is an entirely new application of TFA methodology, one which could be expanded on in future work. Perhaps this simple, mix-and-read approach could be used to evaluate a variety of other bioconguates that include oligonucleotides. Overall, this work has expanded upon the utility of TFA methods.

3.5 Reference

(1) Bracaglia, S.; Ranallo, S.; Plaxco, K. W.; Ricci, F. Programmable, Multiplexed DNA Circuits Supporting Clinically Relevant, Electrochemical Antibody Detection. *ACS Sens* **2021**, *6* (6), 2442-2448. DOI: 10.1021/acssensors.1c00790 From NLM Medline.
(2) Parolo, C.; Idili, A.; Ortega, G.; Csordas, A.; Hsu, A.; Arroyo-Currás, N.; Yang, Q.; Ferguson, B. S.; Wang, J.; Plaxco, K. W. Real-Time Monitoring of a Protein Biomarker. *ACS Sensors* **2020**, *5* (7), 1877-1881. DOI: 10.1021/acssensors.0c01085.
(3) Rossetti, M.; Ippodrino, R.; Marini, B.; Palleschi, G.; Porchetta, A. Antibody-Mediated Small Molecule Detection Using Programmable DNA-Switches. *Anal Chem* **2018**, *90* (13), 8196-8201. DOI: 10.1021/acs.analchem.8b01584.
(4) Yang, X.; Tang, Y.; Alt, R. R.; Xie, X.; Li, F. Emerging techniques for ultrasensitive protein analysis. *Analyst* **2016**, *141* (12), 3473-3481. DOI: 10.1039/c6an00059b.
(5) Hu, J.; Wang, T.; Kim, J.; Shannon, C.; Easley, C. J. Quantitation of femtomolar protein levels via direct readout with the electrochemical proximity assay. *J Am Chem Soc* **2012**, *134* (16), 7066-7072. DOI: 10.1021/ja3000485 From NLM Medline.
(6) Ranallo, S.; Rossetti, M.; Plaxco, K. W.; Vallee-Belisle, A.; Ricci, F. A Modular, DNA-Based Beacon for Single-Step Fluorescence Detection of Antibodies and Other Proteins. *Angew Chem Int Ed Engl* **2015**, *54* (45), 13214-13218. DOI: 10.1002/anie.201505179.
(7) Janssen, K. P.; Knez, K.; Spasic, D.; Lammertyn, J. Nucleic acids for ultra-sensitive protein detection. *Sensors (Basel)* **2013**, *13* (1), 1353-1384. DOI: 10.3390/s130101353.
(8) Beaudet, L.; Rodriguez-Suarez, R.; Venne, M.-H.; Caron, M.; Bédard, J.; Brechler, V.; Parent, S.; Bielefeld-Sévigny, M. AlphaLISA immunoassays: the no-wash alternative to ELISAs for research and drug discovery. *Nature Methods* **2008**, *5* (12), an8-an9.
(9) Rissin, D. M.; Kan, C. W.; Campbell, T. G.; Howes, S. C.; Fournier, D. R.; Song, L.; Piech, T.; Patel, P. P.; Chang, L.; Rivnak, A. J. Single-molecule enzyme-linked immunosorbent assay detects serum proteins at subfemtomolar concentrations. *Nature biotechnology* **2010**, *28* (6), 595-599.
(10) Hu, J.; Easley, C. J. Homogeneous Assays of Second Messenger Signaling and Hormone Secretion Using Thermofluorimetric Methods That Minimize Calibration Burden. *Anal Chem* **2017**, *89* (16), 8517-8523. DOI: 10.1021/acs.analchem.7b02229.
(11) Khuda, N.; Somasundaram, S.; Easley, C. J. Electrochemical Sensing of the Peptide Drug Exendin-4 Using a Versatile Nucleic Acid Nanostructure. *ACS Sensors* **2022**, *7* (3), 784-789. DOI: 10.1021/acssensors.1c02336.
(12) Yan, X.; Le, X. C.; Zhang, H. Antibody-Bridged Beacon for Homogeneous Detection of Small Molecules. *Analytical Chemistry* **2018**, *90* (16), 9667-9672. DOI: 10.1021/acs.analchem.8b02510.
(13) Fredriksson, S.; Gullberg, M.; Jarvius, J.; Olsson, C.; Pietras, K.; Gústafsdóttir, S. M.; Östman, A.; Landegren, U. Protein detection using proximity-dependent DNA ligation assays. *Nature biotechnology* **2002**, *20* (5), 473-477.
(14) Hu, J.; Kim, J.; Easley, C. J. Quantifying Aptamer-Protein Binding via Thermofluorimetric Analysis. *Anal Methods* **2015**, *7* (17), 7358-7362. DOI: 10.1039/c5ay00837a.
(15) Hu, J.; Yu, Y.; Brooks, J. C.; Godwin, L. A.; Somasundaram, S.; Torabinejad, F.; Kim, J.; Shannon, C.; Easley, C. J. A reusable electrochemical proximity assay for highly selective, real-time protein quantitation in biological matrices. *J Am Chem Soc* **2014**, *136* (23), 8467-8474. DOI: 10.1021/ja503679q From NLM Medline.

(16) Li, F.; Lin, Y.; Lau, A.; Tang, Y.; Chen, J.; Le, X. C. Binding-Induced Molecular Amplifier as a Universal Detection Platform for Biomolecules and Biomolecular Interaction. *Anal Chem* **2018**, *90* (14), 8651-8657. DOI: 10.1021/acs.analchem.8b01985.
(17) Zhang, H.; Lai, M.; Zuehlke, A.; Peng, H.; Li, X. F.; Le, X. C. Binding-Induced DNA Nanomachines Triggered by Proteins and Nucleic Acids. *Angew Chem Int Ed Engl* **2015**, *54* (48), 14326-14330. DOI: 10.1002/anie.201506312.
(18) Rossetti, M.; Brannetti, S.; Mocenigo, M.; Marini, B.; Ippodrino, R.; Porchetta, A. Harnessing effective molarity to design an electrochemical dna-based platform for clinically relevant antibody detection. *Angewandte Chemie* **2020**, *132* (35), 15083-15088.
(19) Yang, K.; Huo, M.; Guo, Y.; Yang, Y.; Wu, J.; Ding, L.; Ju, H. Target-induced cyclic DNAzyme formation for colorimetric and chemiluminescence imaging assay of protein biomarkers. *Analyst* **2017**, *142* (19), 3740-3746. DOI: 10.1039/c7an00413c.
(20) Bezerra, A. B.; Kurian, A. S. N.; Easley, C. J. Nucleic-Acid Driven Cooperative Bioassays Using Probe Proximity or Split-Probe Techniques. *Anal Chem* **2021**, *93* (1), 198-214. DOI: 10.1021/acs.analchem.0c04364 From NLM Medline.
(21) Wen, G.; Ju, H. Enhanced Photoelectrochemical Proximity Assay for Highly Selective Protein Detection in Biological Matrixes. *Anal Chem* **2016**, *88* (16), 8339-8345. DOI: 10.1021/acs.analchem.6b02740.
(22) Zhang, H.; Li, F.; Dever, B.; Wang, C.; Li, X. F.; Le, X. C. Assembling DNA through affinity binding to achieve ultrasensitive protein detection. *Angew Chem Int Ed Engl* **2013**, *52* (41), 10698-10705. DOI: 10.1002/anie.201210022.
(23) Heyduk, E.; Heyduk, T. Nucleic acid-based fluorescence sensors for detecting proteins. *Analytical Chemistry* **2005**, *77* (4), 1147-1156.
(24) Joonyul Kim, J. H., Rebecca S. Sollie and Christopher J. Easley. Improvement of Sensitivity and dynamic range in proximity ligation assays by assymetric connector hybridization. *ACS analytical chemistry* **2010**, *82* (16), 6976-6982.
(25) Ren, K.; Wu, J.; Yan, F.; Zhang, Y.; Ju, H. Immunoreaction-triggered DNA assembly for one-step sensitive ratiometric electrochemical biosensing of protein biomarker. *Biosens Bioelectron* **2015**, *66*, 345-349. DOI: 10.1016/j.bios.2014.11.046.
(26) Heyduk, E.; Dummit, B.; Chang, Y.-H.; Heyduk, T. Molecular pincers: antibody-based homogeneous protein sensors. *Analytical chemistry* **2008**, *80* (13), 5152-5159.
(27) Kim, J.; Hu, J.; Bezerra, A. B.; Holtan, M. D.; Brooks, J. C.; Easley, C. J. Protein quantification using controlled DNA melting transitions in bivalent probe assemblies. *Anal Chem* **2015**, *87* (19), 9576-9579. DOI: 10.1021/acs.analchem.5b03432.
(28) Porchetta, A.; Ippodrino, R.; Marini, B.; Caruso, A.; Caccuri, F.; Ricci, F. Programmable Nucleic Acid Nanoswitches for the Rapid, Single-Step Detection of Antibodies in Bodily Fluids. *J Am Chem Soc* **2018**, *140* (3), 947-953. DOI: 10.1021/jacs.7b09347.
(29) Ranallo, S.; Sorrentino, D.; Ricci, F. Orthogonal regulation of DNA nanostructure self-assembly and disassembly using antibodies. *Nat Commun* **2019**, *10* (1), 5509. DOI: 10.1038/s41467-019-13104-6.
(30) Moreno, M.; García-Sacristán, A.; Martín, M. E.; González, V. M. Enzyme-Linked Oligonucleotide Assay (ELONA). In *Nucleic Acid Aptamers: Selection, Characterization, and Application*, Springer, 2022; pp 235-242.
(31) Heyduk, E.; Moxley, M. M.; Salvatori, A.; Corbett, J. A.; Heyduk, T. Homogeneous insulin and C-Peptide sensors for rapid assessment of insulin and C-peptide secretion by the islets. *Diabetes* **2010**, *59* (10), 2360-2365. DOI: 10.2337/db10-0088.

(32) Galanti, M.; Fanelli, D.; Piazza, F. Conformation-controlled binding kinetics of antibodies. *Sci Rep* **2016**, *6*, 18976. DOI: 10.1038/srep18976.
(33) Tian, L.; Heyduk, T. Bivalent ligands with long nanometer-scale flexible linkers. *Biochemistry* **2009**, *48* (2), 264-275.
(34) Tian, L.; Heyduk, T. Antigen peptide-based immunosensors for rapid detection of antibodies and antigens. *Analytical chemistry* **2009**, *81* (13), 5218-5225.
(35) Ogden, N. E.; Kurnik, M.; Parolo, C.; Plaxco, K. W. An electrochemical scaffold sensor for rapid syphilis diagnosis. *Analyst* **2019**, *144* (17), 5277-5283. DOI: 10.1039/c9an00455f From NLM Medline.
(36) Dovgan, I.; Koniev, O.; Kolodych, S.; Wagner, A. Antibody–oligonucleotide conjugates as therapeutic, imaging, and detection agents. *Bioconjugate Chemistry* **2019**, *30* (10), 2483-2501.
(37) Gullberg, M.; Gustafsdottir, S. M.; Schallmeiner, E.; Jarvius, J.; Bjarnegard, M.; Betsholtz, C.; Landegren, U.; Fredriksson, S. Cytokine detection by antibody-based proximity ligation. *Proc Natl Acad Sci U S A* **2004**, *101* (22), 8420-8424. DOI: 10.1073/pnas.0400552101.
(38) Gustafsdottir, S. M.; Schlingemann, J.; Rada-Iglesias, A.; Schallmeiner, E.; Kamali-Moghaddam, M.; Wadelius, C.; Landegren, U. In vitro analysis of DNA-protein interactions by proximity ligation. *Proc Natl Acad Sci U S A* **2007**, *104* (9), 3067-3072. DOI: 10.1073/pnas.0611229104.

Chapter 4

An Electrochemical Proximity Assay (ECPA) for Antibody Detection Incorporating Flexible Spacers for Improved Performance

In this chapter, we introduce another application of the electrochemical proximity assay which was previously developed by our lab for insulin and thrombin detection [1-3], with a brief introduction to commonly use electrochemical techniques for electrochemical biosensor development.

4.1 Commonly used electrochemical techniques in biosensor development

In general, an electrochemical biosensor is referred to as a device which can provide either quantitative or semiquantitative information regarding the presence or absence of a target using a target recognition element in combination with an electrochemical signal transducer such as an electrode [4]. These methods have high sensitivity with appreciable LODs and are amplification-free, whilst being ideal for point of care, point of need sensor development and adaptable for resource poor settings. Kelly and coworkers categorized the commonly used electrochemical techniques into 5 main sections- conductometric, potentiometric, impedimetric, voltametric or amperometric, and field effect-transistors [4]. In voltammetric biosensors, a potential is applied to the working electrode (WE), with respect to a reference electrode and current is measured. Current is generated at the WE surface as a result of oxidation or reduction of the reactant solution and is measured with the increase in potential. The generated current is usually proportional to the analyte concentration [4, 5]. Commonly used voltametric techniques include- linear sweep voltammetry

(LSV), alternating current voltammetry (ACV), cyclic voltammetry (CV) and pulse voltametric techniques (differential pulse and square wave), anodic and cathodic stripping voltammetry [4].

4.1.1 Cyclic voltammetry (CV)

CV is a powerful and very famous technique used in biosensors. The current of a system is monitored while the potential applied at the WE is scanned in both forward and reversed directions. This is a common method which is used to monitor the oxidation or reduction of a specific molecule and also a valuable tool to studying catalytic reactions [4, 6]. Advantages of this technique includes the extensive availability of simple instrumentation and ample theoretical background which aids the users to interpret data with less effort, making it a popular electrochemical technique amongst non-electrochemists [7]. Although CV possesses these two key advantages, it also bears two major shortcomings. If the analyzing system carries two or more electroactive species, identification between them will be difficult if their charge transfer mechanisms exist too close to each other along the axis of scanned potential, which is attributed to peak asymmetry of the current vs voltage plot [7]. Furthermore, only high analyte concentrations can be assessed by CV, which is a result of high capacitive current arising due to the linear potential scan over time [7].

4.1.2 Square wave voltammetry

In order to improve the speed and assay sensitivity, pulse voltametric techniques such as SWV and differential pulse voltammetry (DPV) have been introduced. The concept of DPV is to subtract the current measured right before a potential step, from the current measured after the potential step. To achieve this, the applied pulse potentials are superimposed into a staircase

(**Figure 4.1**) [8]. Due to the pulsing technique, DPV and SWV are considered to be highly sensitive since the capacitive current tends to decay faster than the faradaic currents [8, 9]. Therefore, such techniques have high signal to noise ratio [9]. In SWV, the staircase pulse is combined with a square wave form. The current is generally measured only at the end of each pulsed potential cycle (**Figure 4.2A**) [10]. Due current sampling at the end of a pulse, the capacitive current can be discriminated, improving signal-to-noise ratio resulting in higher assay sensitivity. Furthermore, sensitivity of SWV is improved due to the net difference between forward and reversed voltametric component (or currents) (**Figure 4.2B**) [10]. The small increase in potential of a square wave cycle is controlled by the input step size. The time of one cycle is determined by the input frequency, which also governs the measurement time [9]. Measurement is done at the end of each cycle, right before the next pulse. The rate of SWV is regulated by the frequency and step size [9].

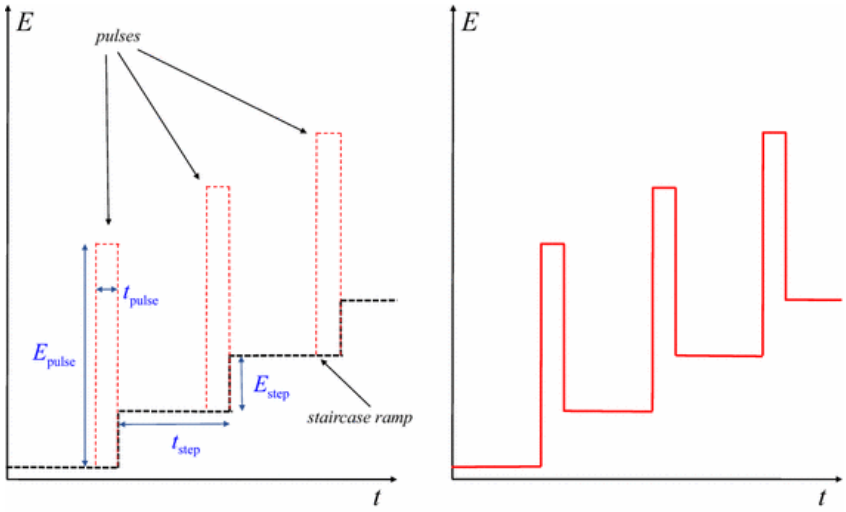

Figure 4.1 A typical DPV plot. Left-Superimposition of staircase ramp with a potential pulses. Right- E vs t post-superimposition. *Reprinted with permission from reference 8. Copyright 2015, Springer Nature.*

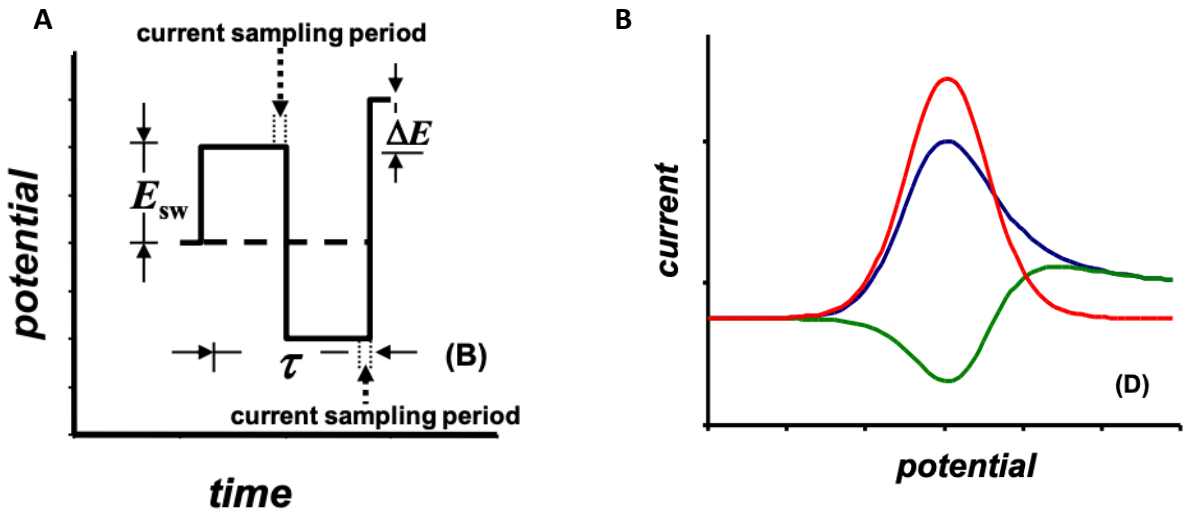

Figure 4.2 Square wave voltammetry. **(A)** Single potential cycle of a SWV, where current is measured at the beginning and end of a single pulse **(B)** A typical current vs potential diagram generated in a SWV. Both forward (blue) and reversed (green) currents are measured, to give the differential current (red). *Reprinted with permission from reference 10. Copyright 2015, Macedonian Journal of Chemistry and Chemical Engineering.*

4.2 Background

Biomarker concentration can be measured with simpler instrumentation as a function of current or impedance using electroanalytical methods. Specifically, DNA-driven electrochemical biosensors leverage the immobilization of oligonucleotide strands tagged with a redox reporter such as methylene blue (MB), [11, 12], or ferrocene[13, 14] on a gold surface using a self-assembled monolayer[15-18]. When a potential is applied, subtraction of non-faradaic current can yield analyte-dependent faradaic current. [19]. Major advantages of electrochemical biosensors are easy-to-operate instrumentation, cost-effective sensing elements, and availability of various efficient and rapid transduction methods; [20-22] and the high sensitivity, good specificity, and compatibility with miniaturization have made electrochemical systems indispensable for point-of-care diagnostics. [23-27]. Different types of electrochemical sensors such as electrochemical aptamer-based sensors (E-

AB),[27-31], E-DNA scaffolds[23, 32-34] molecular pendulum,[13], and a bowtie-shaped DNA nanostructure for immunosensing [35-37], are promising for point-of-care measurements. Previously our group has reported the electrochemical proximity assay (ECPA) capable of detecting proteins as low as the fM range. [2]. ECPA utilizes the proximity binding concept to move an electroactive species (MB) closer to the gold electrode in an analyte-dependent way. [1-3, 38]. Target flexibility, reusability, high sensitivity, and wide dynamic range are notable strengths of the ECPA method. [1, 3]

4.2.1 Electrochemical sensing of antibodies

Antibodies are an important class of biomarkers which are produced in the human body in response to foreign antigens. Immunity against an antigen can be confirmed by identifying the presence and quantifying the level of a specific antibody in the blood. Hence, the detection and quantification of antibodies in human blood is critical for monitoring progression of certain diseases [39, 40]. To develop a simple yet sensitive analytical tool for antibody detection, here we present a novel iteration of ECPA, where the arrangement of the molecular complexes extends from our recently reported thermofluorimetric analysis (TFA) assays (see chapter 2 and 3) for antibody detection [41]. The spontaneous binding of an antibody to DNA-analyte conjugates brings other signaling DNA strands closer to the electrode surface, leading to hybridization with the thiolated DNA. In turn, this brings the redox moiety (MB) closer to the surface, and resultant square-wave voltammetric (SWV) current is proportional to the antibody concentration. Compared to TFA, this electrochemical version of the antibody sensor exhibited better sensitivity and reduced assay time.

Similar to our recent report using fluorescence sensing [41]herein we emphasize the importance of DNA strand flexibility in assay performance. Probe flexibility was achieved by

incorporating polyethylene glycol (PEG) linkers[33, 42-44]into the DNA strands at selected regions. Results demonstrated clearly that including PEG significantly improved analyte-dependent currents. Interestingly, the placement of the spacers provided two distinct enhancements: improved DNA hybridization yield and increased SWV current. Within this chapter, using EC readout gave us a limit of detection (LOD) of 300 pM for anti-digoxigenin antibodies, and the system functioned well in both buffer and human serum.

4.3 Methods and reagents

4.3.1 Reagents

Customized DNA strands were purchased from Integrated DNA Technologies (IDT) (Coralville, Iowa), Biosynthesis (Lewisville, TX) and Biosearch Technologies (Novato, CA). The DNA strand sequences are given in **Table 4.1**. Sodium chloride was obtained from BDH. 4-(2-hydroxyethyl)-1piperazineethanesulfonic acid (HEPES) was from Alfar Aesar. Bovine serum albumin (BSA) was purchased from OmniPur. Tris-(2-carboxyethyl) phosphine hydrocholride (TCEP), mercaptohexanol (MCH), chromium etchant and gold etchant were purchased from Sigma Aldrich (St. Lousi, MO). AZ 40XT positive photoresist and AZ 300 MIF developer were obtained from Microchemicals. Polydinethylsiloxane (PDMS) was from Dow Corning, and dimethyl sulfoxide (DMSO) was purchased from Anachemia. Gold-on-glass (GoG) slides with dimensions of 25.4 mm x 330.2 mm x 1.1 mm (Cr adhesion layer ~5 nm and Au adhesion layer ~100 nm) were purchased from Deposition Research Labs.Inc (St. Charles, MO). Anti-digoxigenin antibody (mouse monolconal) was purchased from Roche and human serum from BioIVT. Necessary buffers and solutions were prepared in deionized, ultra-filtered water (Thermofisher Scientific).

Sequence name	Sequence (5' to 3')
Digoxigenin tagged DNA (D-DNA)	TAGGAAAAGGAGGAGGGTGGCCCACTTAAACCTCAATCCA/3DiG_N/
Thiolated DNA (thiol- DNA)	/5ThioMC6-D/AAAAGCATGGTATTTTTCGTTCGTTAGGGTTCAAATCCGCG
PEG modified thiolated DNA (PEG-thiol- DNA)	/5ThioMC6-D/iSp18/GCATGGTATTTTTCGTTCGTTAGGGTTCAAATCCGCG
Methylene blue **DNA (MB-DNA)**	CCA CCC TCC TCC TTT TCC T AT CTC TCC CTC GUC ACC AUG C/MB-C7/
PEG modified methylene blue DNA (PEG-MB-DNA)	CCA CCC TCC TCC TTT TCC T /iSp18//iSp18/ /iSp18//iSp18/ GTC ACC ATG C[AmC6-Glen][MB-Bios]

Table 4.1 DNA sequences used for Antibody-ECPA

D-DNA, thiol- DNA and PEG-thiol- DNA were purchased from IDT

MB-DNA was from Biosearch Technologies

PEG-MB-DNA was purchased from Biosynthesis

4.3.2 Gold electrode fabrication

A standard photolithographic procedure was followed for gold electrode fabrication, using the positive photoresist, AZ40XT. A photomask of the electrode was designed in Adobe Illustrator and was sent to Fine Line Imaging (Colorado Springs, CO), where a positive photomask was printed (**Figure 4.3A**). Based on this design, 18 electrodes of 2 mm diameter can be fabricated on a gold-on-glass (GoG) slide. After patterning the gold slide, it was dipped in gold etchant (30 s),

followed by chromium etchant (15 s) to remove the unexposed gold and chromium. The AZ photoresist was removed by immersing slides in DMSO for 30 min at 110-150 °C. The etched electrodes were then washed with deionized water and dried with nitrogen.

4.3.3 Electrochemical cell fabrication

The electrochemical (EC) cell was fabricated using polydimethylsilane (PDMS), followed by bonding with fabricated GoG electrode. A 3D CAD file was designed in either Sketchup or Solidworks and the designed mold was printed using the Makerbot Replicator 2 printer, using polylactic acid (PLA) filament (1.75 mm diameter) (**Figure 4.3B**). PDMS and curing agent were mixed in a ratio of 10:1 and poured on to a silicon wafer. The printed 3D mold was then placed on this wafer carefully, followed by baking the PDMS for 1 h at 60°C. After 1 h, the PDMS was removed from the oven and carefully separated from the mold and wafer. The PDMS wells are then placed in an oven at 100°C to complete curing any remaining curing agent, for at least 2-3 h. When the GoG slides are ready to be used, the PDMS is cut into the desired number of wells, depending on the number of electrodes to be used. The etched GoG is cut into the desired number of electrodes and first cleaned with piranha solution (H_2SO_4 : H_2O_2, 3:1) for 1 min. The electrodes are then washed with deionized water and dried with nitrogen. Next, the cut PDMS and cleaned electrodes are sonicated in methanol, followed by drying with nitrogen. The cleaned PDMS and GoG electrodes were then attached to each other by plasma oxidation, to finally form the EC cell (**Figure 4.3C**). Each PDMS well-bound GoG can carry ~100 μL of solution.

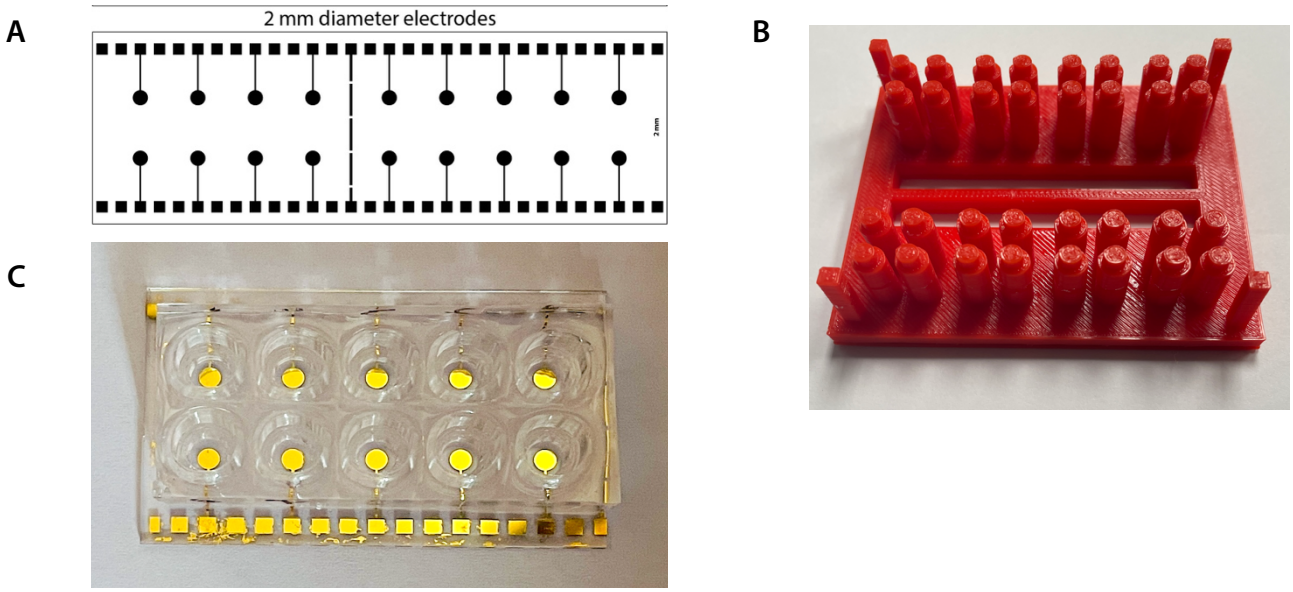

Figure 4.3 (A) Adobe illustrator design of the positive photomask showing, 18, 2 mm diameter electrodes. **(B)** A 3D mold used to fabricate PDMS wells. Figure shows a 32-well mold. **(C)** An EC cell after plasma oxidation. The figure shows 10 independent GoG electrodes ready for thiol-DNA immobilization.

4.3.4 DNA monolayer assembly

Thiolated DNA (thiol- DNA) (20 µM, 1µL) was reduced with TCEP (3 mM, 3 µL), by incubating for 1 hour in dark. This solution was diluted with immobilization buffer (10 mM HEPES, 500 mM or 1000 mM NaCl) to a final concentration of thiol- DNA at 125 nM. 100 µL of this solution was added on to the electrochemical (EC) cell having the gold-on-glass (GoG) working electrode and was incubated for 1 h in dark. Next, 100 µL of 3 mM MCH was added on to the electrode and incubated further for another 1 h (in dark), followed by a 30 min incubation with assay buffer (10 mM HEPES, 500 mM or 1000 mM NaCl and 0.1 % BSA). Monolayer assembled electrodes were stored in the refrigerator, until EC measurements were performed.

4.3.5 Anti-digoxigenin antibody detection

Initially, digoxigenin tagged DNA (D-DNA) and methylene blue DNA (MB-DNA) were mixed and incubated at room temperature for 1 h. Next, anti-digoxigenin antibodies were added to the DNA mixture and was allowed to incubate at room temperature for 30 min. 15 µL of this mixture was added on to the GoG working electrode and was incubated for 40 min at room temperature. During this time, the MB-DNA is expected to hybridize with thiol- DNA. In order to confirm the incubation time for on-electrode hybridization, a kinetic run was performed. Experiment details are given below. The background (BG) included assay buffer, instead of the antibody. Final concentrations of D-DNA and MB-DNA were 50 nM, anti-digoxigenin was 25 nM and thiol- DNA was 125 nM. After the final incubation step, solution was removed from the electrode, followed by the addition of 100 µL of assay buffer, and square wave voltametric (SWV) scan was performed. To generate a calibration curve, a series of anti-digoxigenin solutions ranging from 0-100 nM were electrochemically measured as described above. Final concentrations of D-DNA and MB-DNA were 50 nM, whereas thiol- DNA was 125 nM.

4.3.6 Kinetic experiments

Initially, digoxigenin tagged DNA (D-DNA) and methylene blue DNA (MB-DNA) were mixed and incubated at room temperature for 1 h. Next, anti-digoxigenin antibodies were added to the DNA mixture and was allowed to incubate at room temperature for 30 min. 15 µL of this mixture was added on to the GoG working electrode and was incubated for 40 min at room temperature. During this time, the MB-DNA is expected to hybridize with thiol- DNA. In order to confirm the incubation time for on-electrode hybridization, a kinetic run was performed. Experiment details are given below. The background (BG) included assay buffer, instead of the antibody. Final concentrations of D-DNA and MB-DNA were 50 nM, anti-digoxigenin was 25

nM and thiol- DNA was 125 nM. After the final incubation step, solution was removed from the electrode, followed by the addition of 100 µL of assay buffer, and square wave voltametric (SWV) scan was performed. To generate a calibration curve, a series of anti-digoxigenin solutions ranging from 0-100 nM were electrochemically measured as described above. Final concentrations of D-DNA and MB-DNA were 50 nM, whereas thiol- DNA was 125 nM.

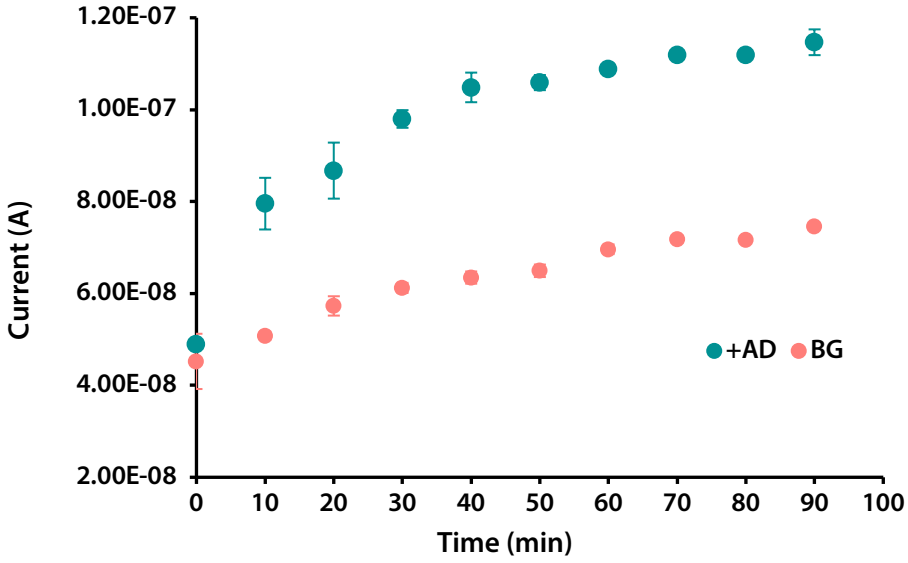

Figure 4.4 Kinetic run to determine on electrode incubation. According to the plot, antibody binding reaches an equilibrium at ~ 30 min. We selected 40 min as the on-electrode incubation time.

4.3.7 Anti-digoxigenin detection in human serum

Electrochemical measurements were performed to detect anti-digoxigenin antibody in 90% human serum. Anti-digoxigenin (20 nM) was analysed in serum, where the incubation steps mentioned previously were followed. 4 M NaCl was spiked to elevate the salt concentration in serum. For the BG of serum experiments, serum of equal volume to that of spiked antibody was added. After the 40 min incubation of 15 µL serum sample on electrode, the solution was removed, followed by addition of 100 µL of assay buffer and SWV measurement.

4.3.8 Electrochemical measurements

All measurements were performed using the Gamry 600 reference potentiostat. When the gold-on-glass (GoG) electrode was ready for measurement, it was connected to create a 3-electrode cell, with a silver/ silver chloride reference electrode (3 M KCl) (BASi) and a platinum counter electrode (CH Instruments). Square wave voltametric (SWV) measurements were performed from -0.45 to 0.00 V vs reference electrode, with a step size of 2 mV and pulse width of 50 mV, at a frequency of 464 Hz. For experiments where broad range SWV frequency scans were performed, a range from 3-1000 Hz was used, with the same step size and pulse width.

4.3.9 Data analysis

Data processing was done using customized MATLAB codes and Microsoft Excel. First, the .DTA files obtained from the Gamry 600 were converted to .txt files using a windows command prompt. The necessary current vs voltage data was then obtained from .txt files by running customized MATLAB codes, where the baseline corrected current vs potential data was exported to Microsoft Excel for further processing (such as obtaining peak currents and percentage change in signal). Detailed data analysis and related graphical demonstrations are given in **Figure 4.5**.

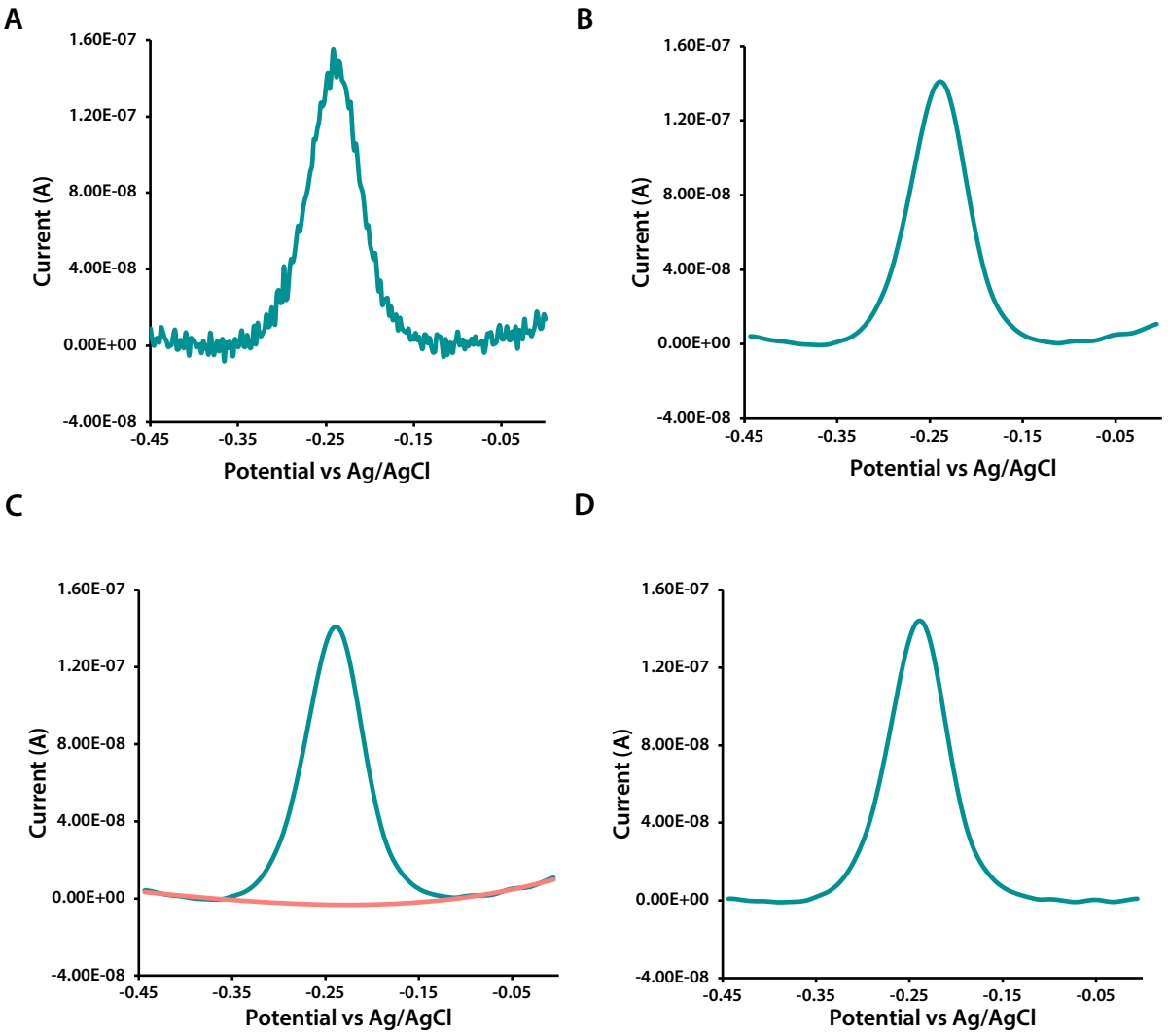

Figure 4.5 A step-by-step depiction of data analysis from customized MATLAB code, plotted in MS Excel for difference current. **(A)** Raw currents obtained from the customized MATLAB code. **(B)** A plot showing the smoothed raw data from (A), where a 21-point smoothing filter is used. **(C)** Baseline correction, using a 3rd order polynomial fit (peach curve shows the baseline fit). **(D)** The baseline corrected faradic current. Peak currents were obtained from the maximum current of the faradaic curve from (D).

4.4 Results and discussion

4.4.1 System design and sensing principle

Earlier, our group introduced the electrochemical proximity assay (ECPA) for insulin and thrombin detection at fM and pM levels respectively [2, 3]. In chapter 3 we quantified anti-digoxigenin antibody (anti-dig) at a limit of detection (LOD) of ~7 nM in buffer using TFA. We also demonstrated how the use of polyethylene glycol (PEG) spacers within DNA strands aids efficient hybridization [41]. With the objective of improving assay sensitivity further and to be able to accommodate the assay for a more miniaturized system leading towards point of care / need, we adapted this method to an electrochemical (EC) surface-based proximity assay.

Herein, we present a modified, surface-based proximity assay for antibody quantification, leveraging three DNA strands- a thiol DNA (thiol-DNA), recognition unit labeled DNA (D-DNA) and a methylene blue labeled DNA (MB-DNA). As illustrated in **Figure 4.6**, each D-DNA is hybridized to a single MB-DNA, through 20 base pairs. Target antibody (Ab) addition induces the spontaneous binding of recognition units, and as an outcome of this event, MB-DNA approaches the thiol-DNA-immobilized gold electrode surface. This close proximity of thiol-DNA and MB-DNA leads to the hybridization of 7 complementary bases, forming an entropically stable structure akin to a DNA hairpin loop which allows efficient electron transfer (ET) at the electrode surface. Therefore, one Ab binding event results in the ET of two MB molecules.

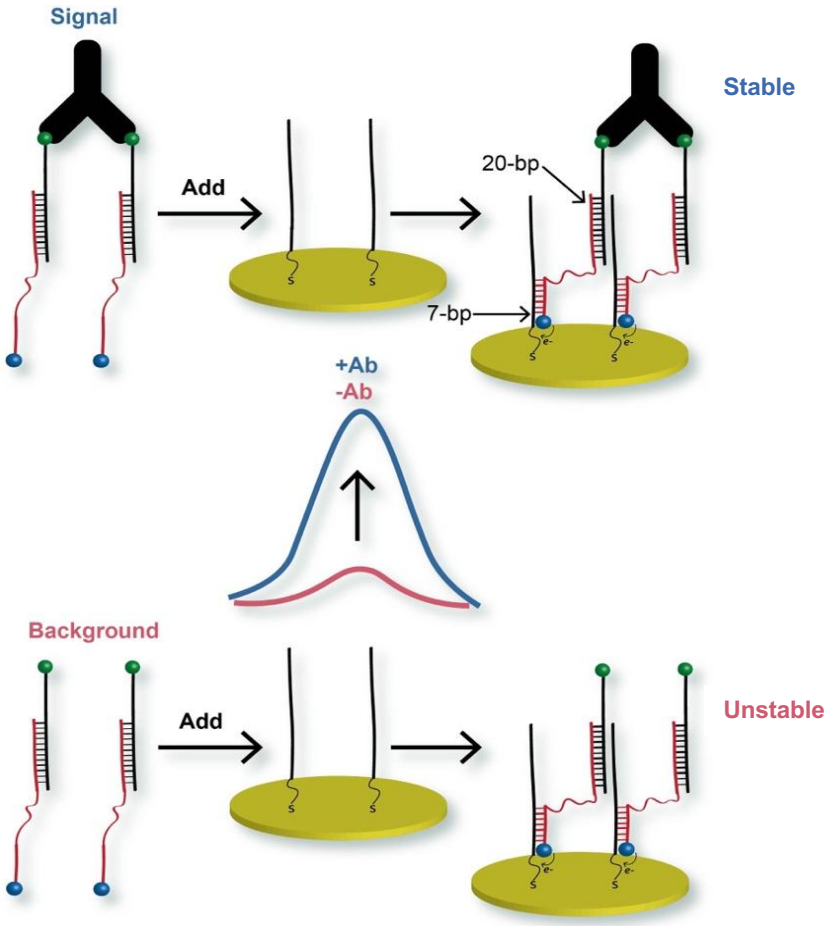

Figure 4.6 Sensing principle of surface based-ECPA for antibody detection. MB-DNA approaches the electrode surface as a result of spontaneous binding of target to its recognition units. Target-induced hybridization leads to an increased current (signal). The absence of target drives weak, spontaneous hybridization, which forms an entropically less stable complex resulting in reduced current (background).

4.4.2 Positional effects of spacers on assay performance

To test our hypothesis and further emphasize on the importance of probe flexibility, we used anti-digoxigenin antibody (Anti-Dig) as the target and digoxigenin, as the recognition unit. For comparison, we first used two types of methylene blue tagged DNA strands. One strand includes a 14-nt ssDNA linker (MB-DNA) separating the 20-bp and 7-bp binding regions (**Figure 4.7A**), which was termed as **original** design. The other strand includes a DNA modified with

polyethylene glycol linker (PEG-MB-DNA) of similar length, which was termed **modification-1** of the original design (**Figure 4.7B**). As mentioned previously, addition of Anti-Dig will push MB-DNA or PEG-MB-DNA closer to gold surface, resulting in its hybridization to thiol-DNA. The generated SWV current will be proportional to the concentration of target antibody. Herein, we detected 25 nM of Anti-Dig (signal) alongside a background (BG) which does not include the target antibody. Target induced hybridization resulted in a higher peak current compared to the BG as shown in **Figures 4.7D, E and F**. More importantly, it is evident that substitution of ssDNA spacer with PEG spacer improved peak currents drastically, giving more separation between the signal and BG peaks (**Figure 4.7E**).

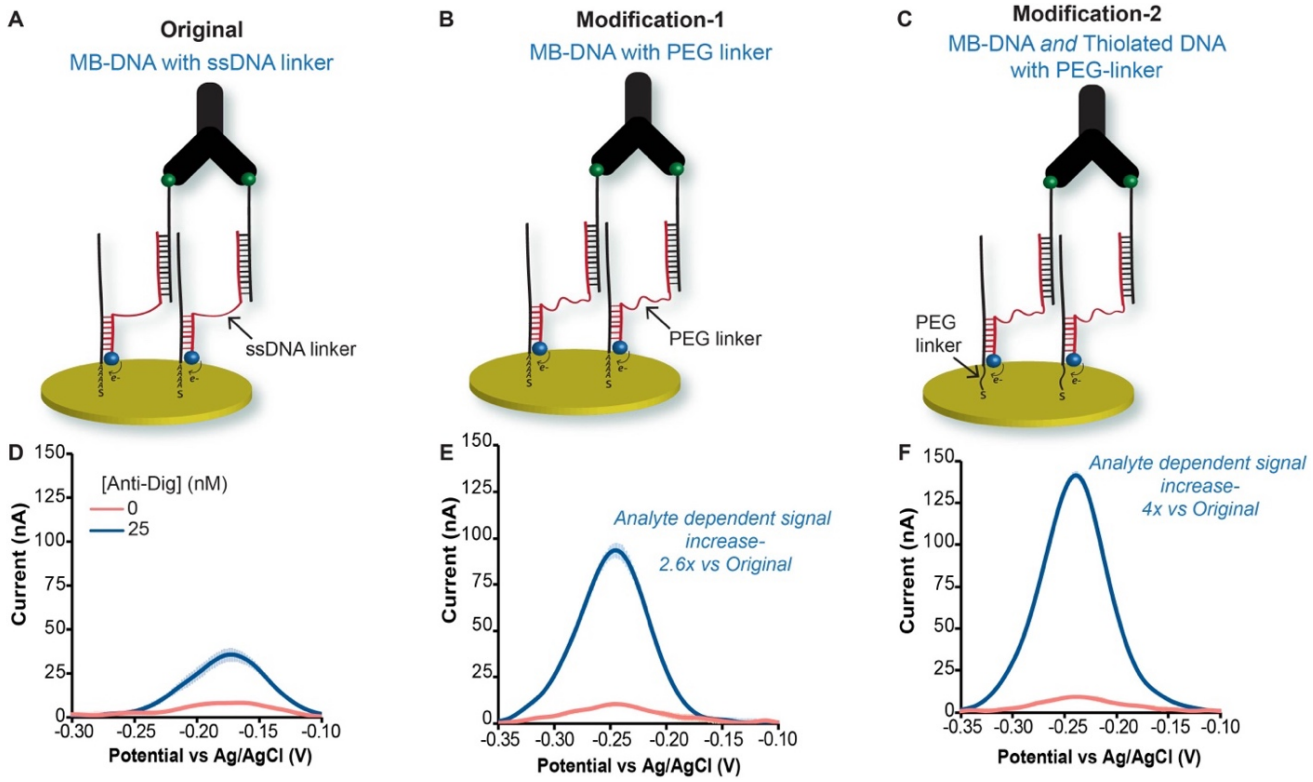

Figure 4.7 SWV peak currents measured at 464 Hz for anti-digoxigenin sensing. **(A)** The original design having a methylene blue DNA with ssDNA linker. **(B)** The first modification for the system where a PEG linker of similar length was added. **(C)** Second modification to the system where the 4A of thiolated-DNA was replaced by a PEG linker of similar length. **(D)** SWV peak current of

original design of AbD detection, with respect to the BG. **(E)** SWV peak current for modification-1, which shows an obvious increase in current (~ 2.6-fold) post- PEG linker substitution. **(F)** SWV peak current for modification-2 shows an increase in peak currents by ~4-fold compared to original, upon further substitution of PEG linker in thiolated-DNA. Error bars represent the standard deviation of measurements from three independent electrodes

In another recent work by our group, it was demonstrated that hybridization of DNA strands at the electrode surface is dependent on the distance between the surface and binding site, which is governed by the electric double layer [45]. It was shown that, more efficient binding of DNA can be achieved if the hybridization site was established at an optimal distance away from the electrode. This was achieved by adjusting the salt concentration in buffer and introducing a short sequence of 4 dA nucleotides at the distal end of thiolated DNA, which either reduced the thickness of electric double layer or pushed the binding region away from the double layer respectively, promoting efficient hybridization [45].

Based on these conclusions, we hypothesized that replacing the 4dA segment of the thiol-DNA with a PEG spacer of similar length can enhance signal due to improved flexibility. As expected, we were able to obtain higher peak currents (in the presence of target) by using both PEG-thiol-DNA and PEG-MB-DNA (**modification-2**), compared to **modification-1** (**Figure 4.7F**). We also carried out a SWV frequency scan from 3-1000 Hz, which was then used to determine the electrochemical critical times[46]of the three systems shown in **Figure 4.7**. As determined by the data in **Figure 4.8A**, the original system exhibited a critical time of 82 ms, and the **modification-1** system gave a similar critical time of 88 ms. This can be explained since the site of modification is positioned away from the electrode, thus it should not significantly alter the electron transfer rate. Notably, the 2.6-fold increase in peak current indicates that the major effect of **modification-1** was to enhance DNA hybridization efficiency (see arrow (1) in **Figure 4.8A**).

By contrast, **modification-2** resulted in a significant change in effective electron transfer rate, giving an electrochemical critical time of 22 ms. We reasoned that this increase in electron transfer rate was a result of increased tethered diffusion rate of the PEG-MB-DNA at the electrode surface. Overall, modification-2 gave a 4-fold increase in both peak current and electron transfer rate (see arrow (2) in **Figure 4.8A**). The effects of flexible spacer position on both critical time and peak current are also shown in **Figure 4.8B**. Overall, these results further confirmed our previous findings that introducing sufficient probe flexibility into a multi-strand-DNA based proximity assay leads to improved assay performance [41].

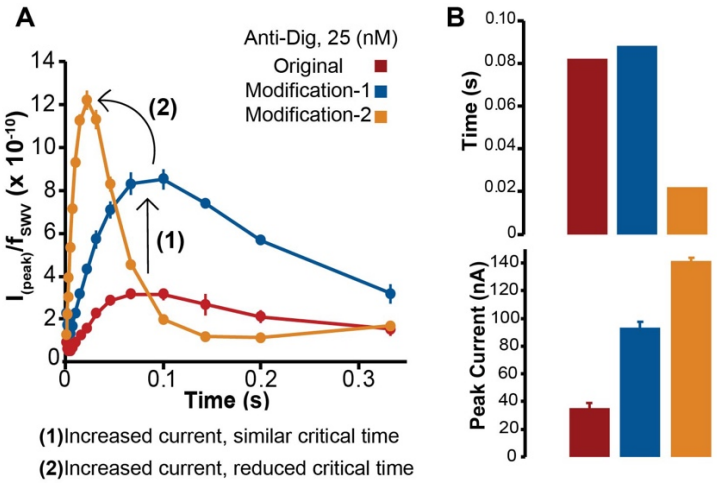

Figure 4.8 Tethered diffusion rates comparing the original with modified designs (1 and 2). **(A)** As the probe flexibility is increased, electron transfer rates begin to shift towards shorter times. **(B)** Bar plots comparing the peak currents and changes in electrochemical critical times for each modification.

4.4.3 Effect of ionic strength on assay performance

Increasing salt concentrations in buffer can reduce thickness of electric double layer, allowing more efficient hybridization of short DNA strands at the electrode surface [45]. Therefore, with the objective of improving assay performance further, we carried out experiments for all three design systems with 1.0 M NaCl in buffer. Despite the increase in target-dependent peak currents with increased salt concentration, we also observed an increase in BG current. We assume that this stabilization of BG is due to the spontaneous hybridization, which is a consequence of the reduced double layer thickness and increased shielding of charge in the DNA backbone by higher salt concentration (**Figure 4.9**). Therefore, based on our results thus far, we used **modification-2** and buffer with 0.5 M NaCl for further experiments.

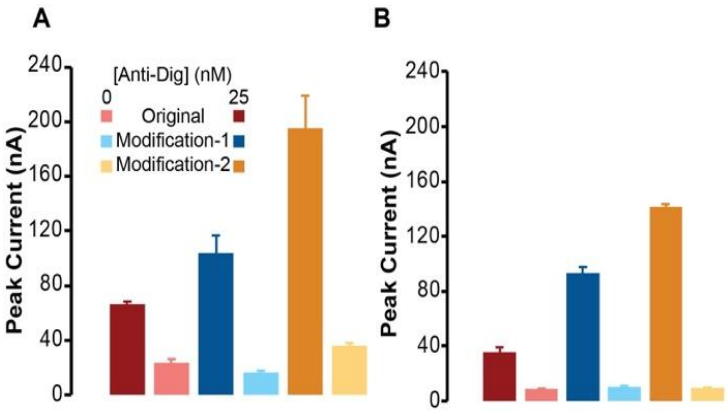

Figure 4.9 Comparison of peak currents with salt concentration. **(A)**Peak currents for the original, modification-1 and modification-2 with 1.0 M NaCl in buffer. **(B)**Peak currents for all three systems with 0.5 M NaCl in buffer. Although peak currents are increased for signal, an increase in BG currents were also observed, indicating the effect of increased salt concentration in promoting spontaneous hybridization.

4.4.4 Sensor calibration

Next, we wanted to study the sensor's response towards varying antibody concentrations. As shown in **Figure 4.10,** the sensor responded as expected, to changes in anti-dig concentrations in buffer. We were able to obtain a 300 pM limit of detection, based on 3σ of blank, with a dynamic range up to 50 nM. However, due to the consumption of probes after saturation, the assay sensitivity begins to drop at higher analyte concentrations, as its ratio exceeds that of the DNA probes (fundamental limitation of proximity assays). The above LOD can be obtained either by using the peak currents at each concentration or percentage change in signal, which was calculated by the formular given below.

$$\%\, Signal\ change = \frac{I_S}{I_{BG}}\ x\ 100$$

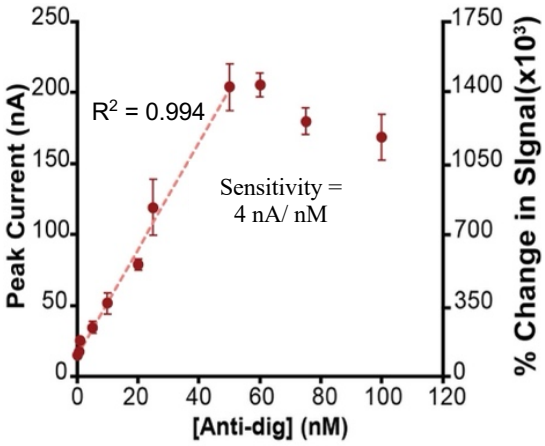

Figure 4.10 Calibration curve for anti-digoxigenin detection. An LOD of 300 pM was obtained by using either maximum (peak) current or percentage change in signal. Furthermore, assay sensitivity begins to drop at higher anti-digoxigenin concentrations due to the increased analyte compared to DNA probes.

4.4.5 Anti-digoxigenin sensing in human serum

To test the functionality of the sensor in biological fluids, we spiked 20 nM of anti-dig into human serum (90%). Initially, in comparison to the buffer control, we did not observe an increase in signal, compared to the BG. Serum has approximately 135-145 mM of salt [47]. As mentioned previously, since salt concentration plays an important role in driving efficient hybridization of surface-based DNA in EC sensors, we hypothesized that a comparatively low salt concentration in serum was inadequate to drive target-dependent DNA hybridization, in combination with other factors such as serum interferents. Therefore, a high concentration of salt (4M) was spiked to increase the final concentration of salt in serum to 415-425 mM. We were able to see improved currents compared to the serum without spiked salt, although raw currents for 20 nM anti-digoxigenin was lower than that of the buffer control (**Figure 4.11A**). However, when percentage change in signal was used, the NaCl spiked serum showed results comparable to that of the buffer control (**Figure 4.11B**). We attribute these differences in peak currents and percentages to the interferents present in serum. However, extensive studies were not done in this work to prove this hypothesis.

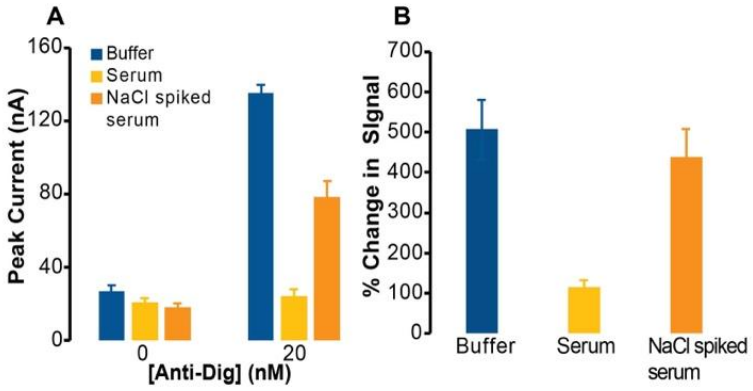

Figure 4.11 Assay functionality in 90% human serum. **(A)** Raw peak currents showing changes or 20 nM anti-digoxigenin spiked in serum and serum spiked with 4 M NaCl. The raw currents are lower for salt spiked serum compared to the buffer control. **(B)** However, the change in % signal

demonstrates comparable results to that of buffer control. The results also show that spiking high concentration of salt can improve assay performance to a degree.

4.5 Conclusions

In this work we have extended the previously developed ECPA for antibody detection. Similar to our recent work leveraging TFA, we have shown the importance of probe flexibility in improving assay performance of proximity-based assays [41]. To achieve this, we compared the original system (exclusively having DNA strands) with two other systems where DNA strands were modified with PEG linkers. Although the original design showed a signal peak in the presence of target, incorporating PEG modified methylene blue- and thiolated-DNA strands showed drastic improvement in target-dependent current. Akin to our recent work [45], here we have shown that although increasing salt concentration improves the signal, it can also lead to stabilized BG currents, since spontaneous hybridization is promoted. Additionally, we have shown that assay performance in biological fluids was improved by increasing the salt concentration accordingly. These observations further supports that it is important to pay close attention to optimizing salt concentration for electrochemical assays involving short DNA strands, as it can influence sensor performance. Although we developed this sensor for anti-digoxigenin antibody detection (as a proof-of-concept), we believe that the sensor can be modified to detect more clinically relevant target antibodies using not only small molecules as recognition units, but also peptides.

4.6 Reference

(1) Bezerra, A. B.; Kurian, A. S. N.; Easley, C. J. Nucleic-Acid Driven Cooperative Bioassays Using Probe Proximity or Split-Probe Techniques. *Anal Chem* **2021**, *93* (1), 198-214. DOI: 10.1021/acs.analchem.0c04364 From NLM Medline.
(2) Hu, J.; Wang, T.; Kim, J.; Shannon, C.; Easley, C. J. Quantitation of femtomolar protein levels via direct readout with the electrochemical proximity assay. *J Am Chem Soc* **2012**, *134* (16), 7066-7072. DOI: 10.1021/ja3000485 From NLM Medline.

(3) Hu, J.; Yu, Y.; Brooks, J. C.; Godwin, L. A.; Somasundaram, S.; Torabinejad, F.; Kim, J.; Shannon, C.; Easley, C. J. A reusable electrochemical proximity assay for highly selective, real-time protein quantitation in biological matrices. *J Am Chem Soc* **2014**, *136* (23), 8467-8474. DOI: 10.1021/ja503679q From NLM Medline.
(4) Labib, M.; Sargent, E. H.; Kelley, S. O. Electrochemical methods for the analysis of clinically relevant biomolecules. *Chemical reviews* **2016**, *116* (16), 9001-9090.
(5) Clifford, A.; Das, J.; Yousefi, H.; Mahmud, A.; Chen, J. B.; Kelley, S. O. Strategies for biomolecular analysis and continuous physiological monitoring. *Journal of the American Chemical Society* **2021**, *143* (14), 5281-5294.
(6) Elgrishi, N.; Rountree, K. J.; McCarthy, B. D.; Rountree, E. S.; Eisenhart, T. T.; Dempsey, J. L. A practical beginner's guide to cyclic voltammetry. *Journal of chemical education* **2018**, *95* (2), 197-206.
(7) Helfrick Jr, J. C.; Bottomley, L. A. Cyclic square wave voltammetry of single and consecutive reversible electron transfer reactions. *Analytical chemistry* **2009**, *81* (21), 9041-9047.
(8) Scholz, F. Voltammetric techniques of analysis: the essentials. *ChemTexts* **2015**, *1* (4), 17.
(9) Osteryoung, J. G.; Osteryoung, R. A. Square wave voltammetry. *Analytical chemistry* **1985**, *57* (1), 101-110.
(10) Mirceski, V.; Guzijewski, D.; Gulaboski, R. Electrode kinetics from a single square-wave voltammogram. *Macedonian Journal of Chemistry and Chemical Engineering* **2015**, *34* (1), 36-42.
(11) Jayawardena, A.; Tan, S. M.; Richardson, M. B.; Chan, J.; Thissen, H.; Voelcker, N. H.; Kwan, P. Industry Viable Electrochemical DNA Detection Sensor Architecture via a Stem-Loop Methylene Blue Redox Reporter and Rapid In Situ Probe Immobilization Method for Pharmacogenetic Biomarker Testing Application. *Journal of The Electrochemical Society* **2022**, *169* (1), 017508.
(12) Li, S.; Lin, L.; Chang, X.; Si, Z.; Plaxco, K. W.; Khine, M.; Li, H.; Xia, F. A wrinkled structure of gold film greatly improves the signaling of electrochemical aptamer-based biosensors. *RSC advances* **2021**, *11* (2), 671-677.
(13) Das, J.; Gomis, S.; Chen, J. B.; Yousefi, H.; Ahmed, S.; Mahmud, A.; Zhou, W.; Sargent, E. H.; Kelley, S. O. Reagentless biomolecular analysis using a molecular pendulum. *Nature chemistry* **2021**, *13* (5), 428-434.
(14) Radwan, O.; Brothers, M. C.; Coyle, V.; Chapleau, M. E.; Chapleau, R. R.; Kim, S. S.; Ruiz, O. N. Electrochemical biosensor for rapid detection of fungal contamination in fuel systems. *Biosensors and Bioelectronics* **2022**, *211*, 114374.
(15) Brothers, M. C.; Moore, D.; St. Lawrence, M.; Harris, J.; Joseph, R. M.; Ratcliff, E.; Ruiz, O. N.; Glavin, N.; Kim, S. S. Impact of self-assembled monolayer design and electrochemical factors on impedance-based biosensing. *Sensors* **2020**, *20* (8), 2246.
(16) Li, S.; Wang, Y.; Zhang, Z.; Wang, Y.; Li, H.; Xia, F. Exploring end-group effect of alkanethiol self-assembled monolayers on electrochemical aptamer-based sensors in biological fluids. *Analytical chemistry* **2021**, *93* (14), 5849-5855.
(17) Mandler, D.; Kraus-Ophir, S. Self-assembled monolayers (SAMs) for electrochemical sensing. *Journal of Solid State Electrochemistry* **2011**, *15*, 1535-1558.
(18) Xu, X.; Makaraviciute, A.; Kumar, S.; Wen, C.; Sjödin, M.; Abdurakhmanov, E.; Danielson, U. H.; Nyholm, L.; Zhang, Z. Structural changes of mercaptohexanol self-assembled

monolayers on gold and their influence on impedimetric aptamer sensors. *Analytical chemistry* **2019**, *91* (22), 14697-14704.
(19) Holtan, M. D.; Somasundaram, S.; Khuda, N.; Easley, C. J. Nonfaradaic Current Suppression in DNA-Based Electrochemical Assays with a Differential Potentiostat. *Analytical chemistry* **2019**, *91* (24), 15833-15839.
(20) Dai, Y.; Liu, C. C. Recent advances on electrochemical biosensing strategies toward universal point-of-care systems. *Angewandte Chemie* **2019**, *131* (36), 12483-12496.
(21) Hai, X.; Li, Y.; Zhu, C.; Song, W.; Cao, J.; Bi, S. DNA-based label-free electrochemical biosensors: From principles to applications. *TrAC Trends in Analytical Chemistry* **2020**, *133*, 116098.
(22) Xie, M.; Zhao, F.; Zhang, Y.; Xiong, Y.; Han, S. Recent advances in aptamer-based optical and electrochemical biosensors for detection of pesticides and veterinary drugs. *Food Control* **2022**, *131*, 108399.
(23) Cash, K. J.; Ricci, F.; Plaxco, K. W. An electrochemical sensor for the detection of protein−small molecule interactions directly in serum and other complex matrices. *Journal of the American Chemical Society* **2009**, *131* (20), 6955-6957.
(24) Downs, A. M.; Plaxco, K. W. Real-Time, In Vivo Molecular Monitoring Using Electrochemical Aptamer Based Sensors: Opportunities and Challenges. *ACS sensors* **2022**, *7* (10), 2823-2832.
(25) Hianik, T.; Wang, J. Electrochemical aptasensors–recent achievements and perspectives. *Electroanalysis: An International Journal Devoted to Fundamental and Practical Aspects of Electroanalysis* **2009**, *21* (11), 1223-1235.
(26) Sassolas, A.; Blum, L. J.; Leca-Bouvier, B. D. Electrochemical aptasensors. *Electroanalysis: An International Journal Devoted to Fundamental and Practical Aspects of Electroanalysis* **2009**, *21* (11), 1237-1250.
(27) Xiao, Y.; Lubin, A. A.; Heeger, A. J.; Plaxco, K. W. Label-free electronic detection of thrombin in blood serum by using an aptamer-based sensor. *Angewandte Chemie* **2005**, *117* (34), 5592-5595.
(28) Arroyo-Currás, N.; Somerson, J.; Vieira, P. A.; Ploense, K. L.; Kippin, T. E.; Plaxco, K. W. Real-time measurement of small molecules directly in awake, ambulatory animals. *Proceedings of the National Academy of Sciences* **2017**, *114* (4), 645-650.
(29) Arroyo-Currás, N. y.; Dauphin-Ducharme, P.; Ortega, G.; Ploense, K. L.; Kippin, T. E.; Plaxco, K. W. Subsecond-resolved molecular measurements in the living body using chronoamperometrically interrogated aptamer-based sensors. *ACS sensors* **2018**, *3* (2), 360-366.
(30) Idili, A.; Gerson, J.; Kippin, T.; Plaxco, K. W. Seconds-resolved, in situ measurements of plasma phenylalanine disposition kinetics in living rats. *Analytical chemistry* **2021**, *93* (8), 4023-4032.
(31) Li, H.; Dauphin-Ducharme, P.; Arroyo-Currás, N.; Tran, C. H.; Vieira, P. A.; Li, S.; Shin, C.; Somerson, J.; Kippin, T. E.; Plaxco, K. W. A biomimetic phosphatidylcholine-terminated monolayer greatly improves the in vivo performance of electrochemical aptamer-based sensors. *Angewandte Chemie International Edition* **2017**, *56* (26), 7492-7495.
(32) Kang, D.; Parolo, C.; Sun, S.; Ogden, N. E.; Dahlquist, F. W.; Plaxco, K. W. Expanding the Scope of Protein-Detecting Electrochemical DNA "Scaffold" Sensors. *ACS Sens* **2018**, *3* (7), 1271-1275. DOI: 10.1021/acssensors.8b00311.

(33) Ogden, N. E.; Kurnik, M.; Parolo, C.; Plaxco, K. W. An electrochemical scaffold sensor for rapid syphilis diagnosis. *Analyst* **2019**, *144* (17), 5277-5283. DOI: 10.1039/c9an00455f From NLM Medline.
(34) Parolo, C.; Idili, A.; Ortega, G.; Csordas, A.; Hsu, A.; Arroyo-Currás, N.; Yang, Q.; Ferguson, B. S.; Wang, J.; Plaxco, K. W. Real-Time Monitoring of a Protein Biomarker. *ACS Sensors* **2020**, *5* (7), 1877-1881. DOI: 10.1021/acssensors.0c01085.
(35) Khuda, N.; Somasundaram, S.; Easley, C. J. Electrochemical Sensing of the Peptide Drug Exendin-4 Using a Versatile Nucleic Acid Nanostructure. *ACS Sensors* **2022**, *7* (3), 784-789. DOI: 10.1021/acssensors.1c02336.
(36) Somasundaram, S.; Easley, C. J. A Nucleic Acid Nanostructure Built through On-Electrode Ligation for Electrochemical Detection of a Broad Range of Analytes. *J Am Chem Soc* **2019**, *141* (29), 11721-11726. DOI: 10.1021/jacs.9b06229.
(37) Gurukandure, A.; Somasundaram, S.; Kurian, A. S.; Khuda, N.; Easley, C. J. Building a nucleic acid nanostructure with DNA-epitope conjugates for a versatile electrochemical protein detection platform. **2023**.
(38) Rossetti, M.; Brannetti, S.; Mocenigo, M.; Marini, B.; Ippodrino, R.; Porchetta, A. Harnessing effective molarity to design an electrochemical dna-based platform for clinically relevant antibody detection. *Angewandte Chemie* **2020**, *132* (35), 15083-15088.
(39) Ballew, J. T.; Murray, J. A.; Collin, P.; Mäki, M.; Kagnoff, M. F.; Kaukinen, K.; Daugherty, P. S. Antibody biomarker discovery through in vitro directed evolution of consensus recognition epitopes. *Proceedings of the National Academy of Sciences* **2013**, *110* (48), 19330-19335.
(40) Xu, W.; Wang, D.; Li, D.; Liu, C. C. Recent developments of electrochemical and optical biosensors for antibody detection. *International Journal of Molecular Sciences* **2019**, *21* (1), 134.
(41) Kurian, A.; Gurukandure, A.; Dovgan, I.; Kolodych, S.; Easley, C. Thermofluorimetric Analysis (TFA) using Probes with Flexible Spacers: Application to Direct Antibody Sensing and to Antibody-Oligonucleotide (AbO) Conjugate Valency Monitoring. **2023**.
(42) Heyduk, E.; Dummit, B.; Chang, Y.-H.; Heyduk, T. Molecular pincers: antibody-based homogeneous protein sensors. *Analytical chemistry* **2008**, *80* (13), 5152-5159.
(43) Heyduk, E.; Heyduk, T. Nucleic acid-based fluorescence sensors for detecting proteins. *Analytical Chemistry* **2005**, *77* (4), 1147-1156.
(44) Tian, L.; Heyduk, T. Bivalent ligands with long nanometer-scale flexible linkers. *Biochemistry* **2009**, *48* (2), 264-275.
(45) Khuda, N.; Somasundaram, S.; Urgunde, A. B.; Easley, C. J. Ionic Strength and Hybridization Position near Gold Electrodes Can Significantly Improve Kinetics in DNA-Based Electrochemical Sensors. *ACS Appl Mater Interfaces* **2023**. DOI: 10.1021/acsami.2c22741 From NLM Publisher.
(46) Komorsky-Lovrić, Š.; Lovrić, M. Kinetic measurements of a surface confined redox reaction. *Analytica chimica acta* **1995**, *305* (1-3), 248-255.
(47) Ackerman, G. L. Clinical Methods: The History, Ohysical and Labaratory Examinations. **1990**, *3rd edition*, Book chapter. From NIH, PubMed National library of medicine.

Chapter 5

Adapting Electrochemical Bioassays from Planar Electrodes to Microelectrodes

As mentioned in the previous sections, electrochemical (EC) techniques are an excellent choice for developing specific and sensitive sensors which can be adopted for point-of-care diagnostics, with simple instrumentation, for usage in limited resource settings [1-4]. Furthermore, EC sensors can be easily miniaturized and integrated with microfluidic devices, facilitating real-time measurement of analytes, using low sample volumes. In this chapter, we focus on adopting our already developed DNA-based EC assays for gold-on-glass (GoG) planar electrodes to gold microelectrode wires for improved assay sensitivity and miniaturization.

5.1 Background

When designing EC-biosensors, it is crucial to pay close attention to the type of conductive material used. An electrode used for biosensing generally includes three parts- electrode that is exposed, connection points, and paths. Therefore, the working electrode will consist of three layers, namely substrate (such as glass), conductive layer, and insulation (which prevents contact of certain electrode parts with biofluids and fouling) [5]. Important factors to be considered when selecting a conductive material includes biocompatibility, stability in biofluids and cell culture media, and optical transparency, etc. Generally, metals such as gold, iridium, titanium, platinum, and tungsten which are deposited on substrates such as glass and silicon are used as the conductive layer. Among these, gold (Au) has been widely used as the metal of choice, due to its good biocompatibility, corrosion resistivity, and conductivity [5]. As noble metals do not adhere well to

substrates such as glass and demonstrates reduced stability when exposed to water, it is important that they are being deposited on a metal layer such as chromium or titanium for improved stability [5]. We employ patterned chromium-plated GoG electrodes to develop DNA-based EC sensors [2, 4, 6-9]. As mentioned in the methods section of chapter 3, a standard photolithographic process is followed to pattern circular 2D electrodes of customized sizes.

Plaxco and coworkers implanted gold microwires within the jugular veins of mice to detect various therapeutic drugs in whole blood, in real time (**Figure 5.1**) [10-15]. Although the fabricated gold electrodes were able to continuously measure analytes in undiluted blood serum over a few hours, they were contaminated over time when deployed in undiluted whole blood [12]. To address this issue, the group developed a microfluidic device which could measure therapeutic drugs in whole blood continuously. Herein, ex vivo measurements were performed, where the blood was drawn from a catheter to the device, reducing possible biofouling [12, 16]. However, this device carried certain disadvantages- the device retained a certain time lag, owing to being ex vivo with the necessity of drawing blood continuously and device complexity [12, 16]. Thus, in order to be able to use the electrodes within live animals for real time continuous measurement of analytes, the group encased the developed microelectrodes in polysulfone membranes, which reduced biofouling. Although longer times of sensor functionality was achieved, considerable drift in baseline was observed. In order to correct for this drift, a "kinetic differential method" (KDM) was used [12]. Furthermore, to improve sensitivity of E-AB sensors, the Plaxco group used electrochemical roughening to increase surface area of the gold microwires. Following electrochemical roughening, more methylene blue tagged aptamers were able to immobilize on electrode surface, resulting in improved signal to noise ratios [11].

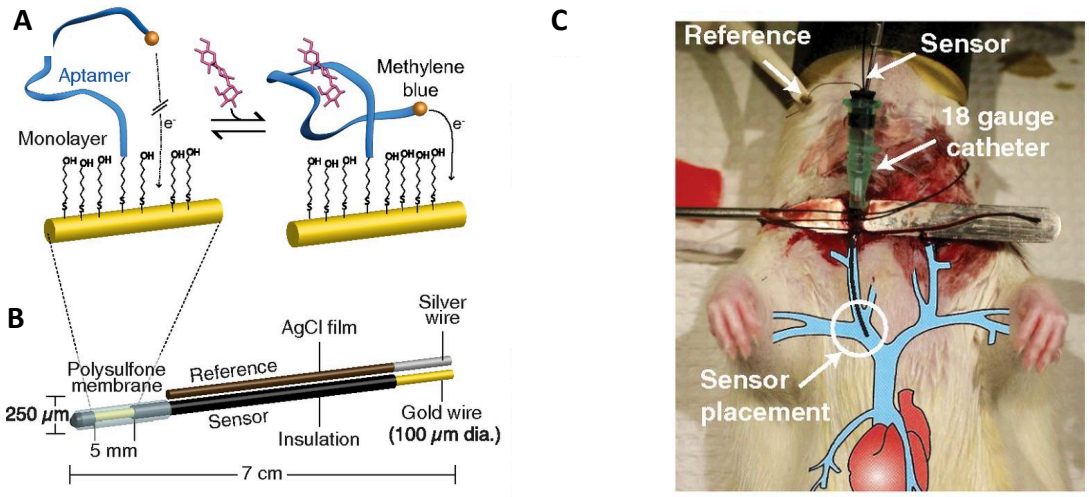

Figure 5.1 Gold microwires implanted in a mouse for real time detection of therapeutic drugs**. (A)** An aptamer carrying a redox tag (methylene blue) is immobilized on a gold microwire. In the presence of small molecule target, aptamer folds to generate EC signal. **(B)** Reference and working electrodes used in the set-up. To prevent biofouling, a polysulfone membrane was used. **(C)** The sensor was implanted inside the jugular vein of a mouse. *Reprinted with permission from reference 12. Copyright 2017, Proceedings of the National Academy of Sciences, USA.*

Inspired from the use of microwires by the Plaxco group, in this project we outline the initial adaptation of gold microelectrodes for our existing DNA-based EC biosensors fabricated on 2D planar GoG electrodes. Currently, DNAs are self-assembled on circular gold surfaces of 2 mm diameter. We aim to reduce electrode fabrication time, improve sensitivity, and integrate microelectrodes with microfluidics.

5.2 Methods and reagents

5.2.1 Reagents

Customized DNA strands were purchased from Integrated DNA Technologies (IDT) (Coralville, Iowa) and Biosearch Technologies (Novato, CA). The DNA strand sequences are given in table 5.1. Sodium chloride was obtained from BDH. 4-(2-hydroxyethyl)-1piperazineethanesulfonic acid (HEPES) was from Alfar Aesar. Bovine serum albumin (BSA) was purchased from OmniPur. Tris-(2-carboxyethyl) phosphine hydrocholride (TCEP), mercaptohexanol (MCH), potassium ferrocyanide, potassium ferricyanide, methylene blue, magnesium chloride hexahydrate, estradiol, chromium etchant and gold etchant were purchased from Sigma Aldrich (St. Lousi, MO). T4 DNA ligase (400,000 units) and adenosine triphosphate (ATP, 10 mM) were obtained from New England Biolabs. Polydimethylsiloxane (PDMS) was from Dow Corning. UV curable 3D printing resin was obtained from Anycubic. Anti-estradiol antibody (ab 116648) was from Abcam. Gold wire (0.25 mm diameter, Premion, 99.998 % metal basis), platinum wire (0.25 mm diameter, 99.9 % metal basis) and silver wire (0.25 mm diameter, Premion, 99.9985% metal basis) were purchased from ThermoFisher Scientific. Necessary buffers and solutions were prepared in deionized, ultra-filtered water (ThermoFisher Scientific).

Sequence name	Sequence (5' to 3')
40 base-pair methylene bue (MB-40)	CGCGGATTTGAACCCTAACGAACGAAAAATGTCACCATGC-[MB]
Thiolated DNA complementary to MB-40 (thiol- DNA)	/5ThioMC6-D/AAAAGCATGGTATTTTTCGTTCGTTAGGGTTCAAATCCGCG
PEG modified thiolated DNA (for nanostructure) (ns_PEG-thiol-DNA)	/5ThioMC6-D/iSp18/GCATGGTATTTTTCGTTCGTTAGGGTTCAAATCCGCG
1-Methylene blue DNA (for nanostructure) (1-MB-DNA)	T [MB] CTC CAC TTC AAC CG
Anchor connector DNA (for nanostrcuture) (Anc-DNA)	**/5Phos**/ GAG ACA CTG TGT CGT CTC CGG TTG AAG TGG AGA /**iAmMC6**/ TAG GAA GAG GTG AGG

Table 5.1 List of DNA sequences used for microelectrode characterization and nanostructure assembly

MB-40, thiol- DNA, ns_PEG-thiol- DNA and Anc-DNA were purchased from IDT

1-MB-DNA was from Biosearch Technologies

5.2.2 Preparation of gold microwires

An approximately 1-inch-long gold wire was cut and wrapped with a breadboard jumper wire, followed by sealing with heat shrink tubing to secure connections (**Figure 5.2A**). Next, the wire was inserted to a 3D printed electrode holder and glued to the holder by using UV curable resin. The resin was cured for 1-2 min to make sure that the gold wire was firmly fixed. Finally, the exposed gold wire was adjusted to 5 mm length, which serves as the gold electrode working area (**Figure 5.2B**). The prepared gold microwire included 0.25 mm diameter and 5 mm length. The custom-designed electrode holders were designed in Solidworks (3D CAD software) and printed in a high resolution 3D printer (Anycubic), using UV curable resin. As shown in **Figure 5.2C**, the holder consisted of 3 holes, one each for the gold working electrode, counter and reference electrodes. The hole for working electrode was 0.3 mm in diameter, whereas the counter and reference electrode holes were 0.35 mm each.

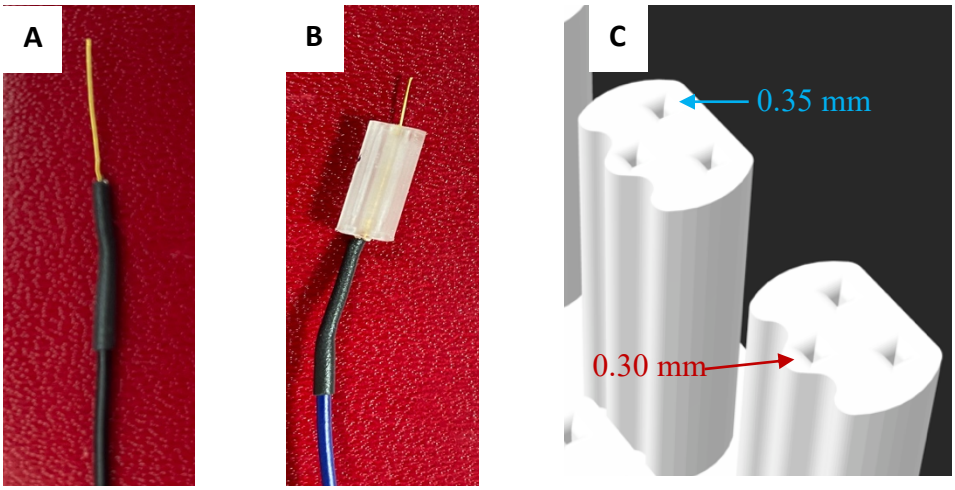

Figure 5.2 Preparation of gold working electrode. **(A)** Gold microwire connected to breadboard jumper cable and sealed with heat shrink tubing. **(B)** Gold microelectrode used for experiments, where the wire was sealed inside a 3D printed microelectrode holder, using UV curable resin. **(C)** 3D CAD designs of microelectrode holders having three holes for working, reference and counter electrodes.

5.2.3 Fabrication of electrochemical cells

Electrochemical cells were fabricated using polydimethylsilane (PDMS), as described in the methods section of chapter 4. For experiments outlined in this chapter wells of two different volumes were used. All experiments were carried out in PDMS wells which were able to carry 65 µL of solution. For experiments where DNA nanostructure was assembled, 20 µL wells were used for adding ligation mixture. When it was ready for experiments, PDMS wells were cut and cleaned with methanol followed by drying with nitrogen. These wells were bonded on to pieces of cut-glass slides either through plasma oxidation or using double sided tape. **Figure 5.3** shows the 3D printed molds used for PDMS molding and a glass-bound well.

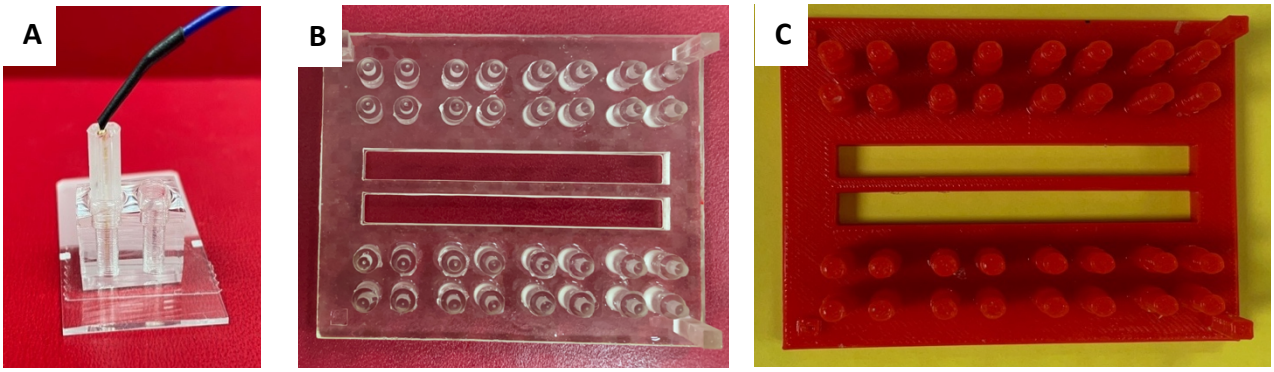

Figure 5.3 3D molds used for electrochemical cell preparation. **(A)** A PDMS well bound to glass, which fits the electrode holder. **(B)** A 3D printed mold for 20 µL wells. **(C)** 3D mold used for 65 µL well fabrication.

5.2.4 Initial electrode functioning and reference electrode selection

To test the feasibility of using gold microwires as electrodes, we first performed experiments with solutions of potassium ferricyanide/ ferrocyanide and methylene blue, of various concentrations. Here we also tested the use of platinum, gold, and silver wires and in-lab fabricated silver-silver chloride as references. Further details are discussed in section 5.3 below.

5.2.5 DNA monolayer assembly and detection of 40 base-pair methylene blue DNA (MB-40)

For experiments where MB-40 was used, the corresponding thiolated DNA (THIOL-DNA) was reduced with 10 mM of TCEP at a ratio of 1:3 for 1 h. This solution was diluted with immobilization buffer (10 mM HEPES and 500 mM NaCl) to obtain necessary concentration of THIOL- DNA. 65 µL of this solution was added to the fabricated PDMS well followed by insertion of gold working electrode. This was left for 2 h at room temperature to form the self-assembled monolayer (SAM) of THIOL- DNA. Next, 65 µL of 3 mM MCH was added to the well and the electrode was incubated for further 1 h. Finally, MB-40 of a fixed concentration was added to the well, followed by electrode incubation for 30 min at room temperature. The solution of MB-40 was removed, and buffer was added before measurements were taken.

5.2.6 DNA monolayer assembly and estradiol nanostructure assembly

Thiolated-DNA (ns_PEG-THIOL- DNA) was reduced with 10 mM of TCEP at a ratio of 1:1, for 1 h. This solution was diluted to a final concentration of 50 nM with immobilization buffer (10 mM HEPES, pH 7.5 and 10mM $MgCl_2$). 65 µL of this solution was added to a well, where the gold electrode was immersed and left for 2 h for SAM formation. This was followed by incubating the electrode with 3 mM MCH for an additional 1 h. Next, the thiol immobilized electrodes were incubated with ligation buffer (10 mM HEPES, 10 mM $MgCl_2$ and 0.1% BSA) for 30 min. The passivated gold electrodes were then incubated for 6 h with 20 µL of ligation mixture which contained 100 nM of 1-MB-DNA, 100 nM estradiol anchor DNA (Anc-DNA), 1 mM ATP and T4-DNA ligase. Afterwards, the electrodes were washed with water, followed by dipping in assay buffer (10 mM HEPES, 500 mM NaCl and 0.1% BSA) and were refrigerated until further use.

5.2.7 Anti-estradiol detection

First, to confirm formation of estradiol DNA nanostructure on gold microwires, square wave voltametric (SWV) scans were performed to measure peak currents in assay buffer. Afterwards, 65 μL of 20 nM anti-estradiol antibody was added and incubated at room temperature for 30 min. Prior to measurement, the antibody solution was removed, and assay buffer was added which was followed by measurement of peak current. In instances where kinetic measurements related to antibody binding were performed, the electrode system was dropped into a solution of 65 μL of 20 nM anti-estradiol antibody, and changes in peak current were measured at 3 min intervals over 1 hr.

5.2.8 Electrochemical (EC) measurements for DNA-based gold microelectrodes

A Platinum (Pt) pseudo reference and Pt counter micro electrodes were used for EC measurements along with the gold working electrode forming a 3-electrode system, as shown in (**Figure 5.4**). The electrodes were connected to the Gamry 600 reference potentiostat. SVW scans were performed from -800 mV to -200 mV vs Pt reference electrode, with a step size of 1 mV and pulse width of 50 mV at selected frequencies.

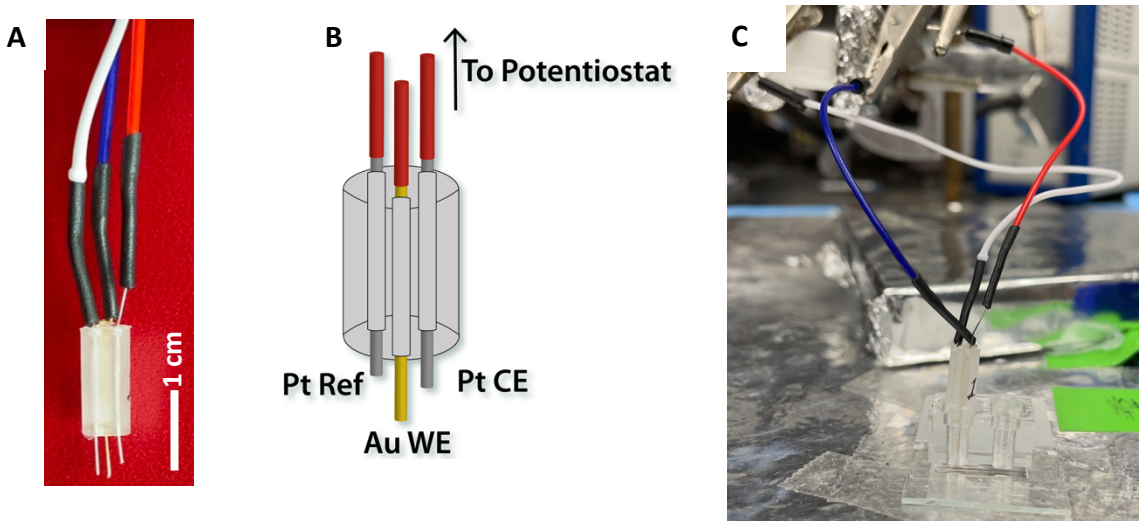

Figure 5.4 Microelectrode assembly for electrochemical measurements. **(A)** Assembled three electrode system in the microelectrode holder. Red- Pt reference, blue- gold working electrode and white- Pt pseudo reference electrode. **(B)** An illustration of assembled electrode to be connected to the potentiostat. **(C)** The electrodes are connected to the potentiostat through breadboard jumper wires.

5.2.9 Data analysis

Data processing was performed using both customized MATLAB codes and Microsoft Excel, as detailed in the methods and reagents section of chapter 4.

5.3 Results and discussion

5.3.1 Initial electrode functionality and selection of reference electrode

As the first step, we tested the capability of using gold microelectrodes (Au-μE) for measuring potassium ferricyanide/ferrocyanide and freely diffusing methylene blue in buffer. Instead of using the commercially available Ag/AgCl reference electrode, we sought to use alternatives, as the end goal is to integrate these electrodes into microfluidic channels. Commercially available reference electrodes are larger in size, which limits their use within

smaller sized channels. Instead of the commercial Ag/AgCl reference electrode, we first used in-house synthesized Ag/AgCl electrodes, as described by the Plaxco group [10, 11, 15]. Herein, a piece of silver (Ag) wire (diameter = 0.25 mm) was dipped in commercial bleaching solution overnight, to form a layer of AgCl. The AgCl was kept exposed, and the remaining portion of silver wire was attached to a breadboard jumper wire. Another Ag/AgCl electrode was generated by electroplating AgCl on a silver wire at 4 V for 5 mins. Furthermore, we used Pt, Ag, and Au wires as pseudo references. A Pt wire was used as the counter electrode for all experiments. **Figure 5.5** below shows the results of measuring 5 mM and 10 mM potassium ferri/ferro solutions using the 5 types of reference electrodes, with the Au-μE. Measurements were done on two consecutive days as well as after five days of preparing the reference electrodes.

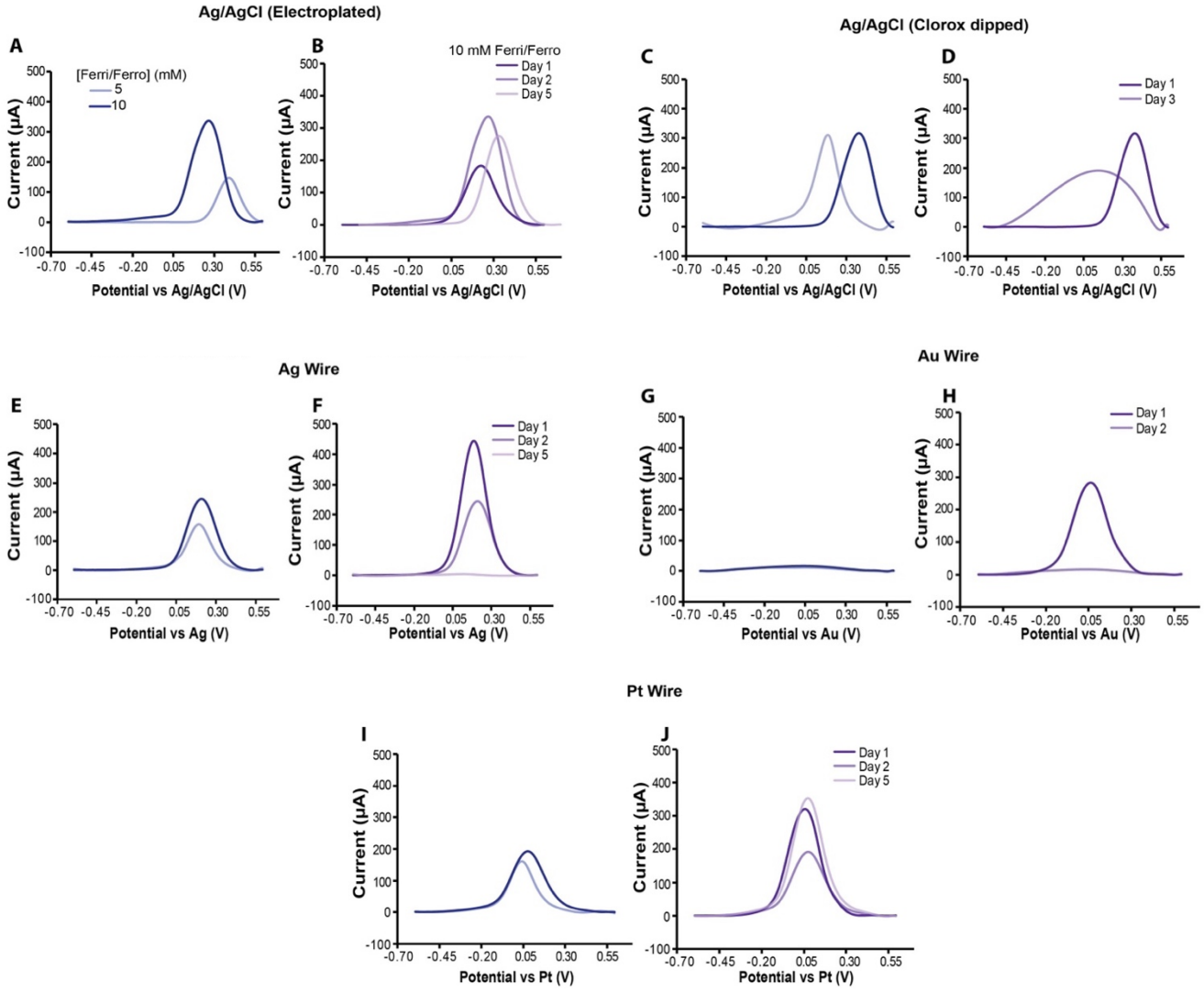

Figure 5.5 Comparison of reference electrodes, where two different concentrations of potassium ferricyanide/ ferrocyanide were measured. **(A)** In-house electroplated Ag/AgCl electrode. A silver wire was dipped in saturated KCl and electroplated at 4 V for 5 min. Figure shows differential peak current at 464 Hz. **(B)** Measurement of 5 mM ferri/ferro using the electroplated Ag/AgCl electrode on three days. **(C)** Measurement using Ag/AgCl reference electrode prepared by dipping Ag wire in Clorox solution. **(D)** EC measurements done using this electrode on day 1 and 3 for 5 mM ferri/ferro solutions. **(E)** EC measurements using Ag wire as the reference electrode. (F) Measuring 5 mM ferri/ferro solution on days 1, 2 and 5. **(G)** Measurements done using Au wire as reference electrode and **(H)** Measurements done on two consecutive days. (I) Measurements done

using Pt reference electrode and **(J)** EC measurements performed on days 1,2 and 5 for 5 mM ferri/ferro solution.

For the electroplated Ag/AgCl electrodes we observed drastic shifts in peak voltages for the two concentrations of potassium ferri/ferrocyanide as well as over the days, combined with observing a possible oxide layer deposition over time. Furthermore, Clorox based Ag/AgCl electrodes as well as Au wire used as reference did not give us any appreciable results. With the Au wires we observed deterioration of performance after a single use, demonstrating to be the least stable of all. The Ag and Pt pseudo reference electrodes showed promising results. However, with the Ag electrode a loss in EC signal was observed after a week. Tarnishing of Ag surface was seen, which prevented its further use. In comparison, the Pt microwires showed less fluctuations in peak voltage shifts even after a week. Variations in peak current over the days may be attributed to improper cleaning of Au-μE. In order to confirm that Pt wires can used as the reference electrode, we measured 3 different concentrations of methylene blue solution (100 μM, 500 μM and 1000 μM). We observed good performance stability with less shift in methylene blue redox potential (data not shown). Therefore, for all the experiments in the following sections, we used the Pt wire as a pseudo reference.

5.3.2 Modification of gold microelectrode (Au-μE) for sensing DNA

After selecting the potentially best reference electrode, we proceeded to modify the Au-μE for DNA sensing. **Figure 5.6A** shows the sensing principle. A thiolated DNA (thiol-DNA) was immobilized on the electrode surface. A 40 bp complementary having a methylene blue DNA (MB-40) was added. After incubation was completed, the peak currents were measured at different SWV frequencies using the Pt pseudo reference electrode and Pt counter electrode. As a reference

system, GoG electrodes immobilized with MB-40 were used. The concentration of thiol-DNA added on to the electrode was 1000 nM and MB-40 was 200 nM. Although we expected to observe a peak current corresponding to MB-40 on the Au-µE, compared to the GoGs, no signal was observed (**Figure 5.6B**).

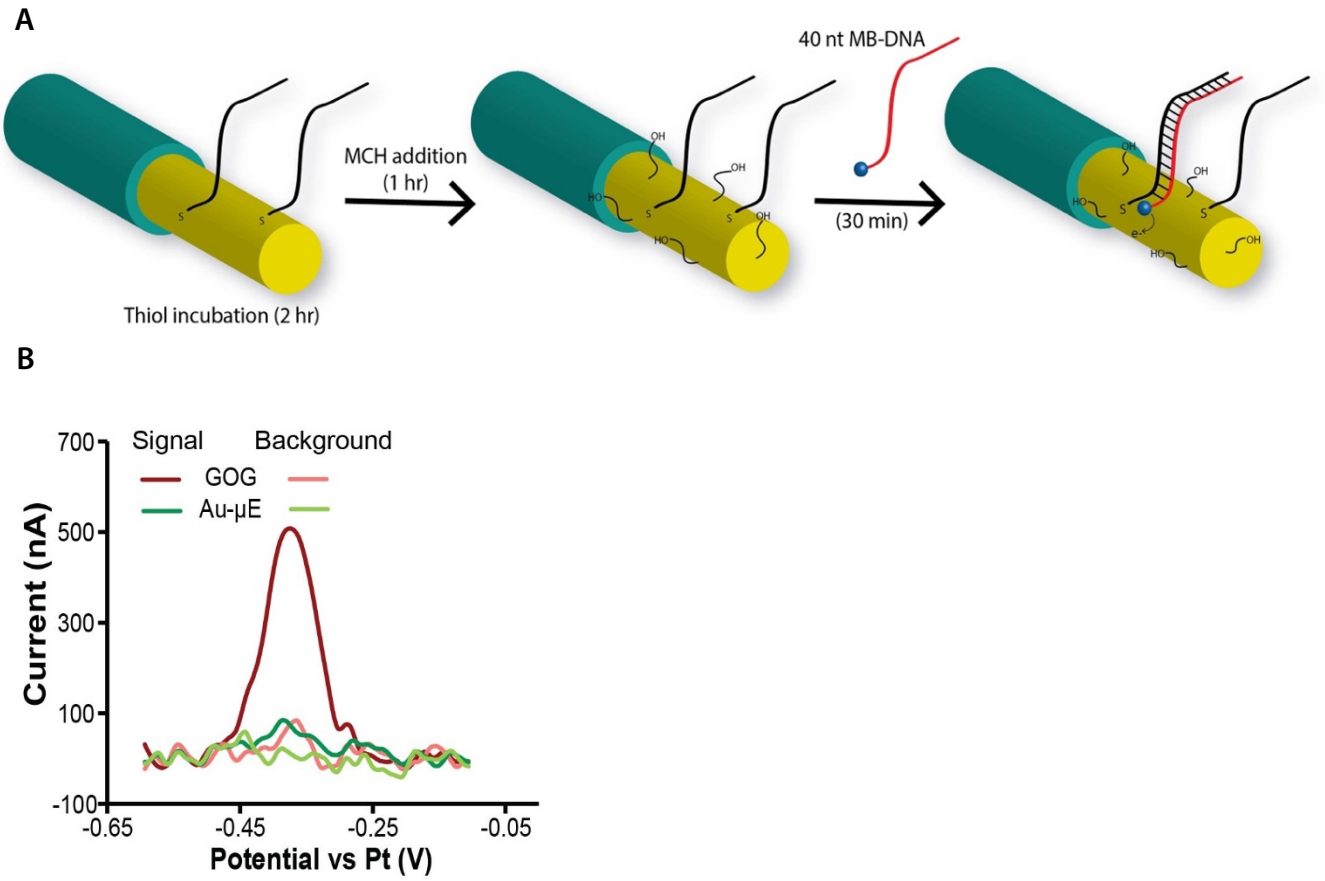

Figure 5.6 DNA sensing using gold microelectrodes. **(A)** A 40 bp complementary methylene blue DNA (MB-40) is added on to the gold surface which carries a monolayer of thiolated DNA. The hybridization of thiol- DNA to MB-40 brings the methylene blue closer to the electrode surface and generates an EC signal. **(B)** Peak currents measured for 200 nM of MB-40, at 464 Hz. It can be clearly obsreved that compared to the GoG electrodes, the Au-µE did not show a peak current in the presence of MB-40.

We reasoned that this might be due to insufficient number of thiol- DNA on the Au-µE surface for hybridizing with MB-40. More specifically we hypothesized that the Au-µEs may require a longer incubation time (> 1 h) to form the self-assembled monolayer of thiol- DNA. To test our hypothesis, we incubated thiol- DNA for 2 h, 3 h, 4 h and overnight at room temperature. As expected, we were able to observe peak currents for MB-40 when the lonegr incubation times were used. Since the peak currents were observed after 2 h of thiol incubation, we selected this time as thiol-incubation time. **Figure 5.7** below shows the results. The SWV peak for 2 h in this figure shows a convolution, which we attribute to be a contamination of the working electrode.

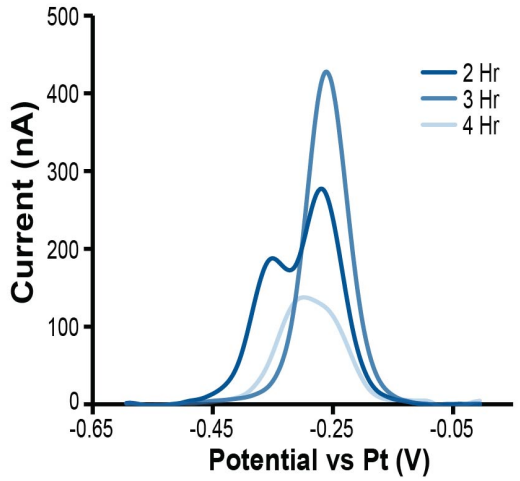

Figure 5.7 variation of thiol- DNA incubation times on microelectrodes. Results indicated that it was important to use an incubation time > 1 h. Although we were able to observe peak currents after 3 and 4 h, we selected 2 h as the incubation time.

For proper assay performance, it was important to make sure that the Au-µE was dipped in the solutions of DNA and respective analytes. A problem faced during this was the formation of air bubbles within the PDMS well after fixing the electrode mold having the Au-µE. Pushing of the mold into the well imposes a pressure, creating air bubbles within the solution (**Figure 5.8A**).

This in turn reduces the volume of solution that is exposed to the Au-µE, which ultimately effects the peak currents of methylene blue at the final measurement step. One of the initial designs of the electrode holder included a completely circular base which created the pressure (**Figure 5.8B**). However, after several testing and design improvements, we utilized an electrode holder which consisted of grooves to release pressure (**Figure 5.8C**). this design helped us reduce or eliminate air bubble formation.

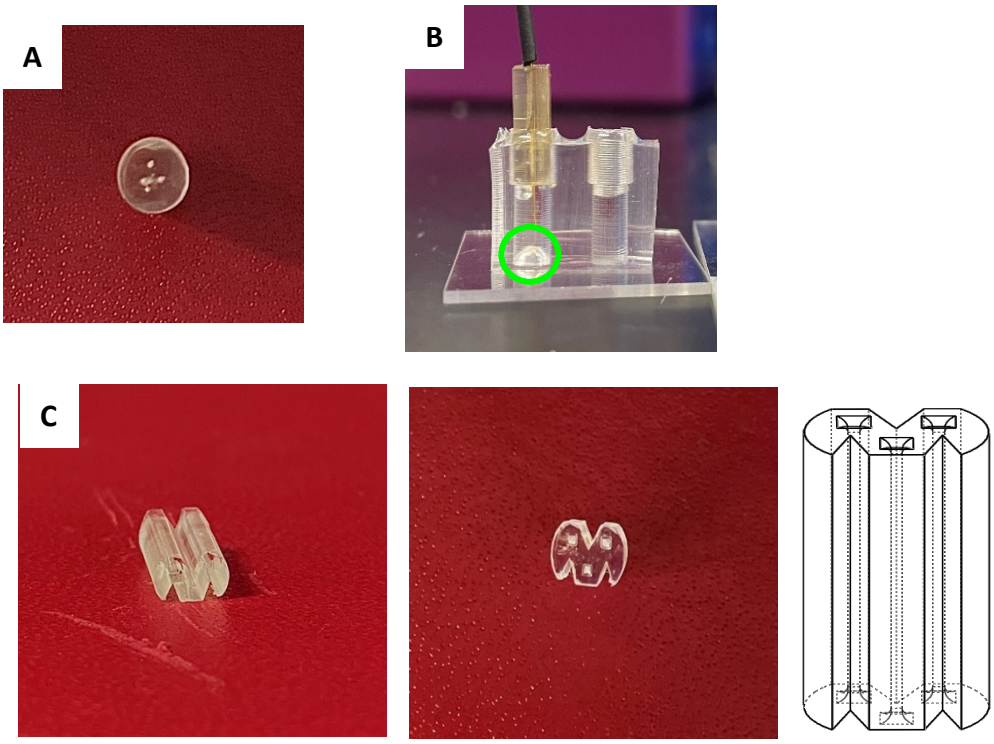

Figure 5.8 Microelectrode holder design modification. **(A)** A cylindrical holder with a perfectly round base. **(B)** Although the holders fitted well, air bubbles were created within solutions filled wells when the holder with electrodes were inserted (as highlighted in green). **(C)** After several trials, "M" shaped electrode holders were designed, and 3D printed. This design was able to reduce or eliminate the formation of air bubbles and allow more Au-µE surface to come in contact with solution.

5.3.3 Assembly of DNA nanostructure on Au-μE for anti-estradiol antibody sensing

Since DNA assembly on microelectrodes was achieved and a 40 bp methylene blue DNA was successfully detected, we moved forward to assembling the DNA nanostructure on Au-μE, which was developed by our lab for biomarker sensing. As discussed in chapter 1, the nanostructure is formed by the ligation of three DNA segments which includes a thiolated-DNA attached to the gold electrode surface, a target recognizing DNA and a methylene blue DNA. Post ligation, a longer continuous DNA strand is formed [2, 4, 7].

Thus far, the nanostructures assembled on 2D planar GoG electrodes employed 30 nM thiolated DNA to form the SAM. With the experiments performed for MB-40 detection, we utilized a thiol-DNA treatment with a concentration of 1000 nM. Therefore, prior to proceeding forward with nanostructure assembly on Au-μE, we decided to detect MB-40 using various concentrations of thiol- DNA. This experiment gave us a rough idea of how low of a thiol- DNA concentration can be used for SAM immobilization on the Au-μE. **Figure 5.9** shows the experimental results. We used 5 different thiol- DNA concentrations (50, 100, 200, 500 and 1000 nM). As shown in **Figure 5.9**, 50 nM of thiol- DNA showed improved peak currents, compared to the other higher concentrations. In nanostructure assembly, it is important to keep the thiol- DNA concentration considerably low, since the electrode surface should have assembled nanostructures at optimized distances, for better sensor performance. If the electrode surface is densely packed, the formed DNA nanostructures will not generate changes in current in the presence and absence of target as hypothesized, due to restrictions in scaffold movement (tethered diffusion) resulting from surface crowding. Therefore, based on these reasons, we used 50 nM of thiolated DNA for nanostructure construction.

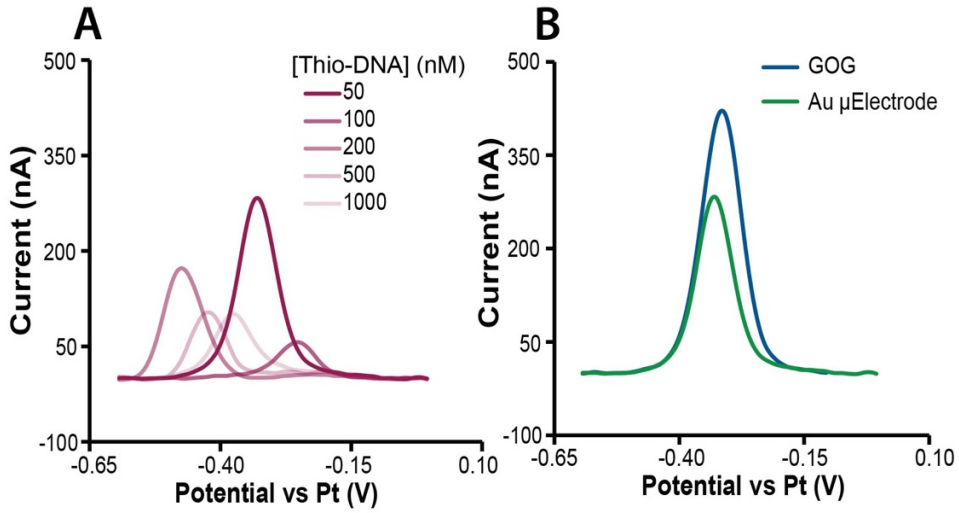

Figure 5.9 Variation of thiol- DNA on Au-µE surface. **(A)** 50 nM thiol- DNA gave higher signals in the presence of 200 nM MB-40. The Pt pseudo reference electrodes were used and we observed thiol- DNA concentration dependent shifts in peak voltages. (**B)** The peak currents for 50 nM thiol-DNA were compared with GoG electrodes.

Using 50 nM of ns_PEG-thiol- DNA, a monolayer of thiols was formed on the Au-µE surface as described in section 5.2.6. For this experiment, we constructed a nanostructure for the small molecule female steroidal hormone, estradiol. **Figure 5.10** below illustrates the principle of ligation. The ligation mixture having 100 nM of estradiol Anc-DNA, 100 nM of 1-MB-DNA, 1 mM of ATP and T4-DNA ligase for added to a PDMS well. The mixture volume was 20 µL. The Au-µE having immolized thiolated DNA was dipped into this well and was left for 6 h at room temperature, to allow ligation and formation of a continuous strand of single estradiol DNA nanostructure (**Figure 5.10A**). **Figure 5.10B** illustrates the sensing principle of estradiol nanostructure. Initially, the constructed nanostructure demonstrates faster tethered diffusion. Upon addition of anti-estradiol antibody, we expect a slower rate of tethered diffusion, which can be observed by a decrease in peak current compared to the former, due to overall change in mass of DNA scaffold and possibly also due to steric effects (**Figure 5.10B, center**). If the solution has

free estradiol, the anti-estradiol antibody will bind to it and not to the electrode, increasing the rate of tethered diffusion of the DNA-nanostructure (**Figure 5.10B, right**). This allows indirect quantification of estradiol, in theory.

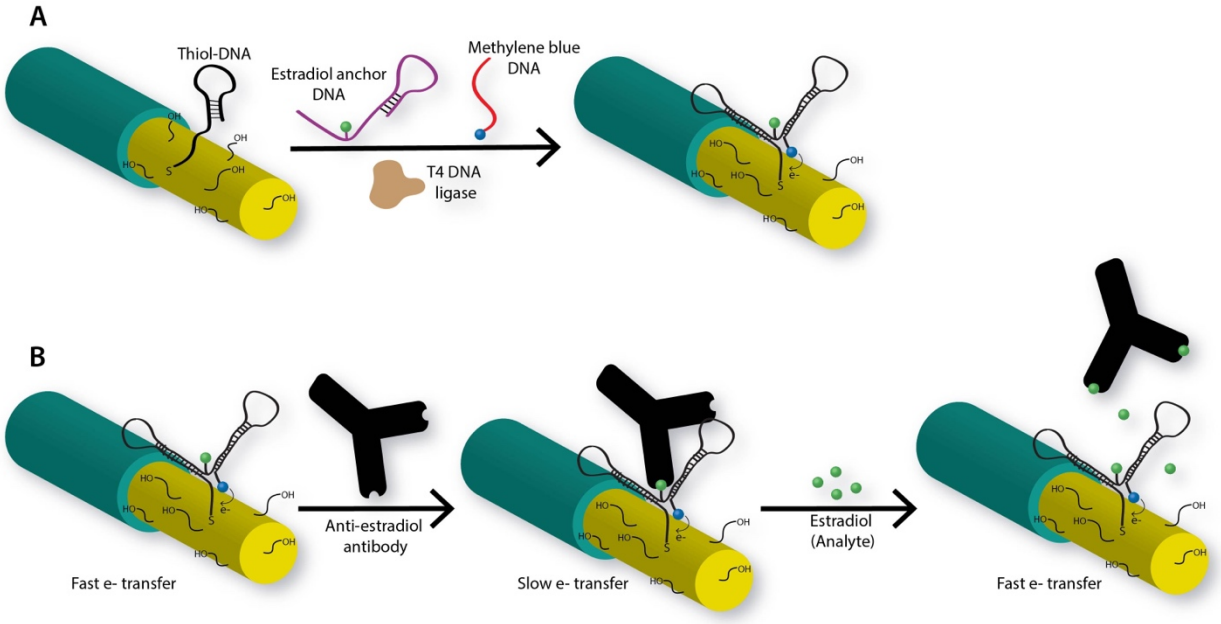

Figure 5.10 Sensing principle and construction of estradiol DNA nanostructure. **(A)** Nanostructure is constructed by ligation of three DNA strands, ns_PEG-thiol- DNA, 1-MB-DNA and estradiol Anc-DNA. **(B)** In the absence of antibody, the nanostructure shows faster tethered diffusion, resulting in higher peak currents. Addition of anti-estradiol antibody will drop the generated peak current. In the presence of free estradiol, the antibody will be shielded from binding to the DNA anchor, which will result in higher peak current.

Recently, we showed that the introduced DNA- nanostructure can be used for detection of sex hormones, on 2D planar (GoG) electrodes, where the respective antibodies and analytes were incubated on the electrode surface for 30 min, post optimization (manuscript in preparation). Thus, based on this work, we incubated 20 nM of estradiol antibody with the fabricated Au-μE for 30

min at room temperature. Prior to antibody addition, the SWV measurements of the Au-μE were performed. **Figure 5.11** below shows the SWV measurements performed before and after addition of anti-estradiol antibody. As hypothesized, we were able to observe a drop in signal with a magnitude of ~ 33 %. Percent change in signal was calculated as follows, where I_o is the initial current measured prior to addition of antibody and I_F is the final current measured after antibody addition. As given in **Figure 5.11A**, we also observed a shift in peak voltage (~ -70 mV) after addition of anti-estradiol.

$$\%\, Signal\ change = \frac{I_0 - I_F}{I_0}\ x\ 100$$

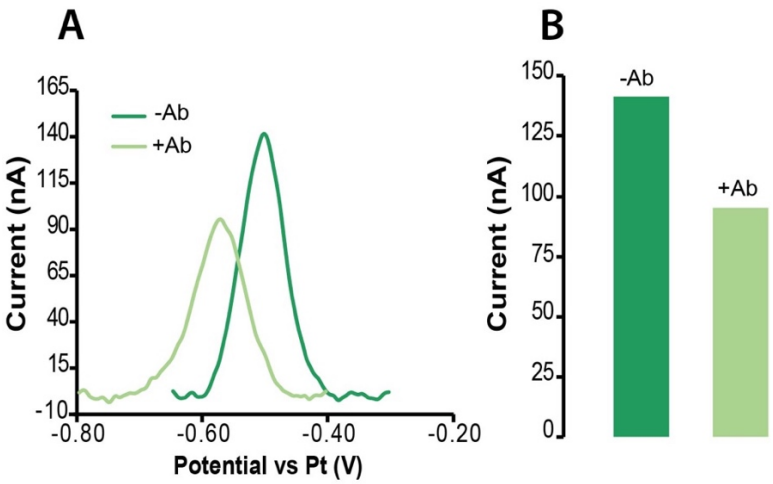

Figure 5.11 Detection of anti-estradiol antibody using Au-μE. **(A)** Current vs potential graph indicating the nanostructure in the absence and presence of antibody. Addition of antibody, slows down the rate of electron transfer, leading to reduced current. **(B)** Peak currents in the absence of presence of antibody. Results are shown for SWV scanned at 464 Hz.

However, ~ 60 % of signal drop was observed for the same concentration of anti- estradiol antibody when the DNA nanostructure was assembled on the GoG electrodes (data not shown). It is noteworthy that when GoGs were used, a thiol-DNA treatment concentration of 30 nM was used. Therefore, we assume that, for the existing Au-µE, the lesser signal suppression maybe due to the use of 50 nM thiol-DNA, which creates a more densely packed surface, which reduces the binding of antibody to anchor recognition unit. However, we still decided to perform a kinetic study to see whether the antibody incubation time can be optimized for the existing thiol-DNA concentration on Au-µE (**Figure 5.12**). Thus, we measured the change in signal every 3 min for 1 h and observed that the system begins to reach a plateau at 45 min. Still, however, the signal suppression was observed to be ~33 %, even after 1 h. With these results, we can conclude that, under the current experimental conditions, the estradiol DNA nanostructure is able to give a 33 % drop in signal, post anti-estradiol antibody incubation. We hypothesize that further signal reduction can be achieved if the thiol-DNA concentration is reduced.

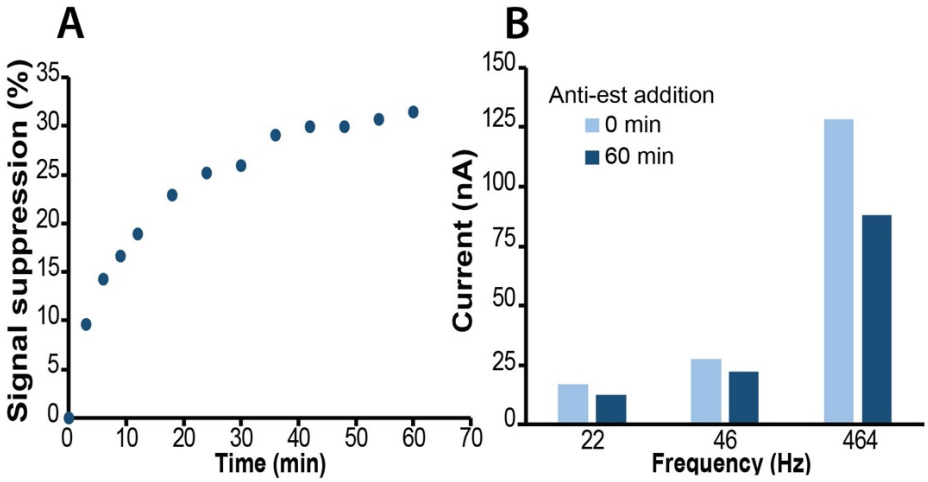

Figure 5.12 Kinetic study for antibody incubation. **(A)** The Au-µE was dipped into a solution of 20 nM anti-estradiol antibody and signal suppression was monitored over 1 h. The sensor showed to plateau off at 45 min (measurement at a SWV frequency of 464 Hz). **(B)** Peak currents of the sensor before antibody addition and 1 h after addition of antibody. The figures indicate that in the

presence of anti-estradiol antibody (20 nM), the sensor under current experimental conditions can achieve ~33 % suppression in signal time after antibody addition.

5.4 Conclusions

Inspired from the Plaxco group on the extensive use of gold microwires as working electrodes, we have shown our attempts of transitioning from 2D planar GoGs to Au-μEs. The end goal of this project is to incorporate the optimized Au-μE with 3D printed microfluidics for detection of biomarkers, specially using the DNA- nanostructure developed by our lab. Thus far, as described in this chapter, we have been able to identify a suitable reference electrode, instead of using a commercial Ag/AgCl electrode. Our reasoning to adapting Pt wire as a pseudo reference is mainly due to the future difficulty of using a commercial reference electrode within microfluidic channels. Furthermore, in this work we have designed custom, 3D printed micro electrode holders which are able to support the three-electrode system, which facilitates the easy handling of such a small structure. Most importantly, in this initial work we have demonstrated the successful assembly of considerably low concentration of thiol-DNA on the smooth Au wire surface, which is important for optimized positioning of the DNA- nanostructures. Although we have been able to achieve the successful assembly of our bowtie DNA nanostructure and observe a drop in signal as hypothesized in the presence of respective antibodies, the system needs to be optimized further for best results in analyte sensing.

5.5 Reference

(1) Dai, Y.; Liu, C. C. Recent advances on electrochemical biosensing strategies toward universal point-of-care systems. *Angewandte Chemie* **2019**, *131* (36), 12483-12496.
(2) Gurukandure, A.; Somasundaram, S.; Kurian, A. S.; Khuda, N.; Easley, C. J. Building a nucleic acid nanostructure with DNA-epitope conjugates for a versatile electrochemical protein detection platform. **2023**.
(3) Hai, X.; Li, Y.; Zhu, C.; Song, W.; Cao, J.; Bi, S. DNA-based label-free electrochemical biosensors: From principles to applications. *TrAC Trends in Analytical Chemistry* **2020**, *133*, 116098.
(4) Somasundaram, S.; Easley, C. J. A Nucleic Acid Nanostructure Built through On-Electrode Ligation for Electrochemical Detection of a Broad Range of Analytes. *J Am Chem Soc* **2019**, *141* (29), 11721-11726. DOI: 10.1021/jacs.9b06229.
(5) Vafaiee, M.; Vossoughi, M.; Mohammadpour, R.; Sasanpour, P. Gold-Plated Electrode with High Scratch Strength for Electrophysiological Recordings. *Scientific Reports* **2019**, *9* (1), 2985. DOI: 10.1038/s41598-019-39138-w.
(6) Holtan, M. D.; Somasundaram, S.; Khuda, N.; Easley, C. J. Nonfaradaic Current Suppression in DNA-Based Electrochemical Assays with a Differential Potentiostat. *Analytical chemistry* **2019**, *91* (24), 15833-15839.
(7) Khuda, N.; Somasundaram, S.; Easley, C. J. Electrochemical Sensing of the Peptide Drug Exendin-4 Using a Versatile Nucleic Acid Nanostructure. *ACS Sensors* **2022**, *7* (3), 784-789. DOI: 10.1021/acssensors.1c02336.
(8) Khuda, N.; Somasundaram, S.; Urgunde, A. B.; Easley, C. J. Ionic Strength and Hybridization Position near Gold Electrodes Can Significantly Improve Kinetics in DNA-Based Electrochemical Sensors. *ACS Appl Mater Interfaces* **2023**. DOI: 10.1021/acsami.2c22741 From NLM Publisher.
(9) Somasundaram, S.; Holtan, M. D.; Easley, C. J. Understanding Signal and Background in a Thermally Resolved, Single-Branched DNA Assay Using Square Wave Voltammetry. *Analytical Chemistry* **2018**, *90* (5), 3584-3591. DOI: 10.1021/acs.analchem.8b00036.
(10) Arroyo-Currás, N.; Dauphin-Ducharme, P.; Ortega, G.; Ploense, K. L.; Kippin, T. E.; Plaxco, K. W. Subsecond-Resolved Molecular Measurements in the Living Body Using Chronoamperometrically Interrogated Aptamer-Based Sensors. *ACS Sensors* **2018**, *3* (2), 360-366. DOI: 10.1021/acssensors.7b00787.
(11) Arroyo-Currás, N.; Scida, K.; Ploense, K. L.; Kippin, T. E.; Plaxco, K. W. High Surface Area Electrodes Generated via Electrochemical Roughening Improve the Signaling of Electrochemical Aptamer-Based Biosensors. *Analytical Chemistry* **2017**, *89* (22), 12185-12191. DOI: 10.1021/acs.analchem.7b02830.
(12) Arroyo-Currás, N.; Somerson, J.; Vieira, P. A.; Ploense, K. L.; Kippin, T. E.; Plaxco, K. W. Real-time measurement of small molecules directly in awake, ambulatory animals. *Proceedings of the National Academy of Sciences* **2017**, *114* (4), 645-650.
(13) Arroyo-Currás, N. y.; Dauphin-Ducharme, P.; Ortega, G.; Ploense, K. L.; Kippin, T. E.; Plaxco, K. W. Subsecond-resolved molecular measurements in the living body using chronoamperometrically interrogated aptamer-based sensors. *ACS sensors* **2018**, *3* (2), 360-366.
(14) Idili, A.; Gerson, J.; Kippin, T.; Plaxco, K. W. Seconds-resolved, in situ measurements of plasma phenylalanine disposition kinetics in living rats. *Analytical chemistry* **2021**, *93* (8), 4023-4032.

(15) Idili, A.; Arroyo-Currás, N.; Ploense, K. L.; Csordas, A. T.; Kuwahara, M.; Kippin, T. E.; Plaxco, K. W. Seconds-resolved pharmacokinetic measurements of the chemotherapeutic irinotecan in situ in the living body. *Chemical science* **2019**, *10* (35), 8164-8170.
(16) Ferguson, B. S.; Hoggarth, D. A.; Maliniak, D.; Ploense, K.; White, R. J.; Woodward, N.; Hsieh, K.; Bonham, A. J.; Eisenstein, M.; Kippin, T. E.; et al. Real-Time, Aptamer-Based Tracking of Circulating Therapeutic Agents in Living Animals. *Science Translational Medicine* **2013**, *5* (213), 213ra165-213ra165. DOI: doi:10.1126/scitranslmed.3007095.

Chapter 6

Concluding Remarks and Future Directions

6.1 Concluding remarks

In this dissertation, we have expanded the applications of DNA-based proximity assays for biomolecular detection utilizing both fluorescence and electrochemical detection platforms, where increased probe flexibility was shown to improve multiple assay types.

We have introduced two novel applications of thermofluorimetric analysis (TFA). Previously this method was used by our lab to detect several analytes at appreciable LODs [1-3]. In this work, we have developed an antibody detection assay leveraging TFA. This is a simple mix-and-read assay which can be performed within a comparatively shorter period of time, compared to methods such as ELISA, and repurposes a commonly available qPCR instrument. Furthermore, we have employed TFA to study the effects of valency on proximity-based assays which utilize antibody oligonucleotides (AbOs) as recognition units. Herein, effects of monovalent and multivalent AbO probe valency were assessed using 12-fold lesser amounts of reagents compared to gel separations, making the method a valuable tool of analyzing precious samples.

Perhaps most importantly, in this TFA work we highlight that proximity assays involving several DNA strands should possess sufficient flexibility to promote the hybridization of the short DNA strands, which can improve assay performance. ssDNA segments were replaced with polyethylene glycol (PEG) linkers which promoted short signaling DNA hybridization[4]. In chapter 2 we introduced the application of TFA in developing a fluorescence assay for biomarker detection

using split broccoli aptamers. Although the system did not demonstrate results as hypothesized, we believe that the assay may be functional in future if the PEG linkers (introduced in chapter 3) can be incorporated into the split aptamers. Careful identification of the location of insertion and optimization has to be done such that the fluorophore (DFHBI) binding pocket is not being disrupted.

The electrochemical proximity assay was introduced by our group previously [5, 6]. In this dissertation, we modified this assay for antibody detection. We adopted the fluorescence-based system developed above to an electrochemical assay by modifying the signaling DNA strands to carry a thiolated-DNA (attached to a gold electrode surface) and complementary DNA strands modified with a methylene blue (redox moiety) molecule. Compared to the develop TFA method, we were able to achieve a lower LOD for anti-digoxigenin antibody detection. To improve assay performance, we again used PEG spacers as mentioned above at selected sections of the DNA strands. Compared to the unmodified electrochemical sensor, the sensor with PEG spacers showed a 4-fold increase in antibody-dependent SWV currents. Moreover, the current sensor design allows two methylene blue molecules to approach the sensor surface in response to one antibody binding event, which also contributes to improved LODs.

Electrochemical techniques have been the method of choice to develop biosensors for the purposes of point-of-care (POC), point-of-need and functioning in limited resource settings [7-9]. Electrochemical sensors in our lab are developed mainly utilizing patterned gold-on-glass (GoG) slides through a standard photolithographic process. The Plaxco group utilized gold microwires to detect analytes within live rats, in whole blood and in real time [10-12]. Inspired from this work, in chapter 5 we have attempted adopting DNA-based sensors developed in our lab on GoG electrodes on gold microwires of 0.25 mm diameter. Herein, we have demonstrated the use of Pt microwires

(0.25 mm diameter) as pseudo references, as opposed to the commercially available Ag/AgCl reference electrodes. This preliminary study presents the assembly of the developed DNA nanostructure and design optimizations done to achieve functional gold microwires.

6.2 Future directions

6.2.1 Antibody detection

Antibodies can be important biomarkers in disease recognition. They have the capability of binding to a variety of biomolecules ranging from small molecules (such as steroids), proteins, cells and viruses. As mentioned in this dissertation, we have introduced both FRET-based TFA and electrochemical proximity assays for antibody detection. Although anti-digoxigenin antibody and its corresponding small molecule antigen, digoxigenin have been used as proof of concept, we believe that the method can be adopted to detect clinically relevant targets.

Antibodies specially related to certain allergy conditions can be targets of interest. The body produces IgE antibodies in response to allergy conditions related to food, certain chemicals etc. It is important that if such allergy conditions are severe, they should be diagnosed and treated promptly. However, identification of specific cause for an allergy may take longer (as much as one month) due to the prevailing methods of testing. We hypothesize that, the developed DNA-proximity-based assay in this work can be of useful for the diagnosis of some common, yet severe allergy conditions within a shorter period of time. Recognition elements (antigens) of interest may not only be limited to small molecules, but also to full peptide molecules, protein fragments (epitopes) and even peptide nucleic acids (PNAs). The developed TFA assay permits modification for multiplexing, where two or more FRET pairs (nonoverlapping absorbances) maybe be used, with slightly modified complementary sequences for the target of interest . The developed antibody ECPA with above suggestions may provide better limits of detection. Furthermore, the effects of

probe packing density has not been extensively studied in this version of ECPA. Therefore, density of the thiolated DNA molecules attaching to the surface can be further optimized with respect to thiol-DNA concentration, as well as respective modifications to thiol-DNA.

6.2.2 Replacing GoG electrodes with microelectrodes

In chapter 5, we have shown the use of gold microwires for DNA nanostructure construction. Although experimental conditions of this system are yet to be optimized, it holds promising benefits over GoG. GoGs have to be fabricated by patterning the electrodes of required size by a photolithographic process. The use of microwires completely eliminates this step, which makes the work load easier. Although Pt wires have been used herein as pseudo electrodes, we have been observing shifts in peak voltages time to time, which is usually minimal in commercially available reference electrodes such as Ag/AgCl. Therefore, we suggest that more characterization has to be done on the use of Pt microwires in terms of stability, such that minimum peak shifting is observed. This can include both electrochemical measurements and surface characterization techniques.

We have demonstrated the successful assembly of an estradiol DNA- nanostructure in the preceding chapter. However, we have been able to achieve only 33 % suppression in signal upon anti-estradiol antibody addition (20 nM), which is lower than what is achieved by GoG. Currently, we attribute this reduction to the thiol-DNA concentration (probe packing density) on the surface. The Au-μE uses 50 nM of thiol-DNA for immobilization, whereas the GoG uses 30 nM. We hypothesize that, the higher concentration of thiol-DNA on Au-μE might be leading to the formation of a more tightly packed surface with DNA nanostructure, which reduces the binding of respective antibody. Therefore, it is important to optimize thiol-DNA concentration, which hints that it should be reduced further. This will ensure enough spacing between the assembled DNA

nanostructures. Followed by this, we intend of using the sensor to measure free estradiol as shown in **Figure 5.10B** (right).

Another issue faced during the use of Au-μE is the sensor-to-sensor variability. It has been shown earlier that planar wires or planar electrode surfaces may suffer from inconsistent results due to the electrode surface not achieving a consistent SAM [11, 13]. Improper probe DNA packing can hamper sensor performance. Therefore, it was shown that such variations can be minimized by enhancing the gold surface area via electrodeposition of gold nanostructures. This has shown to improve electrochemical signals drastically [11, 13, 14]. Thus, for the Au-μE immobilized with the DNA- nanostructure, we suggest electrochemical surface roughening using sulfuric acid. This is an easy technique, where surface roughened electrodes can be generated in few minutes [11]. However, the time needed, number of electrochemical pulses, etc. will have to be optimized, followed by electron microscopy data for best results.

An important goal of adopting our existing nanostructure assays to microelectrodes is to be able to integrate with microfluidics. Recently in our lab, we have been developing microfluidic devices based on 3D printing. 3D printed microfluidic devices bear the advantages of easy fabrication (as opposed to the tedious photolithographic processes followed by conventional microfluidic chip fabrication), requirement of comparatively lesser fabrication time (since high resolution 3D printers are available currently, a chip can be printed within about an hour or so, depending on complexity and requires less technical skill. Recently we integrated such a 3D printed microfluidic chip with a DNA- nanostructure assembled on a GoG for cortisol detection (preliminary study). **Figure 6.1A** shows the assembled microfluidic chip with an electrode. Herein, the Pt microwires were used as pseudo reference and counter electrodes. **Figure 6.1B** shows the

decrease in peak current over time after addition of 10 nM anti-testosterone antibody. A major issue faced during this experiment was the leaking of GoG electrode after assembling on the chip and the practical difficulty of inserting the electrode to the chip, which led to leaking of solution often. As a solution to this, we suggest the use of developed microelectrode system. As shown in **Figure 6.2** the electrode holder can be directly fitted through the chip, such that it comes in contact with flowing solution. This allows easy manipulation of device. We believe that this system will be able to mimic the pumping of bodily fluids (such as serum) and allow mimicking of fluid circulation and real time monitoring.

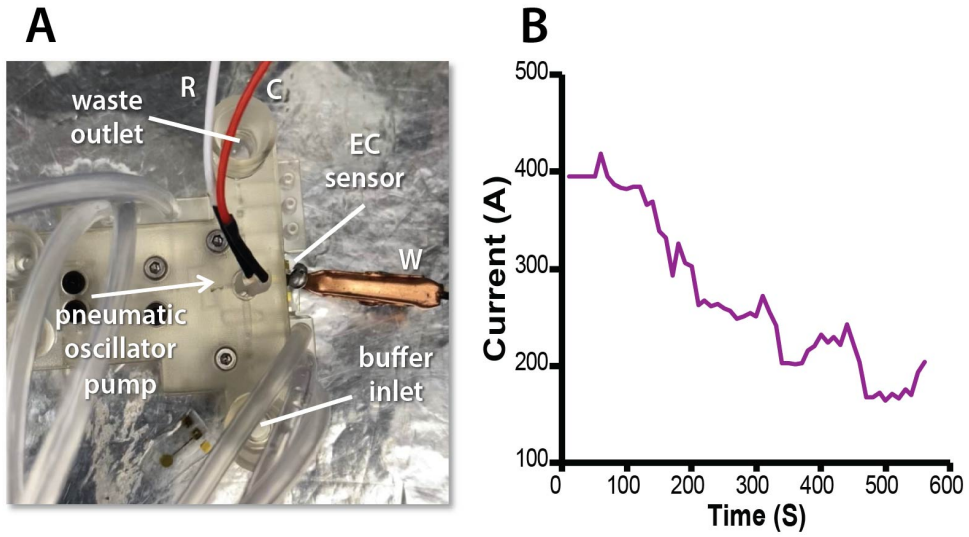

Figure 6.1 Integration of microfluidics with existing GoG sensor. **(A)** A setup which shows a GoG electrode having testosterone DNA- nanostructure assembled on to a 3D printed microfluidic chip. Reference and counter electrodes comprise of Pt microwires. The pneumatic oscillator pumps fluid to the chamber having the electrode. **(B)** Change in current (decrease in signal) after addition of anti-testosterone antibody was measured over time. As expected, a decrease in signal was observed.

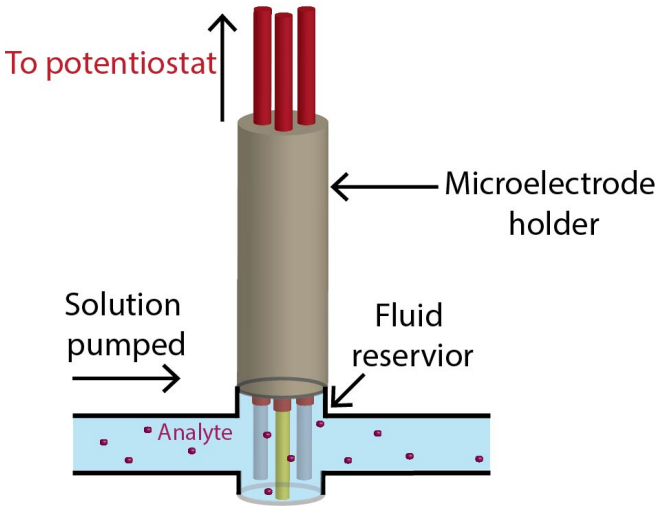

Figure 6.2 An illustration of a proposed microelectrode system fixed to a fluidic reservoir of a microfluidic chip. An oscillator pump will pump small volumes of analyte solution continuously or at controlled intervals. The gold microelectrode will have DNA- nanostructures immobilized, for analyte sensing. While solution flows, an EC signal will be generated in real time.

6.3 Final Comments

Overall, this dissertation work has been able to contribute advancements to several bioanalytical assay platforms. Both fluorescence based (TFA) and electrochemical platforms were extensively studied, with the major application being antibody sensing. The results of these studies point to an important role of probe flexibility, particularly when leveraging hybridization of multiple DNA strands and proximity-dependent binding. Polyethylene glycol (PEG) linkers were used to improve performance of a TFA-based antibody sensor, and electrochemical antibody sensor, and a DNA nanostructure sensor used for various other analytes. While several other studies were also included here (split aptamer sensors, microelectrodes), the probe flexibility improvements were the key advancement. We expect that various other DNA-based (or other) bioassays could be enhanced by carefully considering the flexibility of the probes.

6.4 Reference

(1) Hu, J.; Easley, C. J. Homogeneous Assays of Second Messenger Signaling and Hormone Secretion Using Thermofluorimetric Methods That Minimize Calibration Burden. *Anal Chem* **2017**, *89* (16), 8517-8523. DOI: 10.1021/acs.analchem.7b02229.
(2) Hu, J.; Kim, J.; Easley, C. J. Quantifying Aptamer-Protein Binding via Thermofluorimetric Analysis. *Anal Methods* **2015**, *7* (17), 7358-7362. DOI: 10.1039/c5ay00837a.
(3) Hu, J.; Kim, J.; Easley, C. J. Quantifying aptamer–protein binding via thermofluorimetric analysis. *Analytical Methods* **2015**, *7* (17), 7358-7362.
(4) Kurian, A.; Gurukandure, A.; Dovgan, I.; Kolodych, S.; Easley, C. Thermofluorimetric Analysis (TFA) using Probes with Flexible Spacers: Application to Direct Antibody Sensing and to Antibody-Oligonucleotide (AbO) Conjugate Valency Monitoring. **2023**.
(5) Hu, J.; Wang, T.; Kim, J.; Shannon, C.; Easley, C. J. Quantitation of femtomolar protein levels via direct readout with the electrochemical proximity assay. *J Am Chem Soc* **2012**, *134* (16), 7066-7072. DOI: 10.1021/ja3000485 From NLM Medline.
(6) Hu, J.; Yu, Y.; Brooks, J. C.; Godwin, L. A.; Somasundaram, S.; Torabinejad, F.; Kim, J.; Shannon, C.; Easley, C. J. A reusable electrochemical proximity assay for highly selective, real-time protein quantitation in biological matrices. *J Am Chem Soc* **2014**, *136* (23), 8467-8474. DOI: 10.1021/ja503679q From NLM Medline.
(7) Gurukandure, A.; Somasundaram, S.; Kurian, A. S.; Khuda, N.; Easley, C. J. Building a nucleic acid nanostructure with DNA-epitope conjugates for a versatile electrochemical protein detection platform. **2023**.
(8) Ogden, N. E.; Kurnik, M.; Parolo, C.; Plaxco, K. W. An electrochemical scaffold sensor for rapid syphilis diagnosis. *Analyst* **2019**, *144* (17), 5277-5283. DOI: 10.1039/c9an00455f From NLM Medline.
(9) Somasundaram, S.; Holtan, M. D.; Easley, C. J. Understanding Signal and Background in a Thermally Resolved, Single-Branched DNA Assay Using Square Wave Voltammetry. *Analytical Chemistry* **2018**, *90* (5), 3584-3591. DOI: 10.1021/acs.analchem.8b00036.
(10) Arroyo-Currás, N.; Dauphin-Ducharme, P.; Ortega, G.; Ploense, K. L.; Kippin, T. E.; Plaxco, K. W. Subsecond-Resolved Molecular Measurements in the Living Body Using Chronoamperometrically Interrogated Aptamer-Based Sensors. *ACS Sensors* **2018**, *3* (2), 360-366. DOI: 10.1021/acssensors.7b00787.
(11) Arroyo-Currás, N.; Scida, K.; Ploense, K. L.; Kippin, T. E.; Plaxco, K. W. High Surface Area Electrodes Generated via Electrochemical Roughening Improve the Signaling of Electrochemical Aptamer-Based Biosensors. *Analytical Chemistry* **2017**, *89* (22), 12185-12191. DOI: 10.1021/acs.analchem.7b02830.
(12) Idili, A.; Arroyo-Currás, N.; Ploense, K. L.; Csordas, A. T.; Kuwahara, M.; Kippin, T. E.; Plaxco, K. W. Seconds-resolved pharmacokinetic measurements of the chemotherapeutic irinotecan in situ in the living body. *Chemical science* **2019**, *10* (35), 8164-8170.
(13) Liu, J.; Wagan, S.; Dávila Morris, M.; Taylor, J.; White, R. J. Achieving reproducible performance of electrochemical, folding aptamer-based sensors on microelectrodes: challenges and prospects. *Analytical chemistry* **2014**, *86* (22), 11417-11424.
(14) Das, J.; Kelley, S. O. Tuning the bacterial detection sensitivity of nanostructured microelectrodes. *Analytical chemistry* **2013**, *85* (15), 7333-7338.